FCTUC DEPARTAMENTO DE ENGENHARIA CIVIL
FACULDADE DE CIÊNCIAS E TECNOLOGIA
UNIVERSIDADE DE COIMBRA

# Modelling the Influence of Soil Variability on Geotechnical Structures

**Dissertation submitted for the degree of Master of Civil Engineering in Geotechnics**

**Author**
**Diogo António Carvalho Ferreira**

**Supervisors**
**António M. G. Pedro**
**Paulo Alexandre L. F. Coelho**

Esta dissertação é da exclusiva responsabilidade do seu autor, não tendo sofrido correções após a defesa em provas públicas. O Departamento de Engenharia Civil da FCTUC declina qualquer responsabilidade pelo uso da informação apresentada

**Coimbra, July, 2016**

# AGRADECIMENTOS

Gostaria de começar não sem antes deixar o meu mais profundo agradecimento ao Professor Doutor António Pedro pelo imensurável apoio prestado durante o desenvolvimento desta dissertação. Ao André Mateus, Martim Matos, Izel Issufo e João Carmona pelas diárias discussões que tanto contribuíram para a necessária motivação. Aos docentes do perfil de Geotecnia pela sobre-humana capacidade para transmitir conhecimento e paixão pela área em especial ao Professor Doutor Paulo Coelho e ao Professor Doutor José Grazina por todo o apoio e tempo disponibilizado. Por fim, mas não menos importante, ao José António e Nuno Oliveira por todo o apoio prestado.

Aos meus amigos, em especial aos colegas de curso que me acompanharam durante estes anos quer em trabalho quer em farra em especial ao David Valério, João Sena, Daniel Pereira, Miguel Lucena, Frutuoso Oliveira, Tomás Gonçalves, José Fresta, Laura Seco, Catarina Mouraz e Guilherme Prata sem os quais o percurso teria sido indubitavelmente mais penoso.

À minha Mãe, aos meus Irmãos Rui e Edgar e em especial à minha Avó Maria. Por todo o amor e todo o apoio.

Ao Manuel e Francisco Lobão.

À Mónica.

# RESUMO

A existência de variabilidade nas propriedades de solo e rochas é há muito reconhecida e o seu impacto tem sido alvo de estudo por parte de diversos autores. Com o aparecimento do Eurocodigo 7 tem sido dada uma maior relevância a este temática e conceitos como valor característico e análise probabilística têm ganho notoriedade em detrimento dos conceitos determinísticos usados no passado. Como referido por Uzielli et al. (2006) "*Abordar a incerteza não aumenta o nível de segurança, mas permite um projeto mais racional já que o engenheiro pode em consciência calibrar a sua decisão tendo em conta a performance desejada ou expectável para a estrutura"*.

O presente trabalho tem como principal objetivo modelar numericamente a variabilidade existente em solos e rochas e de avaliar qual o seu impacto no comportamento de obras geotécnicas. Em primeiro lugar será feita a descrição do estado atual do conhecimento desta temática de forma a explicitar a importância do conceito de variabilidade bem como dos principais parâmetros necessários para a sua caracterização. Será feita igualmente a revisão dos algoritmos mais frequentemente utilizados para simular a variabilidade onde será dado destaque ao Método da Subdivisão Local (LAS) usado no presente trabalho.

A simulação numérica da variabilidade exigiu o desenvolvimento de diversos programas de cálculo cuja descrição detalhada é apresentada. Destacam-se entre estes: um gerador de campos aleatórios (UC2DRF) que permite reproduzir a maioria dos tipos de variabilidade existente nos maciços, a adaptação de um algoritmo de elementos finitos (UCGeoCode) para possibilitar correr as múltiplas análises numéricas e um programa intermediário entre ambos (MAT.PROP) que permite aplicar a variabilidade gerada aleatoriamente às propriedades mecânicas desejadas. Referem-se igualmente os diversos softwares que foram desenvolvidos com o intuito de facilitar a interpretação de resultados.

Por último, e com o intuito de aferir o impacto da introdução da variabilidade serão efetuadas três aplicações de prática comum em engenharia geotécnica. Analisa-se em primeiro lugar a capacidade de carga de uma fundação contínua isolada. Posteriormente, avalia-se o comportamento de duas fundações contínuas. E por último, analisa-se o impacto da escavação de um túnel profundo. O estudo destas aplicações irá permitir validar a metodologia usada bem como avaliar o impacto que a variação dos parâmetros selecionados tem na resposta geotécnica e estrutural com a consequente implicação resultante para o dimensionamento destas estruturas.

# ABSTRACT

The presence of variability in soil and rock properties has been widely acknowledged and its impact studied by several authors. With the introduction of Eurocode 7 the impact of variability has become increasingly relevant and notions such as characteristic value and probabilistic analysis have been gaining notoriety in detriment of the deterministic concepts used in the past. As mentioned by Uzielli et al. (2006) "*Addressing uncertainty does not increase the level of safety, but allows a more rational design as the engineer can consciously calibrate his decision on a desired or required performance level of a structure"*.

The present work has the main purpose of modelling numerically the variability observed in soils and rock masses and evaluate its influence on the behaviour of geotechnical structures. Primarily, a description of the current state of knowledge will be provided so that the importance of the concept and of the principal parameters required for its characterization can be understood. A review of the algorithms most commonly used to simulate variability will also be presented emphasizing the Local Average Subdivision (*LAS*) method, which is used in the present work.

Modelling variability in not a direct process and demanded the development of several programs. From these it should be mentioned: the random field generator (UC2DRF) which enables the simulation of diverse types of variability, the upgrade of the finite element code (UCGeoCode) so that multiple analyses could be performed and an intermediate program (MAT.PROP) that allows the application of the randomly generated variability to the desired mechanical properties of the soil. Several other softwares were also developed in order to simplify the interpretation of the numerical results.

Finally, with the objective of assess the influence of the introduction of variability three ordinary applications of the current geotechnical engineering practice will be presented. Primarily, the bearing capacity of a strip footing will be analysed. Subsequently the behaviour of twin strip footings will be assessed. Lastly, the impact of the excavation of a deep tunnel will be discussed. The study of these applications will allow the validation of the used methodology and the evaluation of the impact that the variation of the chosen parameters has on the geotechnical and structural response with the consequent implications for the design of this type of structures.

# TABLE OF CONTENTS

# 1 INTRODUCTION

*"Unfortunately, soils are made by nature and not by man, and the products of nature are always complex… As soon as we pass from steel and concrete to earth, the omnipotence of theory ceases to exist. Natural soil is never uniform. Its properties change from point to point while our knowledge of its properties are limited to those few spots at which samples have been collected. In soil mechanics the accuracy of computed results never exceeds that of a crude estimate, and the principal function of theory consists in teaching us what to observe in the field."*

Karl von Terzaghi

## 1.1 General considerations

The existence of variability in properties of the materials in civil engineering is an undeniable fact. Though manufactured materials like concrete and steel can have the variability in its properties controlled both during production and post production, natural materials like soils and rocks are subject to random chemical and physical processes making it so that their properties cannot be controlled.

In a traditional geotechnical approach samples are retrieved from a few pointwise locations and a more or less refined local representative value of the properties within a given area is estimated. A single calculation based on those values and on a usually rough estimative of the field stresses is performed and structures are then designed to withstand the acting forces by the inclusion of a safety factor. This approach is prone to cause structural failure when the safety factor is not large enough and to have an economic impact when the safety factor used reflects an overestimation of the acting stresses or an underestimation of the properties of the soil. In order to overcome the afore mentioned issues the reliability based approach has been picking up momentum. In a reliability based approach instead of decision making process relying on a safety factor it relies on a probability of failure established accordingly.

So that probability of failure can be accessed methods of generating multiple scenarios, random fields, have been developed. In the present work the Local Average Subdivision (*LAS*) method will be used. Through the generation of random fields multiple calculations can be performed

until the desired reliability revel is achieved making the geotechnical structural design both efficient and impervious.

## 1.2 Goals of the dissertation

This dissertation aims to establish a reliability based design methodology that could be applied to the design of geotechnical structures as well as its validation throughout the process. It is also this work's objective to assess the impact of the variation of parameters related with the statistical distribution and spatial distribution of soil and rock properties on structural response. The approach established will hopefully allow for the analyses of situations where neglecting to consider the existence of variability could have undesired consequences.

So that variability could be included in numerical analyses, a number of tools and procedures will be developed or created allowing for the sequential computation of multiple calculations. Finite elements method will be used to analyse the impact that each random field has on each considered structure.

## 1.3 Structure outline

The dissertation was divided in five chapters. Following this introductory section (Chapter 1) where an introduction to the main topic of the present work and to its main goals are presented, Chapter 2 provides a review on the current state of knowledge regarding the subject of soil and rock variability. In this chapter the most commonly used algorithms to simulate variability are also presented and its advantages and pitfalls discussed in detail.

In Chapter 3 a detailed presentation of the software developed for numerically simulate and evaluate the influence of variability of soils and rocks is provided. Particularly emphasis will be given to the random field generator and to its potentialities when modelling different aspects of inherent variability.

Chapter 4 presents three applications, a strip footing, a twin strip footings and a deep tunnel, in which the influence of a number of parameters related with soil and rock and soil variability is inferred by performing multiple parametric studies.

Finally, in Chapter 5 the final conclusions from the developed work and recommendations about possible future works and developments around the subject are presented.

# 2 VARIABILITY IN SOILS AND ROCKS

## 2.1 General Considerations

### 2.1.1 Concepts

Soil and rocks are materials whose properties are heterogeneous in space and variable in magnitude (Zhang, 2013). The determination of their properties often relies on tests performed in a laboratory or at a few pointwise locations in the field, both limited to a number of samples and conditioned by a certain level of interference (Bourdeau & Amundaray, 2005). The notion of variability implies an observable manifestation of heterogeneity of one or more physical parameters or processes that can be described through the analysis of a sufficient number of samples. The notion of uncertainty reflects the decision making process required when addressing the observed variability (Uzielli et al., 2006). The characterisation of uncertainties in geotechnical engineering, mainly in the input parameters used in the design, allows the evaluation of the impact that variability may cause in the performance of the structure through the assessment of a probability of failure. The existence of ground properties' variability leads to a level of uncertainty both when choosing input parameters in a problem and when analysing its output. Christian (2004) has concluded that regarding uncertainty three methodologies can be followed: (1) it could be ignored by being conservative, as long as the structure or system is robust enough to be able to withstand anything; (2) using observational methods by considering possible designing methods, monitoring their application during construction and modify / adjust them depending on the results; or (3) quantifying uncertainty through a reliability approach derived from the observational method using probabilistic methods.

The spatial variability of soils and rocks is one of the main sources of structural damage and the malfunctioning of built systems. Cases have been identified where the variability of soil stiffness and strength induced differential settlements which had severe consequences on structural response (Breysse et al., 2004). Uncertainty is often described as being related with three main causes (Bourdeau & Amundaray, 2005; Pedro et al., 2012):

(1) inherent soil and rock variability - mostly caused by weathering, in which rocks are subjected to physical, chemical and biological phenomena, being transformed into materials with weaker properties (Dasaka & Zhang, 2012) or soil variability related with depositional processes that occurred during its formation. This kind of uncertainty accounts for intrinsic

variations within a relatively homogeneous soil horizon (Bourdeau & Amundaray, 2005). Inherent variability can also be related with lithological heterogeneity, manifested through intercalation of soft and stiff layers or resulting from large-scale geologic and geomorphic processes (Uzielli et al., 2006).

(2) limited availability of information - most problems on geotechnical engineering are solved on the basis of a few discrete observations (Rackwitz, 2000). The number of samples obtained from each site are often constrained by the time and by the economic resources available and consequently are not enough in order to obtain a representative value of its properties. Even if a high number of samples can be characterised it is not certain that they will properly describe the variability within the area of study.

(3) imperfect information – due to measurement errors, soil disturbance, sample size effect, test imperfections, difference between stress conditions in the field and in the laboratory, a level of uncertainty derives from the fact that site investigation techniques can not properly and accurately quantify soil properties. Therefore, a difference between test results and the actual value of a certain property is expected (Orchant et al., 1988).

Despite the existence of several empirical deterministic expressions in order to evaluate possible modes of failure it is expected that a failure surface will follow the weakest path, that is, through areas where it has lower resistance, and consequently it is paramount to identify such areas. In a traditional approach the soil is considered to be spatially homogeneous, effects of heterogeneity are ignored and consequently there is no uncertainty. Though safety factors are generally applied when using a deterministic approach, not accounting for uncertainty may lead to failure. The introduction of Eurocode 7, the European standard for geotechnical design, in 2010, provides a broad framework for the design of all different types of geotechnical structures with an involved risk analysis approach (Orr, 2012). Eurocode 7 proposes a way of dealing with uncertainties regarding both limited information and imperfect information, while still acknowledging its existence. This is achieved through several recommendations proposed in Application Rule §1.3(2) in EN 1997-1, that specifies conditions regarding both the qualifications of the personnel gathering data and performing the design. A minimum number and type of field and laboratory tests to be performed for soil classification and the requirement of a generation of a Geotechnical Design Report are also enforced by section 3.4.1(1) and by Part 2 of Eurocode 7 (EN 1997-2). To what inherent variability is concerned Eurocode 7 states that the representative value to be chosen when studying any given soil is the characteristic value defined as a cautious estimate of the parameter governing the studied limit state: *“Geotechnical investigations shall provide sufficient data concerning the ground and the ground-water conditions (...) for a proper description of the essential ground properties and a reliable assessment of the characteristic ground parameters to be used in design calculations”*

(EN 1997-1 §1.3.2(1)P). The space, number and depth of the investigation points required by Eurocode 7 is dependent on the type of structure to be built. The minimum number of identification tests to be performed for each parameter proposed by Eurocode 7 is summarized in Figure 2.1a) and depends on the quality of data already available as well as prior knowledge of material properties. In the figure *PSD* refers to particle size distribution, Consistency to Atterberg tests, *P/d* represents particle density determination and *BDD* the bulk density.

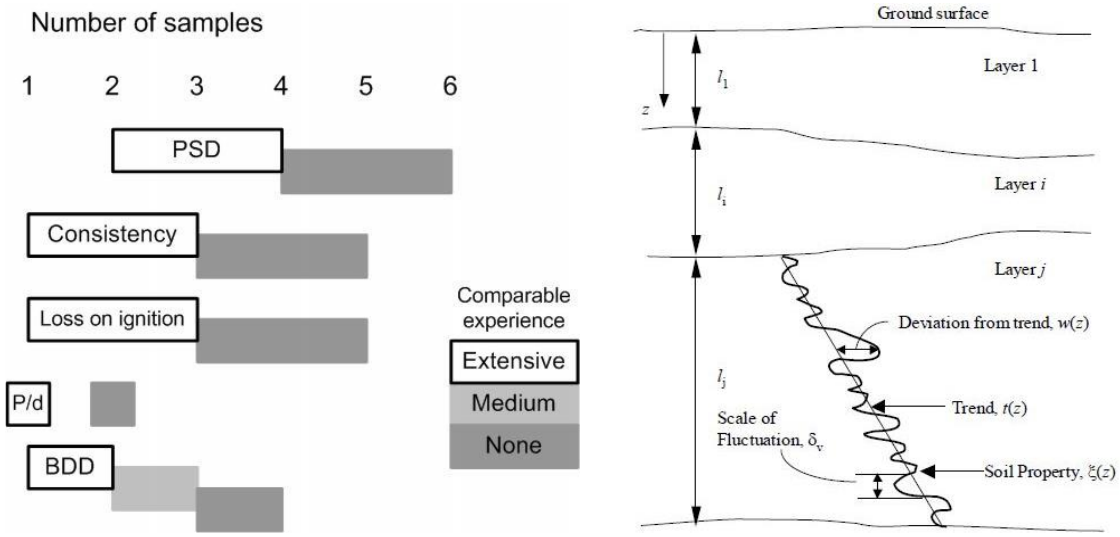


a) b)

Figure 2.1 – a) Number of samples to be tested for each stratum (Bond & Harris, 2008); b) Spatial variation for soil properties (Phoon & Kulhawy, 1999);

While the uncertainty related with limited availability of information and its imperfection is considered epistemic, hence subjective, uncertainty regarding inherent soil and rock variability is considered to be objective but aleatory caused by spatial variability of soil and rock properties (Suchomel & Masin, 2010). The inherent variability causes that ground properties vary from point to point even within the same stratum (Bourdeau & Amundaray, 2005). The variations are caused by multiple factors, acting together or isolated, such as: differences in mineral composition, stress history, water content and mineral composition as well as a number of physical and chemical processes that can occur depending on the environmental conditions. These cause variations in soil and rock strength and stiffness properties that translate directly in the response of the material when loaded.

Anisotropy refers to any directional dependence in a material property. Soils are generally recognized to be anisotropic in their mechanical properties: strength, stiffness and permeability (Nishimura, 2005). Generally soil properties vary in all directions and consequently have an anisotropic spatial variability. Even sedimentary soils which appear homogeneous present properties that vary from point to point. Soil properties vary both horizontally and vertically

mostly due to the depositional environment, degree of weathering, confinement and physical environment (Jones et al., 2002; Cho & Park, 2010), although some degree of homogeneity is usually found in the horizontal direction (Uzielli et al., 2006). In contrast, a residual soil or a rock frequently present anisotropy in all directions. These aspects should be recognized and taken into account in each phase of variability estimation.

In spite of the occurrence of variability, spatial correlation between soil and rock properties in space is expected to happen as a result of its natural or man-made fabric. This means that values of a certain property at location $X$ and the same property at $X+\Delta h$, with $\Delta h$ being the distance between the locations, are correlated. This correlation is dependent on the spatial arrangement, shape, size and condition of the particles and it is highly site specific. The spatial variation of soil properties in a given direction can be described by Equation 1 (Phoon & Kulhawy, 1999):

$$\xi(z) = t(z) + w(z) \quad (1)$$

Where $\xi$ is the value of the soil property in the field, $t$ a deterministic trend component, $w$ a random component and $z$ the depth as shown in Figure 2.1b), though same principle is applied to any given direction. The trend can be determined by fitting a deterministic function to the data or by employing a moving average procedure. The random component can be estimated through methods that will later be detailed. This random component is associated with a scale of fluctuation, which is the difference between the value it assumes and the trend it is expected to follow, and is directly correlated with the standard deviation of a statistical model. The scale of fluctuation presented in Figure 2.1b) is defined as the proportionality constant in the limiting expression of the variance function, and its formulation can be found in Vanmarcke (2010).

The characterisation of variable parameters simply based on their mean and standard deviation is usually not enough since it is frequently observed that two different sites present similar mean and standard deviation values but display significant differences in spatial distribution (Uzielli et al., 2006). Consequently, the determination of the spatial variation when describing soil variability is very important. By acknowledging the existence of spatial variation the representative value of any soil property also became dependent of the volume of the problem to be solved.

### 2.1.2 Typical Statistical Distributions in Soils and Rocks

The use of probability theory is useful when modelling the behaviour of a variable parameter. Data gathered through sampling can be used to extrapolate and fit a statistical distribution for each individual property or for a combination of properties. Based on these distributions probabilistic models can be created and tested, theoretically, under an infinite number of material properties combinations in order to define the most representative behaviour, as shown

in Figure 2.2. The fit of probability density functions is only adequate for practical purposes as long as it applies to well-known soil or rock properties (Arsyad, 2008). In order to perform statistical estimation of soil properties the establishment of the correlation structure is required. This can be achieved through moment estimators, inverse estimation from stochastic interpolations or the maximum likelihood method (Degroot & Baecher, 1993). It can also be performed through bootstrap-resampling in which data sets are numerically generated by randomly subsampling the available data and then compute estimators by summarizing these samples' variability (Bourdeau & Amundaray, 2005).

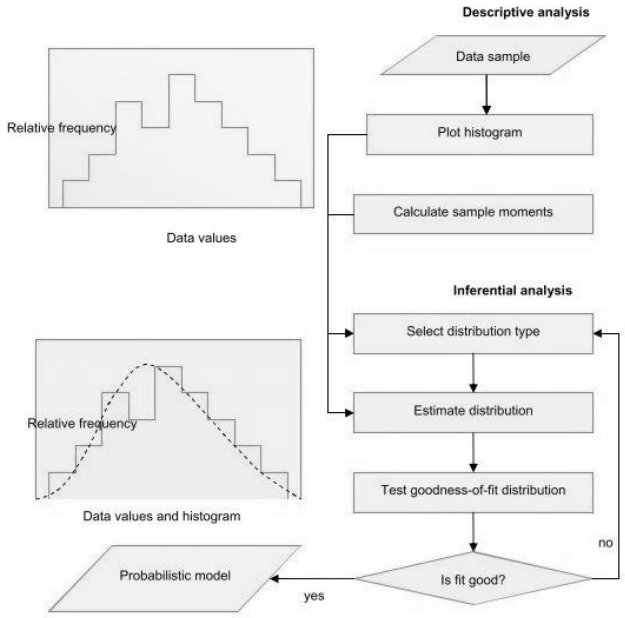


Figure 2.2 – Probabilistic models based on statistical distributions (Uzielli et al., 2006); sample moments: average and standard deviation

Laboratory tests conducted show that properties in natural soils appear to have random variations that follow a Gaussian statistical distribution or a transformation of it, mainly a lognormal distribution, where the exponential of the values fit a normal distribution (Lumb, 1966; Griffiths & Fenton, 2001). As for the strength parameters Wolff et al. (1995) and Lacasse & Nadim (1996) suggest that a Gaussian statistical distribution can also be fitted to the friction angle, $\phi'$, as well as a normal or lognormal distribution for the undrained shear strength, $S_u$, for silty clays and clays respectively. These suggestions were also supported by studies performed by other authors (Suchomel & Masin, 2009; Suchomel & Masin, 2010; Chen et al., 2012). The deformability parameters, $E'$ and $E_u$, are expected to follow an identical function of $\phi'$ and $S_u$ for cohesionless and cohesive soils, respectively. Lacasse & Nadim (1996) also suggested that for CPT results a lognormal probability density function is suitable for sands and a normal or

lognormal probability density function is suitable in silty clays and clays respectively for the tip resistance values.

The evaluation of properties in rocks is even more complex than in soils due to its nature. The heterogeneity observed in these materials is strongly dictated by tectonic movements, physical and chemical processes, faults and joints that affect its strength and stiffness properties making difficult to define a single representative value. As consequence, instead of defining a strength or stiffness variable directly it is usual to estimate those properties through the use of geomechanical classifications. From the several classifications available in the literature the Geological Strength Index (*GSI*), developed by Hoek (1994), is often used since the rock properties can be derived by simple expressions and is intertwined with Hoek-Brown failure criterion (Hoek et al., 2002), which is the most broad criterion employed for accurately reproduce the failure envelope of rock massifs (Cai, 2011). The Hoek-Brown failure criterion is based on the strength of the rock mass and on the *GSI* value which can be estimated though the tables proposed by Marinos & Hoek (2001) or correlated with the Rock Mass Rating system (*RMR*) (Bieniawski, 1973). The strength of the rock mass depends on the properties of the intact rock pieces and also upon the freedom of those pieces to slide and rotate under different stress conditions (Hoek, 2007), while *GSI* value is obtained based on the geological description of the rock structure or block size as well as joint conditions. Block size is dependent on the number of joints, their spacing, orientation, size and persistence, it is, therefore, a volumetric expression of joint density. Studies found that a lognormal distribution could be fit to joint spacing (Dershowitz & Einstein, 1988; Cai, 2011) and its orientation, defined by dip direction and dip, usually follow the von Mises-Fisher distribution (Cai, 2011). The joint size can be described through several statistical distributions though studies found that lognormal was the most suitable (Dershowitz & Einstein, 1988). The joint surface conditions, controlled by alteration, large-scale waviness and small-scale smoothness, follow a Gaussian distribution (Cai et al., 2004; Cai, 2011). The *GSI* values derived from such parameters follow a normal distribution according to the central limit theorem (Cai, 2011). Other parameters such as uniaxial compressive strength and Young's moduli tend also to follow normal distributions. All the afore mentioned conclusions are based on empirical observations and therefore may vary depending on site conditions.

## 2.2 Methods for Simulate the Variability of Soils and Rocks

So that variability can be simulated random fields are used in order to reproduce a number of possible distributions of a given variable within a finite field. A random field is a random process consisting of an indexed set of random variables generated in a defined multidimensional area (Vanmarcke, 2010). Unlike a deterministic approach where only a single calculation is performed resulting in a single Safety Factor value, the analysis of multiple

random fields has the advantage of enabling a reliability based design associated with the concept of probability of failure. In order to characterise a Random Field (*RF*) at least three parameters are required: mean, standard deviation and a function that relates the properties of any two points at any given location, auto-correlation function (Ching et al., 2015). Therefore, when generating a *RF* for a given property a probabilistic model must be assigned to it, as described on the previous section. Furthermore a finite dimension or dimensions for the field must be fixed so that it can be increasingly sub-divided depending on the level of refinement expected or required of it.

Several algorithms have been developed in order to generate scalar multidimensional random fields of a given property A brief explanation of the most commonly used methods will subsequently be provided as well as a detailed characterization of the algorithm used in this work. It should be noted that only the generation of 1D, 2D and 3D random fields are significant since all the methods presented are stationary and variation with time are neglected. One of the presented methods (*TBM*) is unable to perform one dimensional random fields.

In order to thoroughly understand the presented algorithms there is an underlying statistical assumption that must be detailed. In every algorithm that will be introduced only the variables required to characterize a Gaussian field, mean and covariance structure, that is standard deviation, are required. These are referred in technical literature as the first two moments of the target field. In spite of the existence of methods relying on the four sample moments of the field: mean, standard deviation, skewness and kurtosis they will not be referred in this work and a detailed explanation of such methods can be found in Uzielli et al., 2006. Non-Gaussian fields can be obtained from a Gaussian field through a transformation function. However, care must be taken since mean and covariance structure must also be transformed.

### 2.2.1 Covariance Matrix Decomposition (CMD) and Moving-Average Method (MA)

Covariance matrix decomposition (*CMD*) and moving average (*MA*) methods have been thoroughly described by Le Ravalec et al. (2000) and Fenton & Griffiths (2008). These methods rely on the expression of a property as an average of an underlying white noise process. The afore mentioned white noise consists of a Gaussian white noise, that is, a n-dimensional field of uncorrelated normal deviates, random variables with zero mean and unit variance that follow a Gauss probabilistic distribution.

CMD was developed by Cholesky (Tanabe & Sagae, 1992) and it is of relatively simple implementation in one dimension. It consists on the establishment of a covariance matrix that is obtained through the product of an upper and a lower triangular matrix so that one is the transpose of the other. By multiplying the previously determined upper triangular matrix with

a vector of uncorrelated normal deviates and adding the local average expected it is possible to obtain a random distribution of a given property along one dimension.

MA method is considered as an improvement to the *CMD* method. Instead of requiring the use of a covariance matrix it requires the use of a convoluted function, which is the product of a function and its inverse, eliminating the need of the cumbersome matrix decomposition process, thus, making this method of easier computation and consequently more time efficient.

Both methods have several problems within their formulation, namely when it comes to choosing a covariance matrix and function, respectively, due to the nonuniqueness of the triangular matrix resulting from the *CMD* or from the convoluted function obtained from the covariance function in the *MA* method. Another difficulty is related with the necessity of truncating the Gaussian white noise since its possibility of assuming any real value affects the reliability of the results obtained through both methods. Furthermore, it is expected that in two dimensions, when generating a random field of square dimensions using the *MA* method ($K^2$), the number of white noise realizations to be around $rK^2$, with $r$ being the ratio between the incremental distance between points of the underlying white noise and the increment of the physical process (Fenton & Griffiths, 2008), which is significantly larger than in other methods resulting in impractical calculation times and makes the method prone to considerable round-off errors. When calculating a random field for the same square field using the *CMD* method a total of $K^4$ realizations are expected making it only useful to employ when calculating small fields.

### 2.2.2 Discrete Fourier Transform (DFT) and Fast Fourier Transform (FFT) methods

The Fourier Transform methods are based on the spectral representation of homogeneous mean square continuous fields (Griffiths & Fenton, 2008). *DFT* uses a divide and conquer approach that consists on a matrix-vector product that requires $N^2$ complex additions and multiplications in order for it to be evaluated (Duhamel & Vetterli, 1990). The *DFT* method consists on expressing a n-dimensional integral that abides on a spectral representation of mean contiguous fields through a $n$-dimensional sum that is evaluated at each point in space $x$ which makes it so the method can be computationally slow for reasonable field sizes and typical spectral density functions. The underlying idea of the method is to map the original problem into several sub-problems in such way that the effort of performing the mapping of the sub-problems and its evaluation is smaller than the effort required to evaluate the complete problem. The advantage of the method is that the number of divisions can be applied recursively to the sub-problems leading to the reduction of the level of complexity involved.

*FFT* is an efficient way of computing the general equation of the *DFT* method assuming that both space and frequency can be discretized into equispaced points. That factor results on an

efficiency increase of the method. *FFT* takes advantage of the fact that the calculation of the coefficients of the *DFT* can be carried out iteratively, reducing computation time as well as round-off errors associated with the computation of the method (Cochran et al., 1967). However, the assumption that the process associated with the randomization of the field has zero mean and is real and discrete is required (Fenton & Griffiths, 2008; Griffiths & Fenton, 2008). Other of the problems of the *FFT* method is that, regardless of the target covariance function, the covariance function resulting from the algorithm is always symmetric about the midpoint of the field (Fenton, 1994). However, this limitation can be circled around by generating a field with the dimensions twice as big in both directions and keeping only one quadrant of the field. This methodology keeps the variance and average of the field within reasonable values.

### 2.2.3 Turning Bands Method (TBM)

The basic concept of the Turning Bands Method (*TBM*) is to transform a multidimensional simulation into the sum of a series with equivalent unidimensional simulations (Jones et al., 2002). The objective is to preserve the statistics of the true field, particularly the measure of the degree of spatial dependence between samples along a specific support of the stationary random field. In order to use *TBM* it must be assumed that the field has a second-order stationarity, a constant mean and standard deviation, and is isotropic. However, it is possible to transform the normal distribution resulting from the application of the method into other statistical distributions.

In two dimensions the algorithm proceeds as follows: one arbitrary origin within or near the domain of the field to be generated is chosen; a line *i* crossing the domain and having the direction of a random vector is selected; a realization of a one-dimensional process along the line *i* is generated accordingly; the process is repeated orthogonally for as many lines needed until proper discretization of the field is achieved. The field must then be normalized by dividing each unidimensional process by the square root of the number of lines. *TBM* method is, therefore, highly dependent on the knowledge of the one-dimension covariance structure. The method causes errors due to the existence of streaks within the field itself resulting from the lines chosen in order for it to be performed. These streaks can cause paths of reduced resistance or crack propagation if the field is to be submitted to further calculation. Despite that *TBM* is considered the most accurate method when using a larger number of lines though it results in cumbersome computation.

### 2.2.4 Local Average Subdivision (LAS)

The Local Average Subdivision (*LAS*) method is the most difficult to implement amongst the mentioned methods but one of the easiest to use when coded since no decisions have to be made

during the process regarding its parameters (Fenton & Griffiths, 2008). By acknowledging the fact that most properties in engineering practice are represented by the average value within the analysis domain, that is a local average, Fenton & Vanmarcke (1990) developed the *LAS* method. This method allows for random field generation along 3 dimensions with the advantage of keeping the statistics consistent with the field resolution at each level (Pedro et al., 2012). Though the method was developed so that the random field has a stationary Gaussian distribution it can be used to generate random fields with other statistical distributions, namely log-normal distribution, through transformation functions. It is also worth noticing that a systematic bias in the variance field is observed in a two dimensions which magnitude varies with the number of subdivisions and the covariance function though a quantitative analysis of its influence is yet to be performed (Griffiths & Fenton, 2008).

This method is ideal for combined use with finite element modelling using low-order interpolation functions since it guarantees freedom to change mesh resolution without losing stochastic accuracy (Griffiths & Fenton, 2008). In spite of only being suitable for stationary processes due to its formulation, that is processes that can be described by its second order statistics, average and variance, that remain constant throughout the domain, a non-stationary mean and variance can be added to the process through a simple transformation expressed by Equation 2 where X(t) represents the results obtained from the method through a stationary process, μ(t) the average value that varies along one of the directions, *σ(t)* the standard deviation that can also be variable along the same direction and *Y(t)* the resulting non-stationary process. This is useful for simulation of *CPT* results where sometimes the values increase with depth.

$$Y(t) = \mu(t) + \sigma(t) \cdot X(t) \qquad 2$$

In the present work only the case of 1D and 2D generations will be explained since the generated fields employed in this research will be two dimensional and a thorough explanation of the method in 1D is useful in order to fully understand it.

*LAS* starts from a given initial average $Z_1^0$ associated with a pre-determined statistical distribution and standard deviation both constant on the entirety of the domain and divides it equitably from level to level until the required precision is reached. The number of divisions is an input parameter of the method and its definition is dependent on the discretization intended, which is directly related with the number of individual points to be expected as output. This is mostly relevant when it is required for a finite elements mesh to have different properties in each individual Gauss point. In such case the number of divisions must be sufficient to guarantee that the distance of each subdivision is smaller than the distance between two consecutive Gauss points.

In one dimension this method can be easily understandable as having a top-down structure as shown in Figure 2.3a). The algorithm proceeds as follows: the initial field having an initial average $Z_1^0$ is subdivided into two fields having means $Z_1^1$ and $Z_2^1$ obtained from a Gauss distribution which are conditioned on the value of $Z_1^0$, averaging $Z_1^0$. These new fields have a correct standard deviation according to averaging theory and are correlated with each another. This process is repeated for the generation of other levels. The values at each level are obtained through the addition of a random Gaussian noise. The correlation of every value on the same level is accomplished through a covariance matrix obtained from a spatial correlation function.

The definition of the space correlation function is a key point of the method because it establishes mathematically the existing relationship between the values assumed for a given property in two separate points in space. In one dimension the Gauss-Markov expression (Equation 3) is of most common use (Zhang, 2013; Wang, 2014). This equation allows for the determination of the existent correlation ($\rho(|\tau|)$) given a standard deviation ($\sigma$), a distance between averages ($\tau$) and a spatial correlation distance ($\theta$). The spatial correlation distance establishes the length interval in which properties are expected to be correlated. A small correlation distance will imply that significant variations of a properties' value will occur within a smaller space while a higher correlation distance implies that there is small variation on the value of the same property. Theoretically this means that if the space correlation distance is equal to zero the value of the property at each point is uncorrelated with the value of the same property at any other point. In contrast, if the space correlation distance value is infinite the result would be an isotropic uniform field.

$$\rho(|\tau|) = \sigma^2 \times exp\left(\frac{-2|\tau|}{\theta}\right) \qquad 3$$

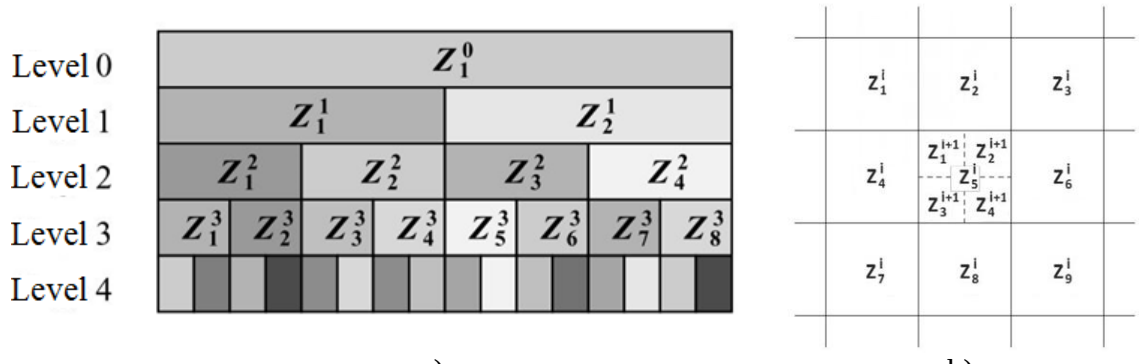


a) b)

Figure 2.3 – *LAS* (adapted from Fenton & Griffiths (2008)): a) 1D; b) 2D

In 2D the algorithm follows similar steps. As shown in Figure 2.3b) the initial field having average $Z_1^0$ associated with a standard deviation and having a statistical distribution constant along the domain is divided into four subdivisions with same dimension and having means correlated with $Z_1^0$ as explained previously.

The main difference between the 1D and 2D algorithms resides on the space correlation function through which the covariance matrix is obtained. The Markov function used is this work has been employed by several authors (Fenton & Griffiths, 2008; Zhang, 2013; Li et al., 2015) and is shown in Equation 4. The Markov expression used represents a circular function if isotropic correlation distances are applied and an elliptical function if anisotropic spatial correlation distances are used. The introduction of rotation to anisotropic random fields is obtained through modifications to the coordinate system of the elliptical function as explained in Zhang (2013).

$$\rho(\tau_{ij}) = \sigma^2 \times exp\left[-2\left(\frac{|\tau_{ij,x}|}{\theta_x} + \frac{|\tau_{ij,y}|}{\theta_y}\right)\right] \quad 4$$

In this equation $\tau_{ij,x}$ and $\tau_{ij,y}$ are the distances between elements *i* and *j* in the *x* and *y* directions, respectively. If the correlation distances in both directions ($\theta_x$ and $\theta_y$) assume the same value than the correlation function is isotropic and can be further simplified. However, if $\theta_x$ is different from $\theta_y$ an anisotropic random field can be generated. In this case the algorithm proceeds as follows: the direction with the smaller space correlation value is stretched so that the reason between the lengths is inverse from the reason between the θ values. As an example if $\theta_x$ is equal to 2 and $\theta_y$ is equal to 1 the length in the *y* direction is multiplied by 2 so that $L_y/L_x=\theta_x/\theta_y$. From there the algorithm proceeds accordingly and after the generation of the field it is cropped to its initial size as shown Figure 2.4. This process does not require code change nor does it result in loss of efficiency, though it is expected, in spite of generally the field being anisotropic, that small neighbourhoods of points in the final resolution tend to follow an isotropic correlation structure because the algorithm itself is incapable of preserving anisotropy (Griffiths & Fenton, 2008).

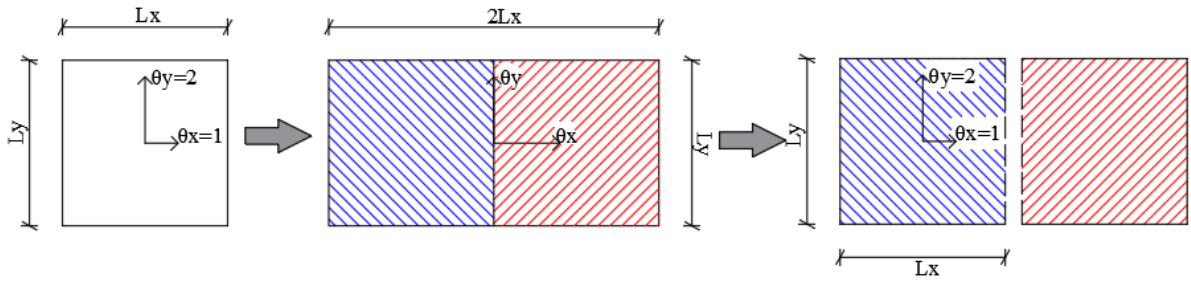


Figure 2.4 – Generation of an anisotropy field with LAS method

The afore mentioned algorithm for the LAS method in 2D generates random fields having the horizontal and vertical axis as the main directions of correlation. As a result they control the directions of variability accounting only for transverse anisotropy which may be insufficient in some problems, per instance, when the direction of the layers of stratification within a soil has an angle with the horizontal direction. Rotated anisotropy can be achieved by introducing the angle $\alpha$ between one of the main directions and the horizontal axis. In such case, and considering that the main directions of the field remain orthogonal, an auxiliary field can be generated having as main axis the horizontal and vertical directions with such dimensions so it can accommodate its rotation to the main directions and its cropping to fit the size of the original field as displayed in Figure 2.5.

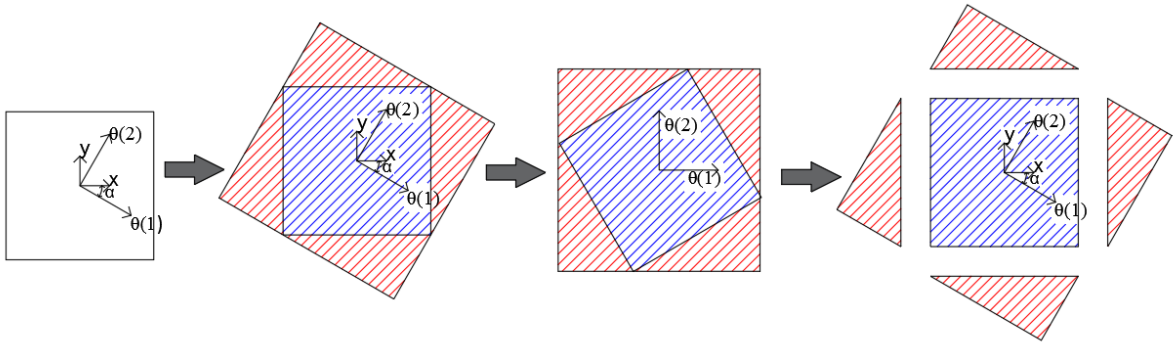


Figure 2.5 – Generation of a rotated field

In order to calculate the values for *i+1* levels the values at level *i* must be known so that a Markov expression can be used. Because of that while computing the *LAS* method storage must be provided for 2N-1 values in one dimension or $4/3(N^2)$ in two dimensions assuming that N is the desired number of intervals of the process. This makes the method cumbersome to compute for a number of subdivisions higher than 10.

### 2.2.5 Comparison of methods

The choice of which method to use to generate a random field must be suited to each particular problem. In the present work LAS will be used since it was already in a late stage of implementation when this work began. In the technical literature only *FFT*, *TBM* and *LAS* methods are advised to simulate variability due to the fact that all the other afore mentioned methods, although potentially accurate, tend to be computationally slow and therefore not suitable for most problems in engineering practice. To what efficiency is concerned *LAS* or *TBM* with a small number of lines are the algorithms with smaller run-times, though this is often a negligible aspect since the time it takes to generate the field is generally insignificant when compared with the time it takes to subsequently process and analyse it.

When it comes to accuracy when keeping the mean and covariance structure Griffiths & Fenton (2008) states that the best algorithm is probably the *TBM* method using a large number of lines, there isn't, however, clear rules regarding the number of lines required to avoid streaking when using the *TBM* algorithm since it depends not only of the dimensions of the field but also of the covariance function used. The *FFT* method requires symmetry in the covariance structure of the realizations and consequently symmetry regarding the standard deviation on the final resolution of the field is expected to occur. This drawback can be surpassed by manipulating the field, although that implies slower run times that increase significantly with the number of dimensions. *FFT* is also the most suitable method when it comes to time dependent applications since it employs spectral density functions. The *LAS* method is the logical choice if the problem requires a local average representation and, as previously stated, is the easier to use once coded and generally the most efficient though a bias in the variance field, especially in two or higher dimensions, is to be expected.

# 3 NUMERICAL MODELLING OF VARIABILITY

## 3.1 Introduction

In order to simulate variability a number of programs were created or further developed so that a level of reliability could be reached. Previous to this work the random field generator (UC2DRF) developed by Pedro et al. (2012) only allowed for the generation of up to 99 fields and had limited capabilities. In the current version (v6.2) the program can generate up to 999 fields and several other features were implemented such as the possibility to generate fields having a lognormal statistical distribution, field rotation, non-stationary processes and layering as well as the combined effect of multiple conditioning. A software (MAT.PROP) capable of serving as an intermediate between the random field generator and the finite element software (UCGeoCode) was developed making the process, which previously had to be done manually, automatic, more user friendly and efficient. The finite element software was updated so it could handle the sequential calculation of multiple fields. Finally, a software that allows for the interpretation of results in bulk was developed since previously it was only possible to output results from single calculations.

It should be emphasized the large increase of efficiency obtained by performing the interpolation of the random fields and the finite element mesh in bulk outside the finite element method software reducing the calculation time. As an example, 100 calculations can currently take less computing time than a single calculation performed previously if all the process is taken into account. Soil and rock correlations from the literature were also implemented in order to obtain variability in multiple parameters from single variable random fields.

In the following sections the main features of all the software upgraded and developed during this research are going to be presented and discussed in detail.

## 3.2 Random Field Generator

UC2DRF is a software developed at the Geotechnics Laboratory of the Civil Engineering Department of University of Coimbra that is currently on version 6.1. This program allows for the generation of 2D random fields using the *LAS* method. It can create random fields for a single variable with isotropic or anisotropic spatial correlations. In its current version the software allows for:

- Different dimensions of the field, making it suitable for problems where the relationship between the horizontal and the vertical dimensions of the domain are not 1:1. However, the generated field must always be rectangular which is not always the case in real case studies namely slope stability, though this apparent limitation can be overcome when the interpolation between the field and the finite elements mesh is performed.

- Generation of multiple random fields, allowing for up to 999 different fields to be generated with the same initial characteristics. If needed several instances of software can be run with the same input though studies have suggested that the use of 200 fields is sufficient to establish a pattern (Fenton & Griffiths, 2008; Pedro et al., 2012).

- High levels of subdivision of the field, the software generates $4^n$ points for every subdivision level being *n* the number of subdivisions. As explained this feature is relevant when trying to achieve variability within every Gauss point of a finite element mesh. For most cases the generation of 8 levels has proven to be reasonable amounting a total of 65536 different points.

- Random or fixed seed generation which makes the user able to control the starting point from which the stochastic white noise process has its beginning. This feature allows the generation of the same field more than once making it possible to reproduce performed calculations as well as clearly assess the influence of every change in each input characteristic.

- Normal or log-normal types of statistical distributions for the variables, since they were proven to be the most common statistical distributions of properties in natural soils and rocks. Other statistical distributions can be added by using transformation functions as stated in 2.2.4.

- Option to generate uniform fields, useful for calculations using standard techniques such as EC7 methodology. This can be achieved by two methods. Through the truncation of the variable by imposing a minimum and maximum values equal to the average value or by defining the standard deviation as having zero value.

- Truncation of the distribution, this can be done in order to avoid negative or extreme and non-acceptable low/high values. This is due to the fact that the domain of the normal distribution is infinite introducing inaccuracy when estimating properties. As an example due to its formulation *GSI* cannot assume a value above 100, if truncation of the highest value wasn't performed there would be a probability that some points would assume values that surpass the acceptable threshold. Identical case occurs for the angle of shear

strength that cannot assume values above π/2 radians. The truncation of lower values, particularly negative, can be avoided by employing a lognormal distribution which domain goes from zero to infinity.

- Anisotropy of the field, the spatial correlation distances in the horizontal and vertical directions relative to the field can be adjusted in order to simulate in-situ conditions.

- Layering, at the current stage of development it can only perform horizontal layering. The presence of several materials with different properties can be simulated. This is particularly interesting when studying the behaviour of geotechnical structures in the presence of multi-layered soil conditions.

- Rotation of the field, accounting for every condition of soil deposition as well as tectonic history that may have rotated the layers of the soil from the horizontal position. In the current version the assumption that the main directions of the variability remain orthogonal after rotation is made, making it impossible to generate fields with generalized anisotropy (non-orthogonal) and rotated generalized anisotropy (non-orthogonal).

- Increment with depth of the average assigned to the property, allowing for non-stationary random field generation accounting for variations of properties with depth related with gravity forces and confinement that cause the increase of properties' values with the increase of depth within soil layers as illustrated in Figure 2.1b).

In the following sections the several features and potentialities of the program will be exemplified and discussed.

### 3.2.1 Normal and Lognormal Distributions

As mentioned UC2DRF can generate random fields following normal and lognormal distributions. In Figure 3.1 two fields were generated having the field size of $100\times100m^2$ with a single layer, 8 subdivision levels, a stationary average value of 100, standard deviation of 50, isotropic spatial correlation distances of $\theta_x=\theta_y=10$ and truncated between the values of 0 and 200. As can be observed Figure 3.1 (a) presents the result of a Gaussian statistical distribution and (b) the result of a lognormal distribution. In Figure 3.1(c) the theoretical curves (*T*) for both statistical distributions are plotted against the results obtained from UC2DRF (*RF*). It is possible to verify that the results obtained closely resemble the theoretical curves validating the implementation. An accumulation of values can be observed at the truncation limits resulting from the fact that the domain of both statistical distributions is infinite, therefore, theoretically, there is probability of occurrence of values that fall outside the acceptable range of the field. In such case the values obtained automatically take the value of the minimum and maximum

values allowed. It is worth noting that due to the mathematical formulation of the lognormal statistical distribution, for the same average, the value with higher frequency, that is the mode, tends to be smaller than in the case of a normal distribution.

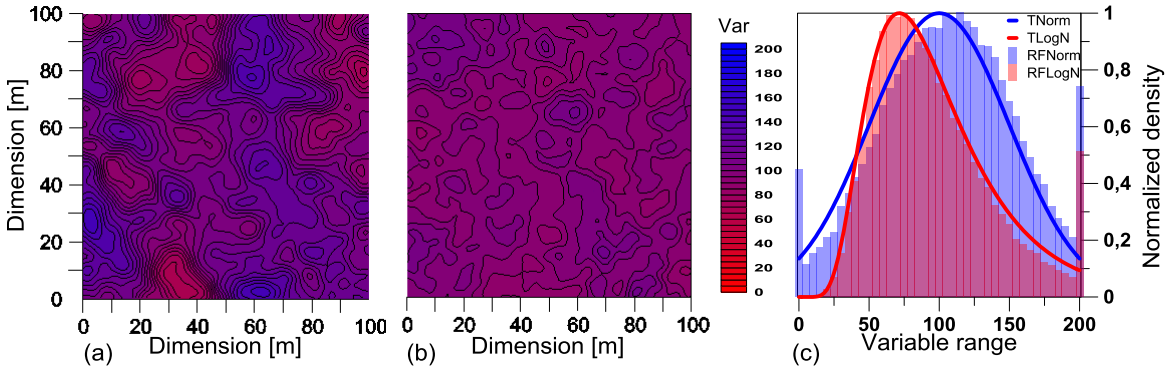


Figure 3.1 – Normal and lognormal distributions

### 3.2.2 Number of levels

The number of subdivisions performed directly affects the resolution of the field. In Figure 3.2 the discretization of the field with 3 (a), 6 (b) and 9 (c) levels of subdivision is presented. As can be observed the increase of the number of subdivisions results in a higher resolution of the field, though it may not be noticeable for high levels of subdivision due to the size of the plot, due to the increasing number of points with different properties generated. The amount of levels of subdivision must be appropriate for the problem at hand. In case of problems where fields with large dimensions are required it is advised to perform a high number of subdivisions (8 to 9 levels recommended) in order to achieve variability in every point of the field, whereas in a field with reduced dimensions that may not be required with the advantage of reducing the computation time needed.

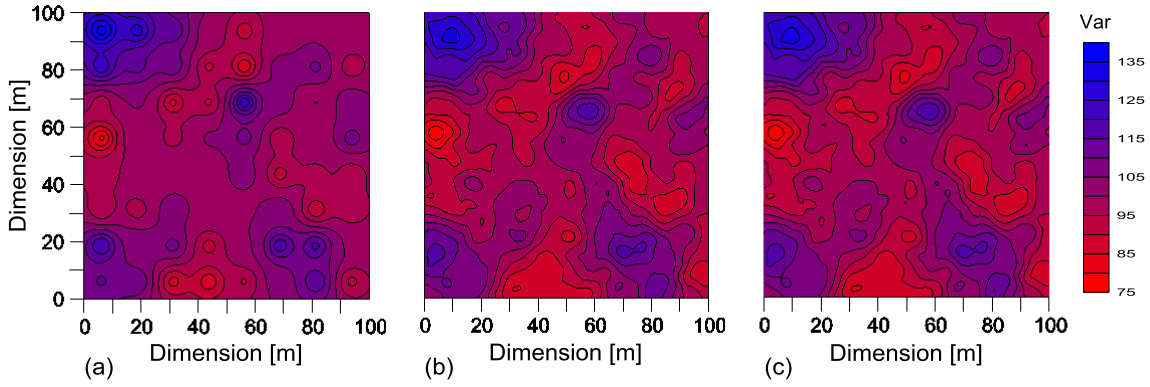


Figure 3.2 – Number of levels

### 3.2.3 Standard deviation

The increment of variability within the field can be shown as a direct result of increasing the value for the standard deviation of the model. In Figure 3.3 5 fields were generated for a field size of 100×100m$^2$ with a single layer, 8 subdivisions, a stationary average value of 100, isotropic spatial correlation distances of $\theta_x$=$\theta_y$=10 and truncated between the values of 0 and 200 with a Gaussian statistical distribution. The standard deviation assumed the values of 0 (a) resulting in a uniform field, 2 (b), 10 (c), 25 (d) and 50 (e). The resulting fields are plotted in Figure 3.3(a)-(e), respectively and, as expected, show that the increase of the standard deviation corresponds to a proportional increase of variability in the field. In Figure 3.3(f) the theoretical normalized curves (*T*) for normal statistical distributions as well as the results obtained through the generation of the random fields (*RF*) for the corresponding standard deviation values of 0, 10 and 50 are displayed. The comparison reveals a good agreement between the theoretical curves and the results of the field for all standard deviation tested. Naturally, for a standard deviation of 0 all the points are concentrated in the average value of 100.

Similar conclusions can be asserted for the lognormal distribution. In Figure 3.4 are plotted the results obtained from the random field generation with lognormal statistical distribution in the same conditions as before. Similarly, as in the Gauss distribution case, is possible to observe that an increase in the value of the standard deviation increases the variability within the field, however, for small standard deviations that difference is not as evident as in the fields generated using a Gauss distribution, given the formulation of the lognormal distribution. In spite of that in Figure 3.4(f), by superimposing the theoretical curves (*T*) corresponding to a lognormal distribution with standard deviations of 10 and 50 with the correspondent results obtained through the software (*RF*), it is possible to confirm that the range of values obtained depends of the standard deviation value initially imposed.

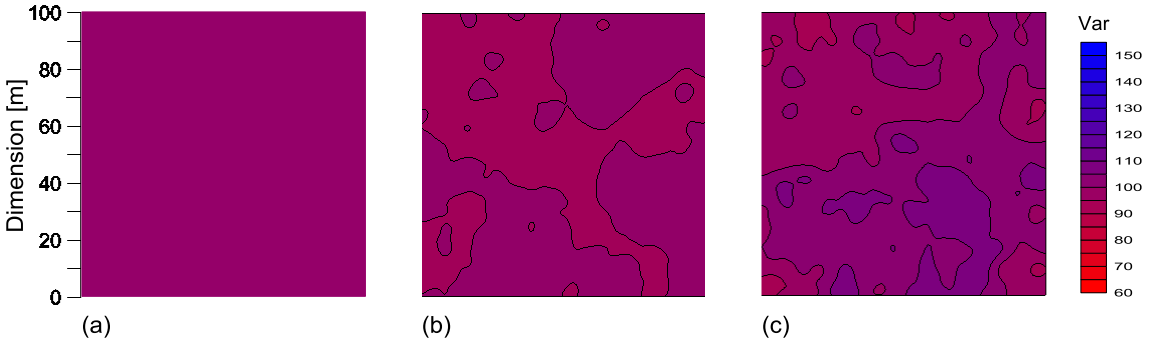

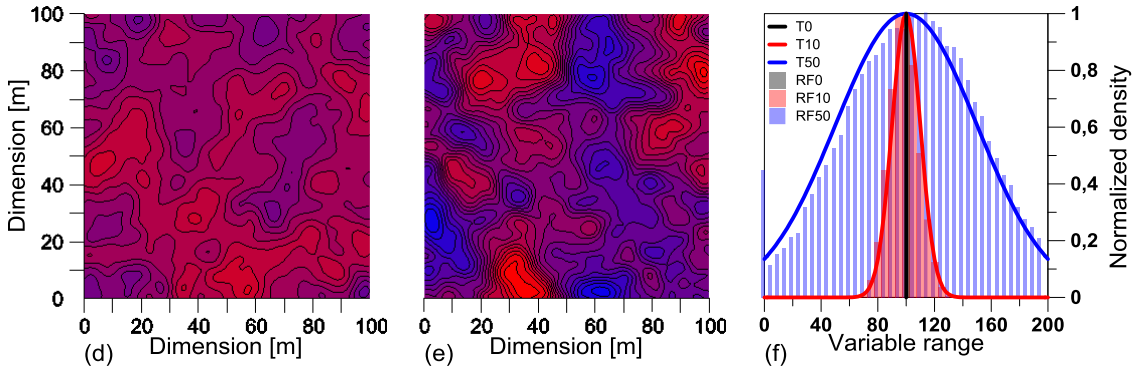


Figure 3.3 – Effect of standard deviation on normal distribution

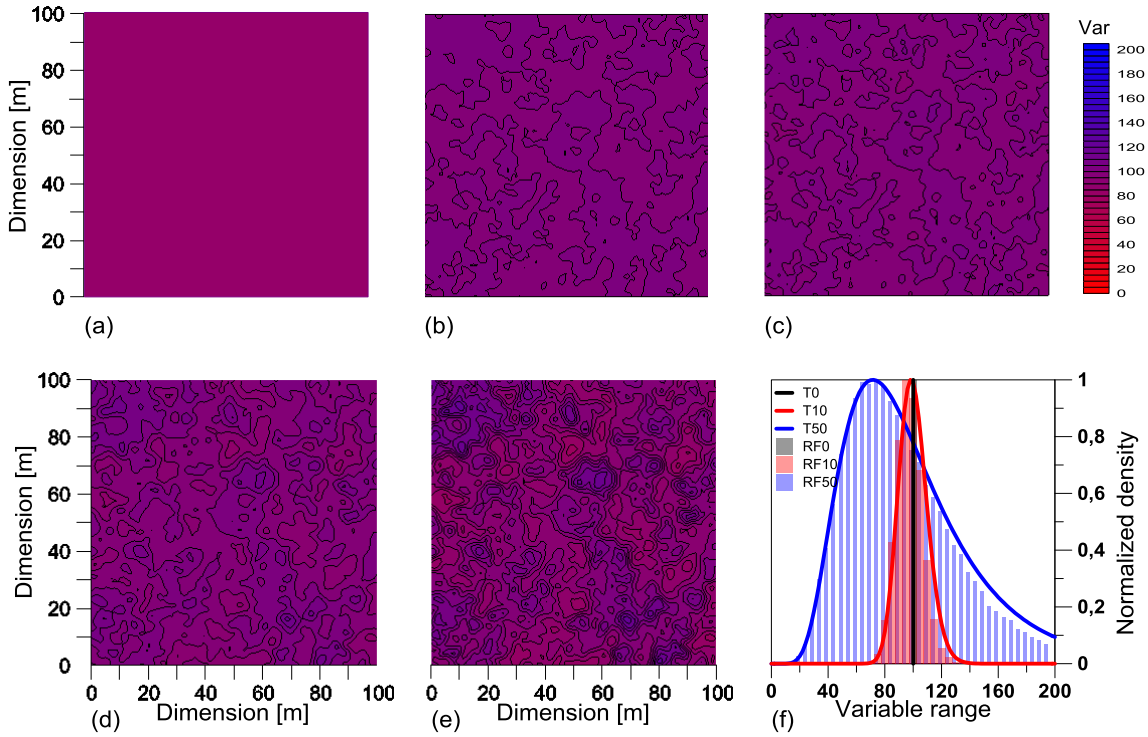


Figure 3.4 – Effect of standard deviation on lognormal distribution

### 3.2.4 Truncation

The limits for truncation are usually set as the lower and upper limits the variable within the field is desired to present in the field's final resolution. As mentioned this aspect is relevant when studying properties that are strictly positive or have upper limits such as the friction angle. However, they must be carefully chosen taking into account the average and the standard deviation of the field so that the values obtained for the property still follow the desired statistical distribution. If the truncation limits are not large enough the variable may have a uniform distribution with emphasis on the boundaries that will be more pronounced when the difference between the mean value and the truncation limits tends to zero. The effect of the

truncation applied to the field is shown in Figure 3.5 for 3 situations: (a) lower truncation at 80, (b) upper truncation at 120 and (c) both lower (80) and upper (120) truncation. In Figure 3.5(d)-(e) are the respective normalized probability density functions as well as the results obtained for each field. As expected the plots of the distribution show clearly the effect of the truncation performed with concentrated peak values in the limit values imposed. The effect on the fields is more difficult to visualise although some variations in the colour pattern can be observed.

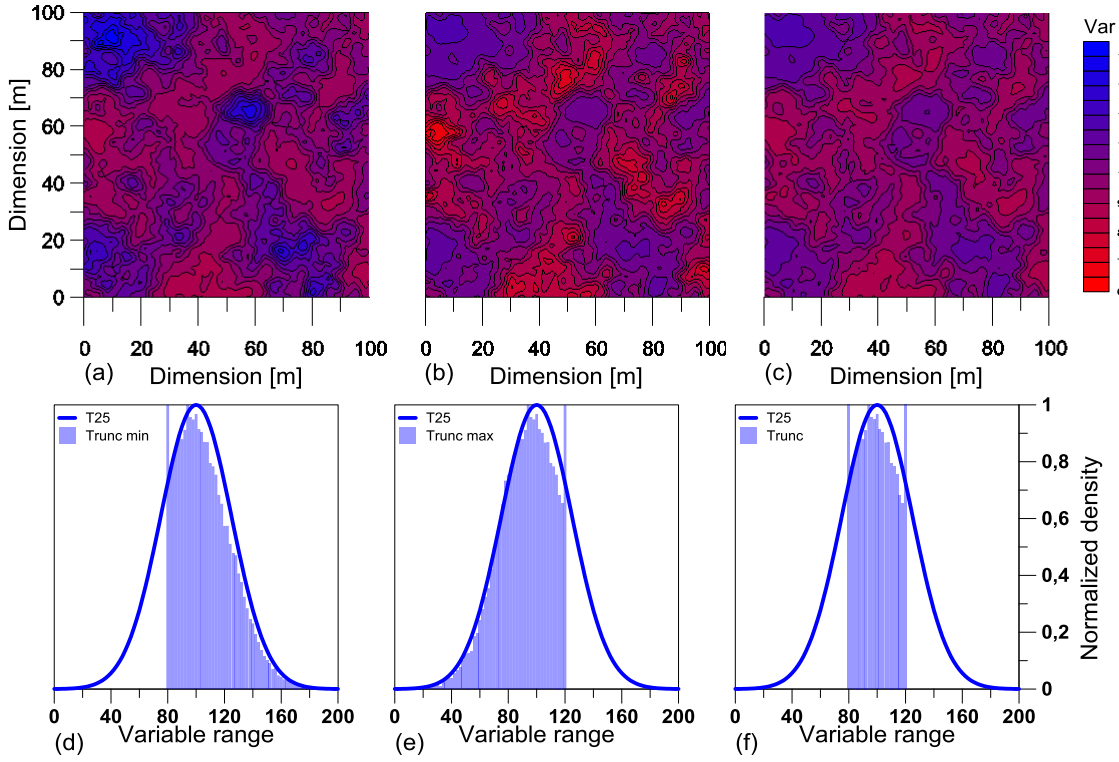


Figure 3.5 – Effect of truncation

### 3.2.5 Spatial correlation and anisotropy

In order to evaluate the influence of the spatial correlation distance 3 random fields with dimensions of 100×100m$^2$ were generated following a Gauss statistical distribution with mean value of 100 and standard deviation of 25 truncated between the values of 0 and 200. The isotropic spatial correlation distances used in the fields were $\theta_x$=$\theta_y$=10 (a), 50 (b) and 100 (c). Figure 3.6 displays the generated fields for the 3 cases. The results show that variability decreases when the spatial correlation distance increases. These results are in agreement with the theoretical premises of the method, which state that when the spatial correlation distance assumes an infinite value a uniform field is generated and when it assumes a null value every point in the field assumes different uncorrelated values for the property for which the simulation is intended.

The influence of anisotropy was evaluated by generating three random fields in identical conditions but having an anisotropic correlation. For this case the value of $\theta_x$ was maintained equal to 10 and the value of $\theta_y$ was varied. Values of $\theta_y$=10 (a) (isotropic), 20 (b) and 100 (c) were tested. In Figure 3.7 are displayed the fields generated with UC2DRF and is possible to verify a decrease on variability in the direction where the spatial correlation distance was increased. For a ratio ($\theta_x/\theta_y$) of 10 the field appears to be layered in the vertical direction. This feature is extremely useful to simulate conditions where directional anisotropy is expected to exist, such as in sediment deposition and rock foliation.

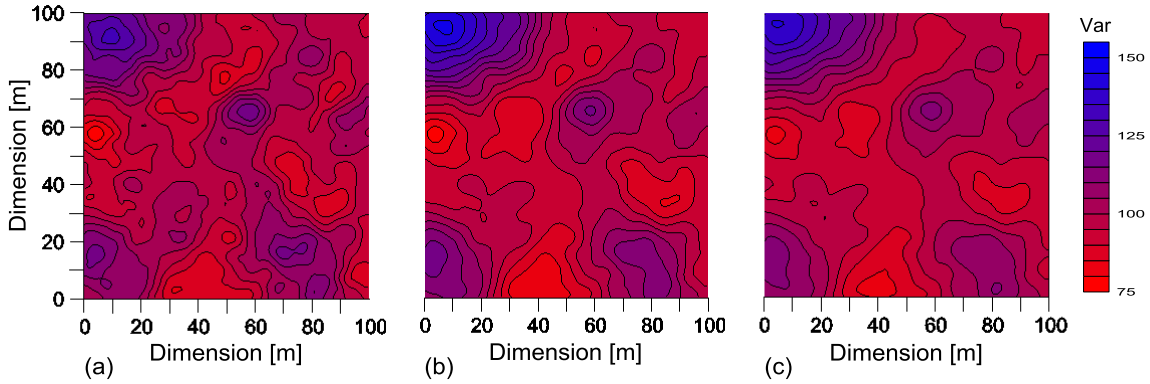


Figure 3.6 – Isotropic spatial correlation

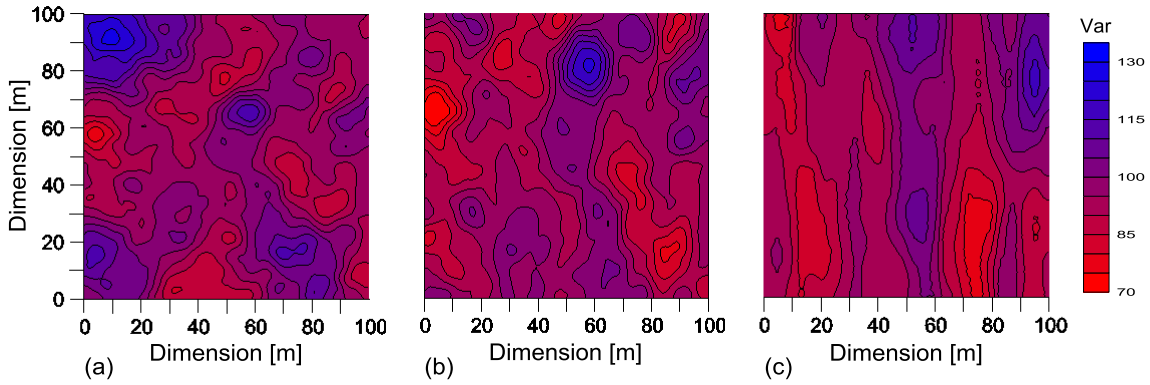


Figure 3.7 – Anisotropic spatial correlation

### 3.2.6 Anisotropy direction

By varying the angle between the directions of the field and the horizontal and vertical cartesian axis is possible to introduce anisotropy directions in the field. In order to demonstrate this possibility 3 random fields with dimensions of 100×100m$^2$ were generated following a Gauss statistical distribution with mean value of 100 and standard deviation of 25 truncated between the values of 0 and 200. In all cases an anisotropy ratio of 5 ($\theta_y$=10; $\theta_y$=50) was imposed. The anisotropy directions tested where: (a) the axis of the field are parallel to the horizontal and vertical cartesian axis; (b) an angle of 45º and; (c) an angle of -45º. Figure 3.8 shows the results

obtained for the 3 fields where a noticeable rotation in the axis of the field can be visualised. This feature, in combination with anisotropic spatial correlation distances, can simulate conditions similar to those resulting from tectonic actions and stress conditioning.

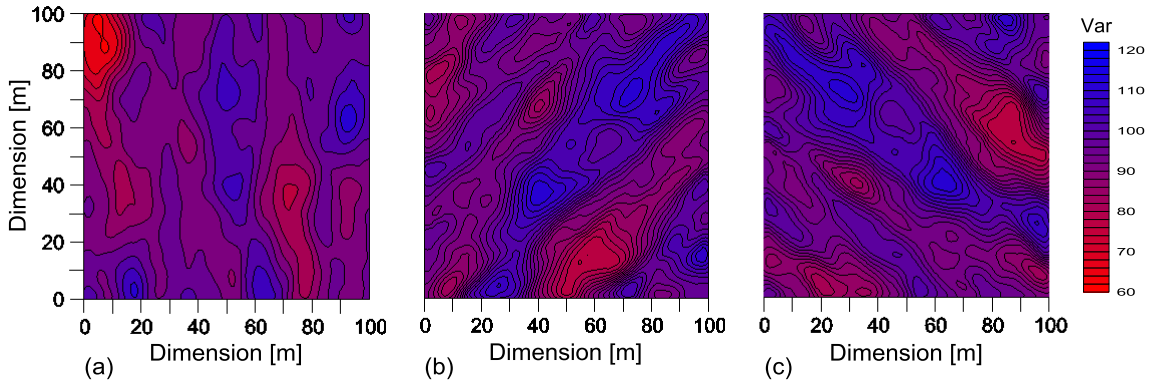


Figure 3.8 – Anisotropy direction

### 3.2.7 Multi-layering

As mentioned previously in its current version the UC2DRF program is able to create a multitude of layers with independent characteristics. As an example in Figure 3.9 are presented random fields with (a) one layer; (b) two layers and (c) four layers having different statistical distributions. This option, combined with other features, is ideal for simulate the results from in-situ tests such as *SPT* and *CPTu*, since allows the generation of fields that express directly the output of the tests performed making them more realistic.

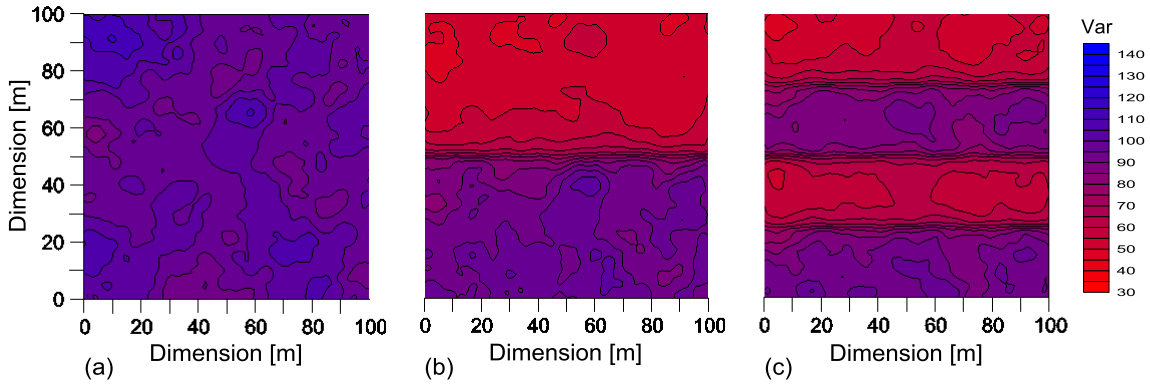


Figure 3.9 – Multi-layering

### 3.2.8 Average increment with depth

A non-stationary average process is attained by adding an increment depending on depth to the values obtained from the stationary process of the *LAS* method. This allows for the generation of random fields that can account for the presence of gravity forces that result in increments both in pressure and confinement. In Figure 3.10 the effect of the average increment in the

generation of two random fields is shown. In (a) a random field of 100x100m$^2$ was generated with a Gaussian statistical distribution having values of mean, standard deviation and isotropic correlation distance of 100, 10 and 10, respectively, whilst in (b) a field with identical conditions was generated with the only difference of having an average increment per metre depth of 0.5. The differences can be observed in (c) where the resulting values as well as the average value and the increment at $x$=1m are plotted for both the stationary and non-stationary processes. This process can be applied to any given number of layers. In Figure 3.10 (d) the generation a random field with 2 layers having different statistical distributions as well as characteristics is presented and in (e) the generation of the same field but with an average increment with depth per metre of 1 and 0.5 for the first and second layers, respectively, is shown. The impact of the average increment in both layers can be asserted through the observation of (f) where the resulting values on a random $x$ coordinate are plotted for both cases as well as the averages and theoretical increments for both layers. The results obtained in both cases highlight the differences when considering an increment of the average value with depth and validate the non-stationary average process implemented in UC2DRF.

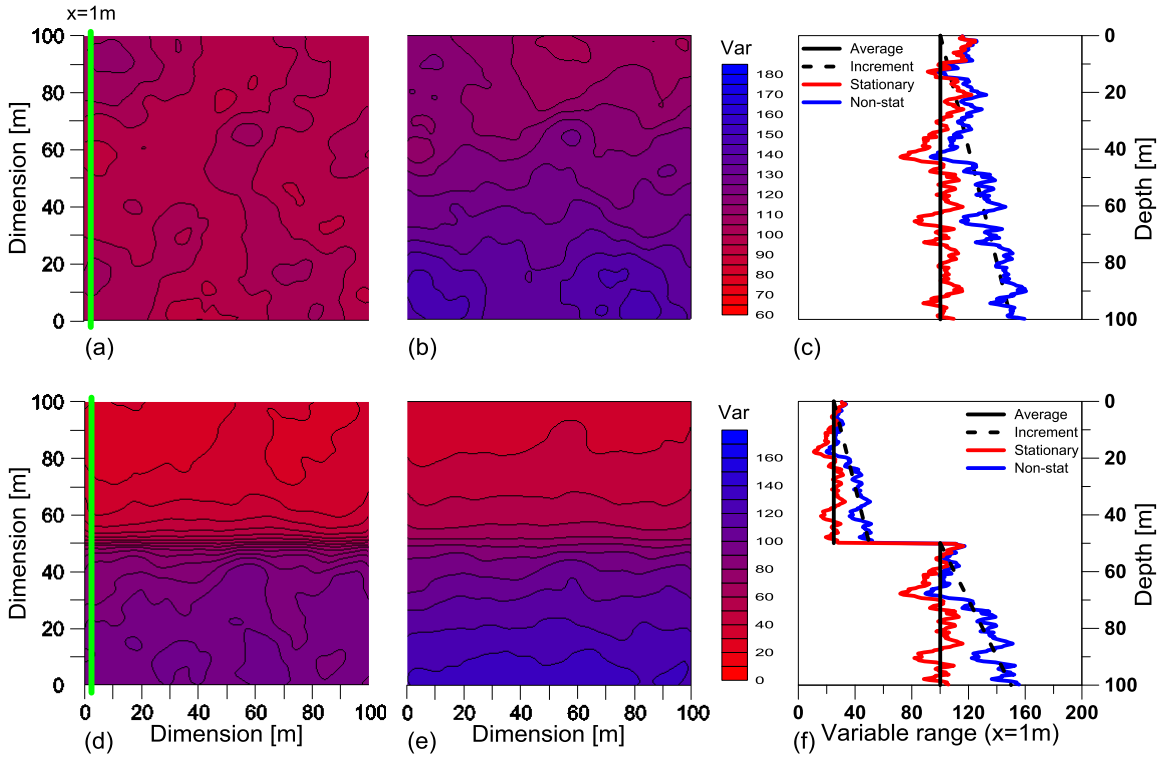


Figure 3.10 – Average increment with depth

### 3.2.9 Extreme cases

By combining several options available within the software it is possible to generate extreme cases for situations that occur in nature. In Figure 3.11 are presented examples of random fields

displaying those characteristics generated through the software. In (a) spatial correlations distances $\theta_x$ and $\theta_y$ of 100 and 10, respectively, were used resulting in layers having horizontal direction, simulating sedimentary deposits of soils. In (b) values of $\theta_x$=10 and $\theta_y$=100 were used resulting in a random field with predominantly vertical orientation, which can simulate the vertical faults of rock massifs. Finally, in (c) is shown a case where the properties of the soil have singular random points with either lower or higher resistance. This is achieved by having anisotropic correlation distances ($\theta_x/\theta_y$=10) as well as having a very small correlation distance in one of the directions relatively to the field size ($\theta_y$=1m). With this type of field is possible to simulate boulders in soil and weathered rocks massifs.

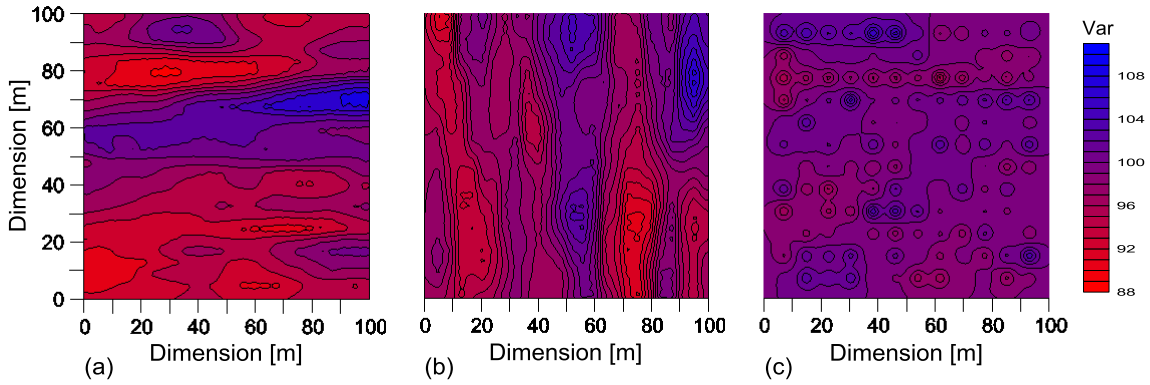


Figure 3.11 – Extreme cases

### 3.2.10 Real Cases

The software can and should be used to recreate and model the parameters of a given region based on reliable data collected in the field and tested in the laboratory. In Figure 3.12 an example is presented from data gathered through a *CPTu* test. Having as reference the tip resistance, $q_c$, measured during the test it was fitted based on a trial-and-error approach, where rough estimates were used, a layering and a set of statistical distributions that could reproduce as accurately as possible the real results. The division, average, standard deviation and spatial correlation distance were estimated and fitted based on the *CPTu* data. In total the deposit was divided into 7 different layers and for each of them a Gaussian distribution was selected with average values of 1, 25, 1, 3.5, 1, 3 and 7.5 MPa and standard deviations of 1, 7.5, 0.3, 3.5, 0.7, 1 and 3 MPa (from the surface to the maximum depth). It must be noted that in the case presented it was assumed anisotropy in the depositional plane and consequently a ratio of 10 ($\theta_x/\theta_y$) was chosen. However, these assumptions were solely based from a single *CPTu* test which in practice may not be advised since the deposit may not present a horizontal stratification. In Figure 3.12 (b) and (c) the results of the *CPTu* are plotted against the output of UCRF2D in two $x$ coordinates ($x$=1m; $x$= 19m). The agreement between the random field and the *CPTu* result is very good and prove that the code developed can be employed to simulate real cases of variability.

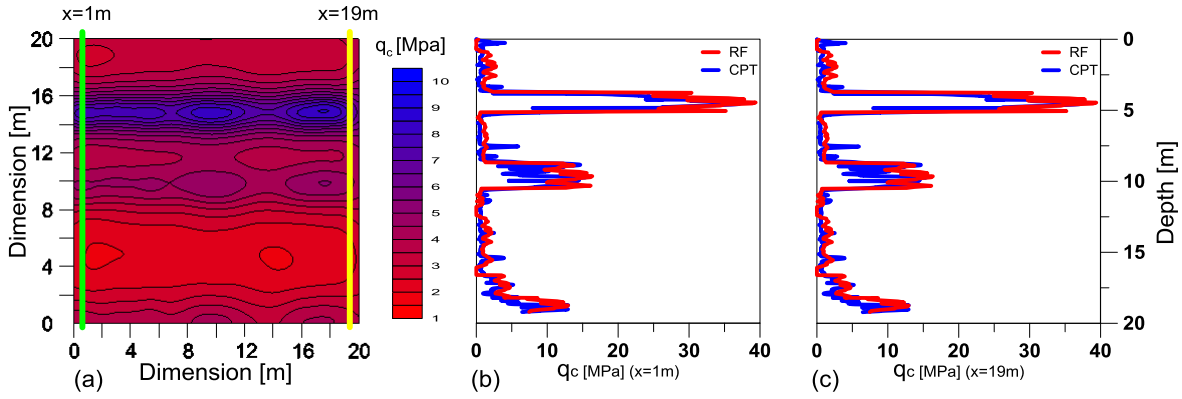


Figure 3.12 – CPTu modelling

The parameters used to generate a random field can be, at first, based on an observational analyses of the area that is meant to be studied. In Figure 3.13 3 real cases of rock masses presented by Zhang (2013) are displayed. The first case (a) is a granite with an isotropic structure; (b) represents a rock mass with foliation and; (c) shows also a rock mass with rotated foliation. In an attempt to enhance the applications of the program 3 random fields were generated with the purpose of trying to visually reproduce the distributions observed in the 3 mentioned cases.

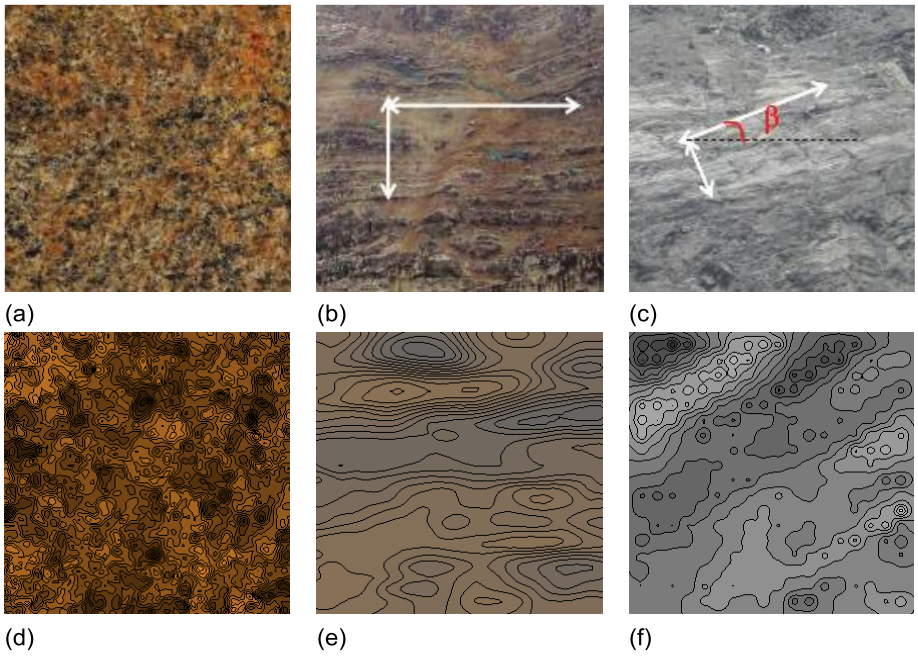


Figure 3.13 – Real cases, visual representation

The adjustment achieved after a couple of trial-and-error attempts, where only the average and standard deviation of the $q_c$ value were iterated, is illustrated in Figure 3.13 (d), (e) and (f), respectively, and can be considered very satisfactory in all 3 cases. However, it must be stated

that the generated random fields only represent approximations of the observable characteristics and that the variable fitted does not correspond to any property in particular but a set of characteristics that allow for the visual representation.

## 3.3 Analytical and Theoretical Correlations for Soils and Rocks

The random variables generated by UC2DRF do not always represent a direct property or a parameter of a constitutive law since random fields can be used to simulate field tests (*CPT*, *SPT*). Therefore there is a need for transform the output of UC2DRF into a property that a finite element program can use. With that purpose the program MAT.PROP was developed during the period of this research. This program serves as an intermediate between UCRF2D and UCGeoCode, the finite element software that was used in this work and that will later be explained. It allows for the integration of random fields in the finite element calculations making it possible to run numerical models that include variability in rock and soil properties.

MAT.PROP starts by reading the input file of UCGeoCode so that it can determine the coordinates of the Gauss points of the finite element mesh. Afterwards, having as reference the random field coordinates and output values it defines through interpolation the value that the variable should assume in each Gauss point of the finite element mesh, assuring that there is compatibility between the random field and the finite element mesh used in the analyses. This process is highly dependent on the resolution of the random field as well as the number of elements in the finite elements mesh. After interpolation, the variable that is calculated for each Gauss point can be modified by selecting a pre-defined correlation. In the current version of the program there are implemented several empirical correlations that allow the conversion of one or a multitude of properties defined solely based on the input variable. As output the software writes a file containing for each Gauss point of the finite element mesh the soil properties in a format that can be directly read by UCGeoCode. The software also allows for the processing of multiple random fields conditioned to a single finite element mesh providing individual output files for each random field and queue file useful for UCGeoCode automation.

As mentioned previously it is very important that the resolution of the finite element mesh be coherent with the discretization of the field. Figure 3.14 presents the results of a study where that problem is highlighted. In (a), (b) and (c) three random fields generated with UC2DRF with 3, 5 and 7 subdivision levels are presented. Subsequently, the program MAT.PROP was used to interpolate the three random fields for three different meshes that had a discretization of 16, 256 and 4096 elements. In (d), (e) and (f) the interpolation performed between the mesh with 16 elements and each random field is shown; in (g), (h) and (i) the interpolation that was made for the mesh with 64 elements is presented; while in (j), (k) and (l) the interpolation between the mesh with 4096 elements and the three reference random fields is displayed.

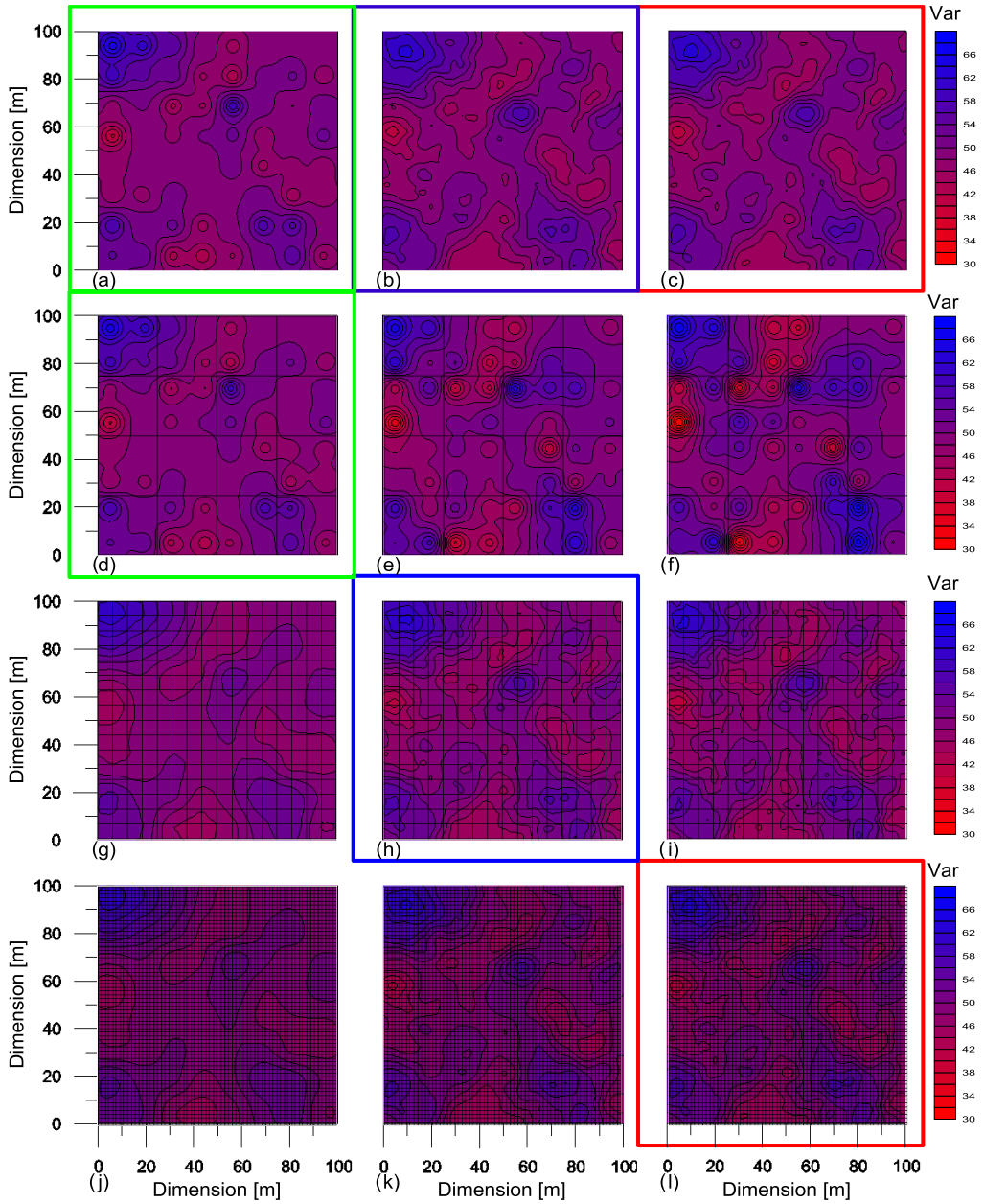


Figure 3.14 – MAT.PROP interpolation

It should be noted that each finite element is quadrangular and has 4 Gauss points. The number of elements used in each mesh was defined so that it could be directly related with the three reference random fields generated. As a result the mesh with 16 elements had the same number of Guass points as the field generated with 3 levels of subdivision. The mesh of 256 elements corresponds to the field with 5 levels of subdivision and finally the mesh with 4096 elements matches the field generated with 7 levels of subdivision. These 3 pairs are highlighted in Figure 3.14 and correspond to the (a) – (d) in green, (b) – (h) in blue and (c) – (l) in red. As expected for these 3 pairs the interpolation performed is almost exact since the number of points in field

and mesh are equal. A different scenario is observed in the extreme cases. When fields with high number of subdivision (c) are interpolated to a poor mesh (16 elements), (e) and (f), the results reveal great discrepancies with the gauss points of the mesh being excessively highlighted making the distribution of properties uneven and centred in their location. In the opposite scenario is possible to observe that fields with low subdivision levels (a) when interpolated for highly refined meshes, (g) and (j), lose resolution and originate much smoother contours. As a conclusion the ideal is to have some degree of compatibility between random field subdivision and mesh discretization in order to avoid smoothing and accentuated contours.

The available correlations were taken from the available literature and represent empirical approximations that may not apply to the reality of every situation and whose validation is required in every application performed.

### 3.3.1 Available parameters

MAT.PROP allows the user to set the variable of the random field to a corresponding soil or rock parameter associated with a constitutive numerical model implemented in UCGeoCode. The parameters currently available are presented in Table 1. When this option is selected the material property assumes directly the random variable value while all the other parameters of the constitutive model selected remain constant.

Table 1 – Available parameters in MAT.PROP

| UCGeoCode constitutive model | Soil parameter | Units |
|---|---|---|
| Mohr-Coulomb | Angle of shear resistance | º |
| Mohr-Coulomb | Cohesion | kPa |
| All models | Deformability Modulus | kPa |
| Tresca | Undrained strength | kPa |
| Tresca | Undrained deformability modulus | kPa |
| Hoek-Brown / Simplified Hoek-Brown | Compression strength | kPa |
| Cam-Clay / Simplified Cam-Clay | Inclination of the virgin compression line | - |
| Cam-Clay / Simplified Cam-Clay | Inclination of the swelling line | - |
| Cam-Clay / Simplified Cam-Clay | Gradient of the critical state line | - |

### 3.3.2 Available correlations

Through UC2DRF only a random field of a single variable can be obtained. In this stage of development of the program only one variable is independent and consequently in order to introduce variability in more than one parameter a correlation with the input variable must be used. The application of correlations in order to derive soil and rock parameters is very common in geotechnics due to the difficult in characterise the soils and rocks appropriately. Most of them are found through experimentation and have a regional validity, although in most cases

their range of application is generalised. A list of several correlations have been compiled by several authors such as Kulhawy & Mayne (1990) and Ameratunga et al. (2015). In the current version of MAT.PROP the following correlations are implemented:

(1) Geological Strength Index (*GSI*)

This option is available for Hoek-Brown and Simplified Hoek-Brown failure criteria. Besides the field variable (*GSI*) this correlation requires the input of the constant of the intact rock $m_i$, the deformation modulus of the intact rock $\sigma_{ci}$ and the disturbance factor *D*. The *GSI* correlation proposed by Hoek et al. (2002) and Hoek & Diederichs (2006) affects several parameters (Equations 5, 6, 7 and 8) making them variable although related with the *GSI*.

$$m_b = m_i \cdot exp\left(\frac{GSI - 100}{28 - 14D}\right) \quad (5)$$

$$s = exp\left(\frac{GSI - 100}{9 - 3D}\right) \quad (6)$$

$$a = \frac{1}{2} + \frac{1}{6} \cdot \left(e^{GSI/15} - e^{20/3}\right);\ a = 0.5\ if\ Simplified\ Hoek\ Brown\ is\ selected \quad (7)$$

$$E_m = E_i \cdot \left(0.02 + \frac{1 - D/2}{1 + e^{\left(\frac{60+15D-GSI}{11}\right)}}\right) \quad (8)$$

(2) Undrained Shear Strength ($S_u$) (Duncan & Buchignani, 1976)

This correlation is an option available for Tresca failure criterion where the undrained shear strength, $S_u$, acts both as the input random variable and output parameter and the undrained deformability modulus, $E_u$, is also an output parameter. Duncan & Buchignani (1976) proposed the correlation presented in Figure 3.15a) where the overconsolidation ratio *OCR* and the plasticity index *PI* are also required as input. Through nonlinear multiple regressions it was possible to fit the data in the figure to Equations 9, and 10 which were implemented in the software.

$$\text{If } 0 \leq \text{PI} < 30\ (R^2 = 0.902) -\ E_u/S_u = 1494.360 - 930.255 \cdot log(OCR) - 19.186 \cdot PI \quad (9)$$

$$\text{If } 30 \leq \text{PI} \leq 50\ (R^2 = 0.919) -\ E_u/S_u = 970.276 - 403.796 \cdot log(OCR) - 11.359 \cdot PI \quad (10)$$

$$\text{If } 50 \leq \text{IP} < 100\ (R^2 = 0.917) -\ E_u/S_u = 421.763 - 213.082 \cdot log(OCR) - 2.320 \cdot PI \quad (11)$$

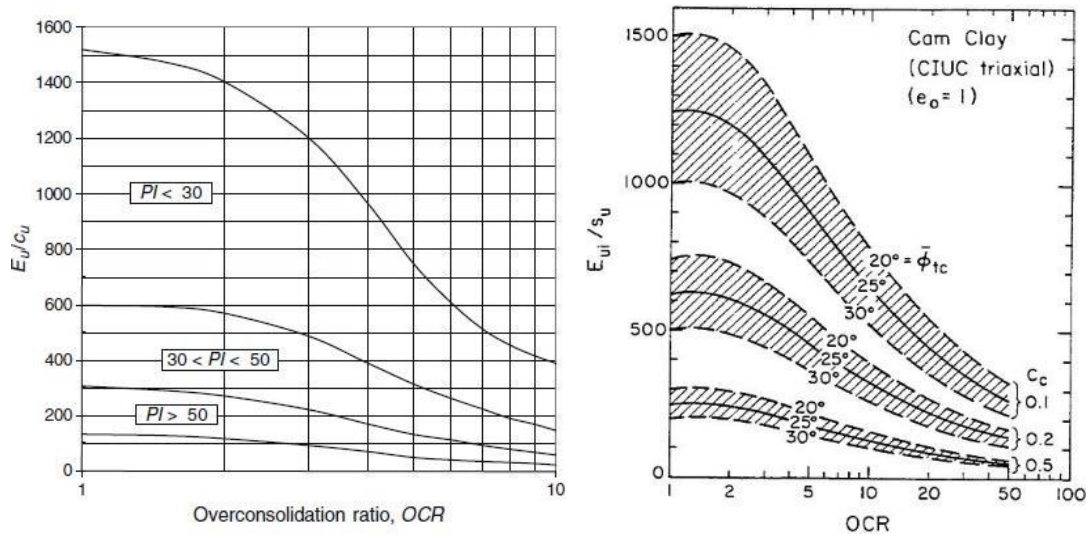


Figure 3.15 – Correlations proposed: a) Duncan & Buchignani (1976); Kulhawy & Mayne (1990)

(3) Undrained Shear Strength ($S_u$) (Kulhawy & Mayne, 1990)

This is also an option available for Tresca failure criterion where, in similarity with the previous correlation the $S_u$ is the random variable and one output parameter along with the $E_u$. Kulhawy & Mayne (1990) proposed the correlation presented in Figure 3.15b) where the angle of shear resistance in triaxial compression $\phi'_{tc}$, the compression index $C_c$ and the *OCR* are also required as input. In this case it was also used a nonlinear multiple regression in order to fit the data of the figure to Equations 12 and 13 which were then implemented in the software.

If $0.1 \leq C_C < 0.2$ ($R^2=0.942$):

$$E_u/S_u = 573.471 - 31.743 \cdot \phi_{tc} - 1550.215 \cdot log(C_C) - 637.383 \cdot log(OCR) \quad (12)$$

If $0.2 \leq CC \leq 0.5$ ($R^2=0.886$):

$$E_u/S_u = 447.376 - 10.444 \cdot \phi_{tc} - 587.033 \cdot log(C_C) - 237.455 \cdot log(OCR) \quad (13)$$

(4) N (SPT) for cohesive soils

This correlation is available for Tresca failure criterion. Besides the field variable *(N(SPT))* it requires the input of parameters *A*, *m* and *K*. Based on the number of blows of the *SPT* the general expressions 14 and 15 were implemented in the software for estimation of the undrained shear strength and of the undrained deformability modulus. In Table 2 are presented values suggested in the literature for the additional input parameters required by this correlation.

$$S_u = A \cdot N^m \quad (14)$$

$$E_u = K \cdot S_u \quad (15)$$

Table 2 - *SPT* recommended parameters for soils with cohesion

| Reference | *A* | *m* | *K* |
|---|---|---|---|
| Hara et al. (1974) | 29 | 0.72 | - |
| Kulhawy & Mayne (1990) | 6 | 1 | - |
| Bowles (1996) | | | |
| - Clay and silt (PI>30%) | - | - | 100 - 500 |
| - Silty or sandy clay (PI<30%) | - | - | 500 - 1500 |

(5) *N (SPT)* for cohesionless soils

This correlation is available for Mohr-Coulomb failure criterion. The field variable is either the number of blows, *N*, or the normalised number of blows for energy rate and atmospheric pressure, $N_1(60)$. Besides one of these parameters it requires the input of up to 5 additional parameters *A*, *B*, *m*, *K* and *M*. The general expressions implemented are presented in Equations 16, 17, 18 and 19 and are employed depending on the selection of the field variable, *N* or $N_1(60)$. The effective vertical pressure $\sigma'_{v0}$, required by some expressions, is automatically determined by the software based on the input file from UCGeoCode. The values suggested in the literature for the required additional parameters are presented in Table 3.

Normalised value *N1(60)*:

$$\phi' = (A \cdot N_1(60))^m + B \quad (16)$$

$$E' = K \cdot (N_1(60)) + M \quad (17)$$

Non-normalised value *N* (Kulhawy & Mayne, 1990):

$$\phi' = tan^{-1}\left[\frac{N}{12.2 + 20.3\left(\frac{\sigma'_{v0}}{100}\right)}\right]^{0.34} \quad (18)$$

$$E' = K \cdot \left(\sqrt{\frac{100}{\sigma'_{v0}}} \cdot N + M\right) \quad (19)$$

Table 3 - *SPT* recommended parameters for cohesionless soils

| Reference | *A* | *B* | *m* | *K* | *M* |
|---|---|---|---|---|---|
| Shioi & Fukui (1982) | 0.45 | 20 | 1 | - | - |
| Décourt (1989) | 362036.6 | 4.8 | 0.22 | - | - |
| Hanataka & Uchida (1996) | 20 | 20 | 0.5 | - | - |
| Webb (1970) | - | - | - | 479 | 15 |
| Bowles (1996) | | | | | |
| - Sand | - | - | - | 500 | 15 |
| - Saturated sand | - | - | - | 250 | 15 |
| - Gravelly sand | - | - | - | 1200 | 6 |
| - Clayey sand | - | - | - | 320 | 15 |
| - Silts, sandy silt | - | - | - | 300 | 6 |

(6) *CPT* tip resistance $q_c$ for cohesive soils

This correlation is available for Tresca failure criterion. Besides the field variable, $q_c$, it requires the input of parameters *N* and *K*. General expressions were implemented in the software, presented in Equations 20 and 21. Table 4 presents the values recommended in the literature for the afore mentioned parameters. As in previous expressions the value of the effective vertical pressure is automatically calculated and therefore not required as an input parameter.

$$S_u = \frac{q_c - \sigma'_{v0}}{N} \quad (20)$$

$$E_u = K \cdot S_u \quad (21)$$

Table 4 - *CPT* recommended parameters for soils with cohesion

| Reference | *N* | *K* |
|---|---|---|
| Bowles (1996) | 15±7 | - |
| Bowles (1996) | | |
| - Clay and silt (PI>30%) | - | 100 - 500 |
| - Silty or sandy clay (PI<30%) | - | 500 - 1500 |

(7) *CPT* tip resistance $q_c$ for cohesionless soils

This correlation is available for Mohr-Coulomb failure criterion. Besides the field parameter, $q_c$, it requires the input of parameters *A*, *B* and *K*. In order to calculate the angle of shear strength the user can choose between Robertson (2012) expression and a general expression containing the afore mentioned parameters. These expressions are presented in Equations 22, 23, 24 and 25 and Table 5 contains the values recommended in the literature for the additional parameters.

As is the case of previous expressions the effective vertical pressure, when required, is automatically calculated by the software.

$$\phi' = tan^{-1}\left[\frac{1}{2.68}\cdot\left(log\left(\frac{q_c}{\sigma'_{v0}}\right)+0.29\right]\right. \qquad Robertson, 2012 \qquad (22)$$

$$\phi' = A + B\cdot log\left(\frac{q_c}{\sigma'_{v0}}\right) \qquad \text{General expression} \qquad (23)$$

$$\phi' = A + B\cdot log\left(\frac{q_c}{1000}\right) \qquad \text{EC2: Part 2 (2007)} \qquad (24)$$

$$E' = K\cdot q_c \qquad (25)$$

Table 5 - *CPT* recommended parameters for cohesionless soils

| **Reference** | ***A*** | ***B*** | ***K*** |
|---|---|---|---|
| Mayne (2007) | 17.6 | 11 | - |
| Robertson & Campanella (1983) | 17.2 | 11.6 | - |
| Bowles (1996) | | | |
| - Sand | - | - | 2 – 4 |
| - Saturated sand | - | - | 3.5 – 7 |
| - Clayey sand | - | - | 3 – 6 |
| - Silts, sandy silt | - | - | 1 – 2 |

## 3.4 Finite Element Program

UCGeoCode is a Finite Element code designed specifically for soil calculation whose development at University of Coimbra started by Almeida e Sousa (1998). Written in FORTRAN language it was developed to perform 2D calculations and later being updated in order to perform 3D analyses. The software as suffered several updates along the years making it able to handle elasto-plastic calculations. The program as a wide range of constitutive models that make it suitable to simulate the behaviour of different types of materials. The implemented loading and boundaries conditions allow for the numerical modelling of the detailed construction sequence of almost all geotechnical structures. In the latest development the consolidation theory was implemented (Cruz, 2008) which provided an additional and useful feature to the already vast capabilities of the program. Since the program was already developed and only minor adjustments were performed in this research it will not be given in this dissertation a detailed description of how the program runs. More detailed information can be found in Almeida e Sousa (1998) and Cruz (2008). However, for facilitate the integration of

UCGeoCode with the remaining software employed is displayed in Figure 3.16 the representative flowchart of UCGeoCode structure.

It is just worth mention that in this dissertation the UCGeoCode code was adapted in order to be able to perform calculations considering variability on all materials. This was achieved by connection the output of MAT.PROP program to the input of UCGeoCode. Furthermore, it was developed the possibility of performing up to 999 calculations using the same finite element mesh but associated with up to 999 different random fields of one or multiple properties, as defined in MAT.PROP.

## 3.5 Interpretation of Results

Interpret is a software that was upgraded in order to process the output of up to 999 UCGeoCode sequential analysis. It automatically reads the output from each calculation and has the possibility of create a file with the desired results at any or every stage of the calculation for specific nodes (displacement) or Gauss points (stresses) of the finite element mesh used in the analysis. It is also able to create files containing stage results for each calculation that can be read by post-process program GID so that graphical analyses can be obtained if required (GID, 2012). It was also coded in the program the output of the envelopes of displacements and stresses of all the analysis processed.

Additionally, two more software's were developed in this research for the analyses of specific applications. Though these software's already existed, substantial alterations had to be performed so that they would be able to handle with up to 999 fields. Forces1RF and Forces2RF were developed for a single deep tunnel and twin superficial tunnels applications specific analyses. Both are capable of calculate the forces, hoop and bending moment, applied on the lining and the pressure around the contour of the excavation. The latter has also the possibility of output the displacements, vertical and horizontal, at ground surface and in the contour of the excavation of both tunnels.

Moreover, a form was developed for Microsoft Office Excel that automatically processes the data outputted either from Interpret, Forces1RF or Forces2RF dividing it into bins so that the distribution of values within every batch of calculations can be quickly analysed and visualised through an histogram. As default the number of bins is calculated from $N = \sqrt{n}$ being $N$ the number of bins and $n$ the number of observations which results in 32 bins if $n$=1000. However, it is possible to ignore the recommended number of bins and select the number desired. In that case the limits of each bin as well as average values, frequency and cumulative density are recalculated automatically and the output and histogram are adapted to the modifications.

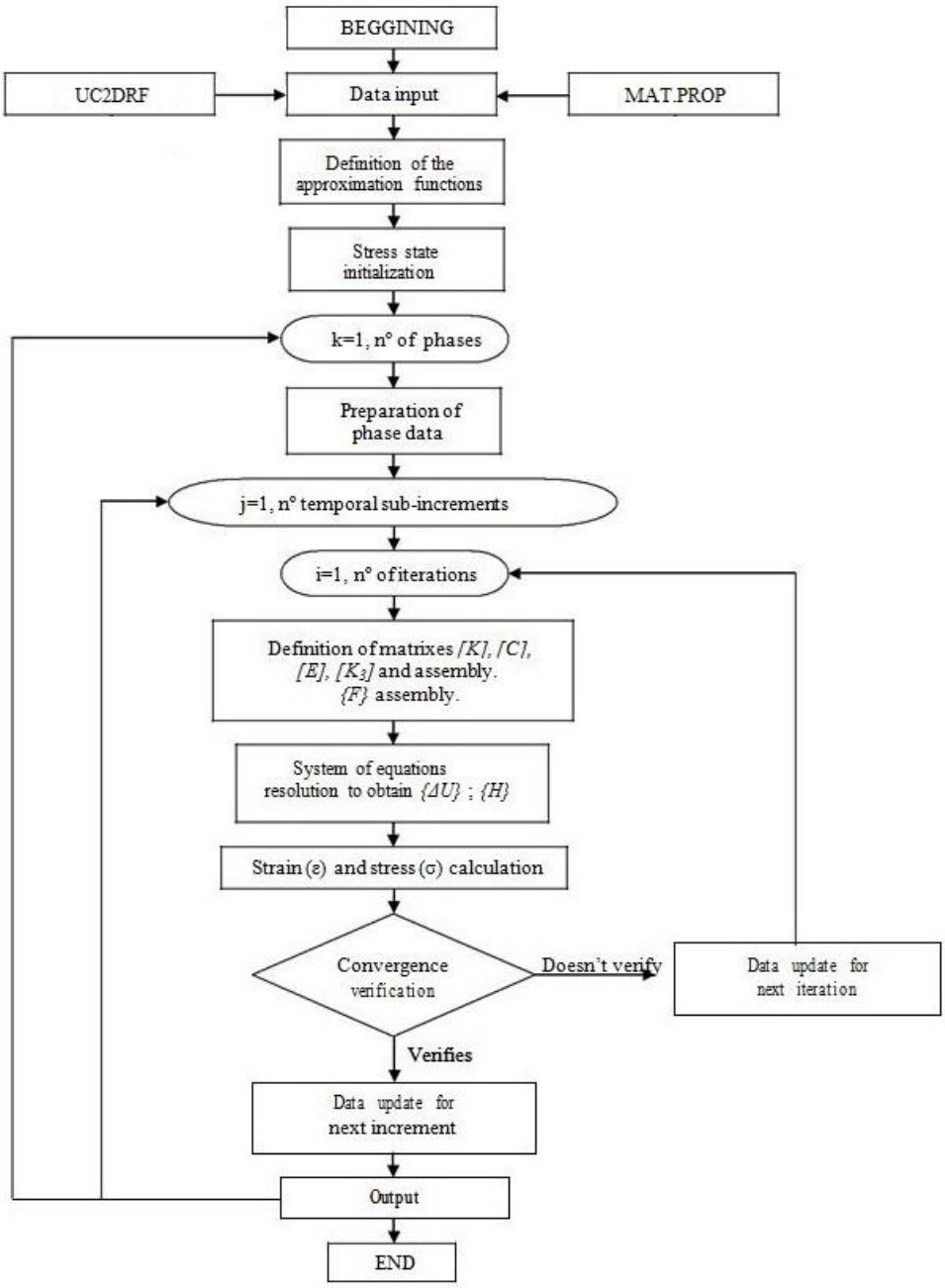


Figure 3.16 – Representative flowchart of UCGeoCode structure, adapted from Cruz (2008)

# 4 APLICATIONS

## 4.1 Introduction

So that the implication of introducing variability when modelling geotechnical structures could be verified in a tangible way, three applications are going to be analysed. These are purposely simple applications, common to the geotechnical engineering practice, so that the direct impact of the introduction of variability in the behaviour of each examined structure could be clearly assessed.

The first application aims to infer the impact of the statistical distribution chosen to describe the random variable. The type of distribution, normal or lognormal, and the impact of its standard deviation will be assessed through the study of the bearing capacity of a strip rigid footing loaded under undrained conditions. The obtained results will be compared with both the solution obtained through a deterministic analysis as well as the theoretical solution established by Prandtl (1920). In the second application the influence of other parameters that control the generation of the random fields and the effect of considering multiple variable parameters will be analysed through the study of two twin strip footings subjected to vertical loading. In order to highlight the importance of introducing variability the results will be compared to those obtained with the deterministic analysis, allowing the observation of multiple aspects that a simple deterministic analysis cannot capture and that can influence the design of such structures. Finally, the third application aims to evaluate the implications of the introduction of variability on a rock mass when studying a deep tunnel excavated under an isotropic stress state. Beside the analysis of the influence of the standard deviation of the input variable (*GSI*) and of the isotropic spatial correlation distance, particularl attention is given to the assessment of the degree and direction of anisotropy in the rock mass.

In all applications the following methodology was followed: generation of random fields with the desired parameters using UC2DRF; employment of constitutive models and interpolation for the finite element mesh of each application with MAT.PROP; calculation of all analysis using UCGeoCode; extraction of the desired results for interpretation using the several programs developed and presented in 3.5.

## 4.2 Strip Footing

### 4.2.1 General Considerations

The present analysis aims to quantify the influence of the type of statistical distribution selected and of the standard deviation used in the generation of the random fields. A simple case of a single strip footing with 2m width, *B*, placed on the soil ground surface was analysed. The soil was assumed to have an elasto-plastic behaviour with a Tresca yield surface where only undrained bearing is considered. The soil properties adopted in the deterministic analysis were: $S_u$=100kPa; $\upsilon$=0.49; $E$=100MPa and $\gamma$=20kN/m$^3$. The footing was considered to be rigid and the analyses were performed under displacement control meaning that uniform vertical displacements, d, were imposed at the entire base of the footing. The displacements applied were increased throughout 23 stages until a ratio of d/B=0.03 was reached. The 2D mesh (assuming plain strain conditions) considered in the analysis is shown in Figure 4.1 and comprises 634 quadrilateral elements with 8 nodal points and 4 Gauss points for tension control. It has dimensions of 40×10m, which were considered to be adequate given the dimension of the footing. In terms of boundary conditions, all displacements were restricted in the bottom boundary while no horizontal displacements were allowed along the vertical boundaries of the mesh.

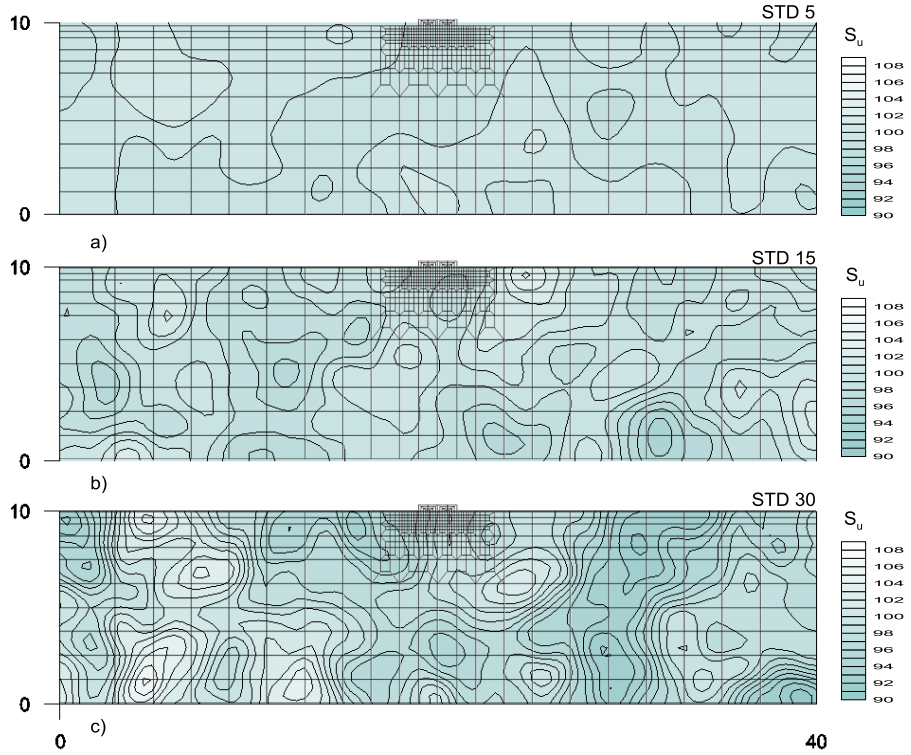


Figure 4.1 – Mesh used ($\theta_x$=$\theta_y$=2): (a) standard deviation of 5; (b) standard deviation of 15; (c) standard deviation of 30

The capacity of a vertically loaded shallow strip footing on undrained conditions can be expressed by Equation 26 were $Q_{max}$ is the maximum vertical load applied, $A$ is the area of the footing, $S_u$ the undrained strength of the soil and $N_c$ the bearing capacity factor (Potts et al., 2001). In the present study, considering a continuous footing, the area is equal to the foundation width, 2m, and the $S_u$ equal to 100kPa. The bearing capacity $N_c$, for the present conditions should theoretically be equal to 5.14 ($2+\pi$) (Prandtl, 1920) for both smooth and rigid footings though it is shown to vary with the smoothness of the footing as well as the interface considered between the soil and the footing (Potts et al., 2001). Based on these values the theoretical bearing capacity of the footing analysed in this case would be 1028kN.

$$Q_{max} = AS_uN_c \quad (26)$$

The introduction of the variability was considered assuming that $S_u$ is the variable parameter within the field and all the other soil properties remain constant throughout all analyses. In the generation of the variable fields the spatial correlation distances were kept isotropic and equal to 2m and the $S_u$ values below 0 and above 200 were truncated. A total of 2 cases were studied in this application and its analyses are summarised in Table 6. The first one aims to infer the impact that the type of statistical distribution of the input variable has on the maximum bearing capacity of the footing and the second one aims to establish the influence of the standard deviation of the input variable. The variability considered for the fields is well illustrated in Figure 4.1 where 3 of the multiple random fields used in the analyses with (a), (b) and (c) corresponding to fields with lognormal distributions having standard deviations of 5, 15 and 30, respectively, are shown. The simple visualization of the figure allows to understand the influence of this parameter in the soil parameters.

Table 6 – Single strip footing study cases

| **Case** | | ***STD*** | **Input distribution law** |
|---|---|---|---|
| 1 | Statistical distribution | 15 | Normal – Lognormal |
| 2 | Standard deviation (*STD*) | 5; 10; 15; 20; 30 | Lognormal |

Given the random nature of the fields running one single analysis is not enough to define the pattern of the behaviour. The introduction of variability implies that multiple calculations have to be performed in contrast with the deterministic case where only one analysis is required. Fenton & Griffiths (2008) recommend the minimum of 500 realizations for each variable parameter. In the present work 999 realizations were performed for every case in order to establish a reliable pattern. In Figure 4.2 the moving average results of the bearing capacity of

the footing determined for the last stage of all analysis is presented for a case having a standard deviation of 15 and a lognormal statistical distribution. From the figure is possible to observe that the number of realizations performed is sufficient to establish a trend. However, there is a slight difference of about 7% between the trend value and the theoretical bearing capacity which can be justified due to the plastification that occurs in the analyses where poor soil strength characteristics are found. These analyses translate in a much lower bearing capacity that cannot be compensated by the other analysis where better soil properties are found leading to the difference observed.

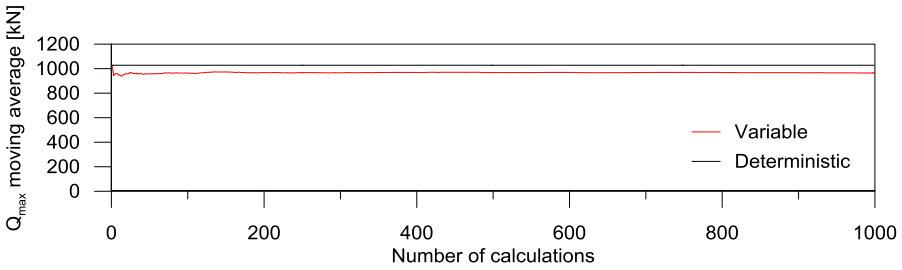


Figure 4.2 – $Q_{max}$ moving average

### 4.2.2 Case 1: Statistical distribution

In order to evaluate the influence of the type of distribution two cases were analysed. In the first a normal distribution was assumed for the $S_u$ while in the other a lognormal distribution was considered. For each case a total of 999 calculations were performed in order to establish a pattern as demonstrated previously. In both cases a standard deviation of 15 and an isotropic correlation distance of 2m were considered in the generation of the random fields.

In Figure 4.3 the minimum, average and maximum load-vertical displacement (normalised by the width of the footing) curves for a point located in the centre of the footing of all the analysis performed are presented in (a), (b) and (c), respectively. The minimum and maximum envelopes determined are a direct result of the chosen statistical distribution with the normal distribution displaying a wider range of values given its formulation. As expected, the difference between distributions is particularly larger for the minimum curves due to the tail of the normal distribution, while for the maximum a smaller discrepancy is observed. The average value of the load displacement curve appears to be independent of the statistical distribution chosen for the input variable and is a direct result of the standard deviation adopted. These results enhance the impact of introducing variability with differences of almost 50% in comparison with the deterministic curve and the theoretical value.

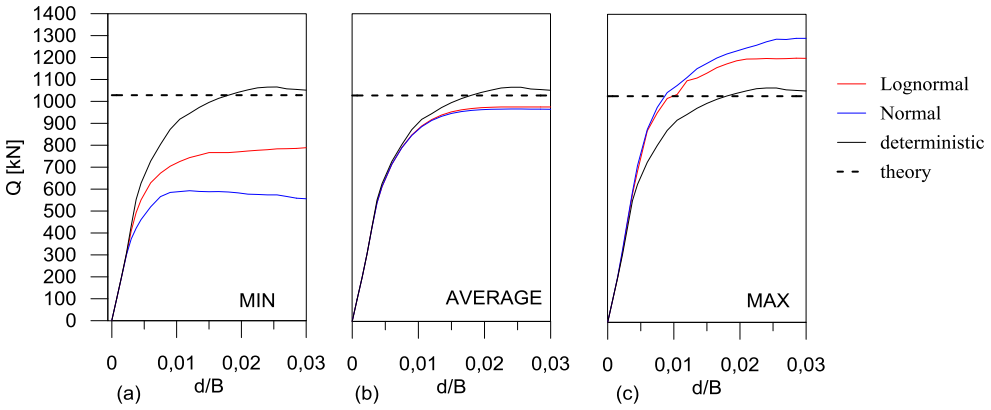


Figure 4.3 – Minimum, average and maximum load displacement curves effect of statistical distribution

The distribution of the bearing capacity values obtained in the 999 analysis for both statistical distributions are presented in Figure 4.4 for 4 different levels of imposed displacements. For the lowest displacement (a), d/B=0.0025, a concentration of values around the deterministic value is obtained and the results resemble a lognormal distribution regardless of the type of the input distribution, which is justified since for the level of displacements imposed the soil is mostly within elastic range. With the displacement increment the distribution of values changes its shape and became similar to a normal distribution, even for the lognormal input curve, which is justified due to the generalised increase of plastification in the soil. It is possible to verify that the range of values obtained increases in proportion with the imposed displacements with the wider range corresponding to a normal statistical distribution as input in all the stages, which is directly related to the tails of this distribution. It can also be noticed that with the increase of displacement the average bearing capacity value progressively became smaller than the deterministic result. As mentioned previously, this difference may be explained by the different levels of plastification of the soil. Based on the obtained results it is possible to conclude that the input distribution has some influence in the results, and particularly on the extreme cases when a normal distribution is employed. However, the output results are essentially dependent of the constitutive laws and tend to follow a normal distribution if plasticity occurs, regardless of the input distribution type.

The fitting parameters for a normal distribution of the resulting bearing capacities (*d/B=0.03*) are displayed in Table 7 for the last increment of displacement and show an overall good agreement for both input distributions, with the input lognormal distribution presenting the best adjustment (K-S provides the Kolmogorov-Smirnov goodness of the fit relative to zero, with negative values representing a deficit and positive a surplus). In the table are also presented the probabilities of the bearing capacity falling within certain ranges (having the theoretical value as reference). The probability results are higher in the lognormal input case and show that for an interval of ±5% only 21.6% of the bearing capacity values will occur. With the introduction of variability a variation of nearly ±20% was found in the bearing capacity highlighting its

impact and the benefits of its consideration in comparison with a traditional deterministic approach.

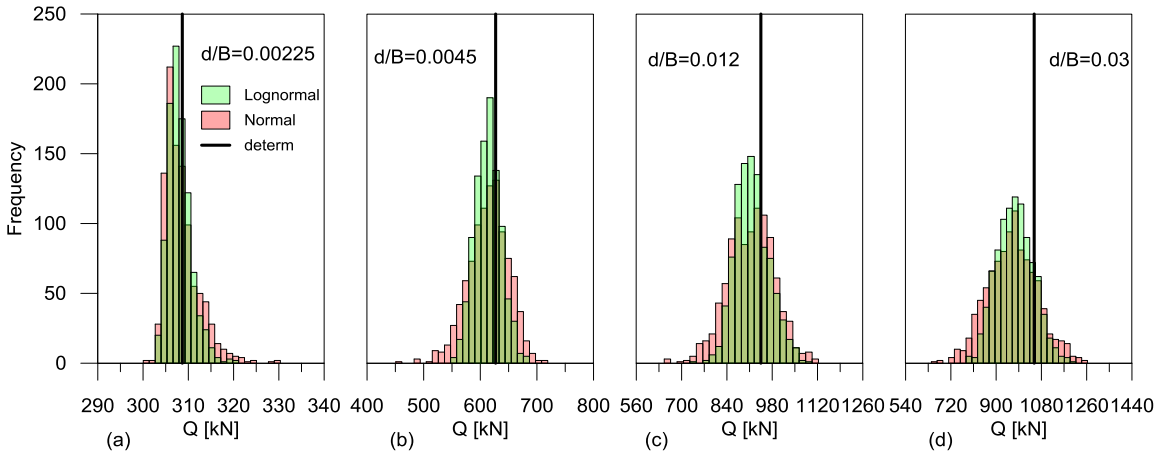


Figure 4.4 – Bearing capacity distribution – statistical distribution; (a) *d/B*=0.0025, (b) *d/B*=0.0045, (c) *d/B*=0.012, (d) *d/B*=0.03

Table 7 – Fitting parameters and probability of bearing capacity with statistical distribution of the input variable

| Input distribution | Fitting parameters of normal distribution | | | Probability of bearing capacity within interval | | |
|---|---|---|---|---|---|---|
| | μ (kN) | σ (kN) | K-S | 1028±5% | 1028±10% | 1028±20% |
| Normal | 965.4 | 98.3 | -1.94 | 17.0% | 33.3% | 82.4% |
| Lognormal | 975.2 | 71.9 | -0.34 | 21.6% | 41.9% | 98.3% |

### 4.2.3 Case 2: Standard deviation

For this analysis a lognormal statistical distribution was used for the value of the undrained strength of the soil since it is the one recommended in the literature as presented in 2.1.2. As expected the variation of the standard deviation of the input variable has a noticeable effect on the bearing capacity of the footing. In Figure 4.5 the minimum (a), average (b) and maximum (c) curves obtained for each standard deviation value considered are presented. As expected the increase of standard deviation will result in wider range of values, since more variability can be found in the field. This is particularly evident for the minimal envelope since smaller standard deviations imply poor strength characteristics of the soil, hence, more plastification and lower bearing capacity. On the upper bound the influence of the standard deviation is not so expressive since, regardless of the standard deviation, there is always plastification once a level of displacement is imposed. The average value of the load displacement curves can be shown as to be inversely proportional to the increment of the standard deviation value. This fact can be justified by two factors. As a result of the statistical distribution used, since the median value

of $S_u$ decreases with the increment of its standard deviation due to the non-symmetry of the lognormal distribution, and also due to the plastification of the soil as mentioned.

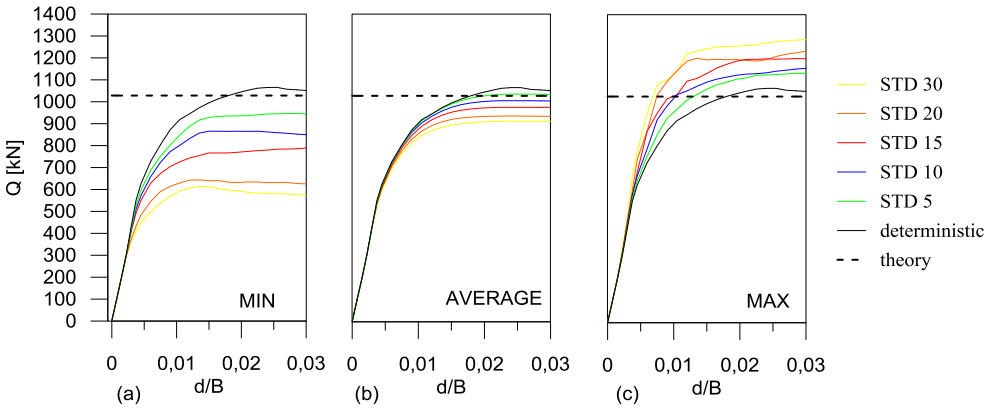


Figure 4.5 – Minimum, average and maximum load displacement curves effect of standard deviation

The distribution of the bearing capacity of the 999 analysis performed is presented in Figure 4.6 for 4 different levels of displacements imposed and for the standard deviations of 5, 15 and 30. Just like in the previous case studied the results show that for small levels of displacements imposed (a) a lognormal distribution is obtained. With the increase of displacements the results tend to follow a normal distribution. However, it is noticeable that for all displacements levels the distributions obtained are directly related with the standard deviation considered for the input variable. The increase of this parameters results in a wider range of values and on an average value of the bearing capacity that progressively decreases in comparison with the deterministic value. The results presented in Figure 4.7 and Table 8 are conclusive regarding the influence of the standard deviation of the input variable. In the figure are represented the average bearing capacity (a), the standard deviation (b) and the covariance (c) of the fitted normal distributions to the results of the last displacement level. In (a) a noticeable decrease of the average value of the bearing capacity is observable resulting from the formulation of the lognormal distribution and of the fact that the higher the standard deviation, the higher the probability of zones with lower resistance underneath the footing. The standard deviation of the bearing capacity (b) increases significantly with the increase of the standard deviation of $S_u$ resulting in a wider range of values for the bearing capacity. The combined effect of both parameters can be directly translated in the evolution of the covariance (c). This property tends to increase with the increment of the standard deviation and can be associated to a measurement of the increase of variability that is achieved with the increase of the standard deviation of the input variable.

The probability of the bearing capacity falling within certain ranges (having the theoretical value as reference) are presented in Table 8. As expected the results show that the increase of the standard deviation of the input variable translates into a considerable decrease of the

probability of occurrence. For the higher value of the standard deviation analysed only 10.7% of the bearing capacity values will occur within the ±5% interval while it is expected that more than 30% of the values fall outside the ±20% range.

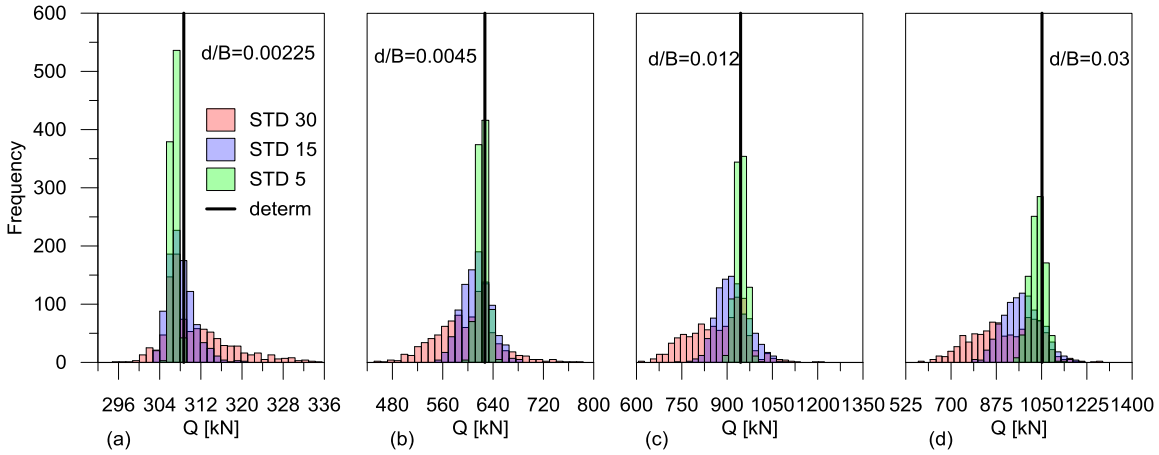


Figure 4.6 – Bearing capacity distribution - standard deviation; (a) *d/B*=0.0025, (b) *d/B*=0.0045, (c) *d/B*=0.012, (d) *d/B*=0.03

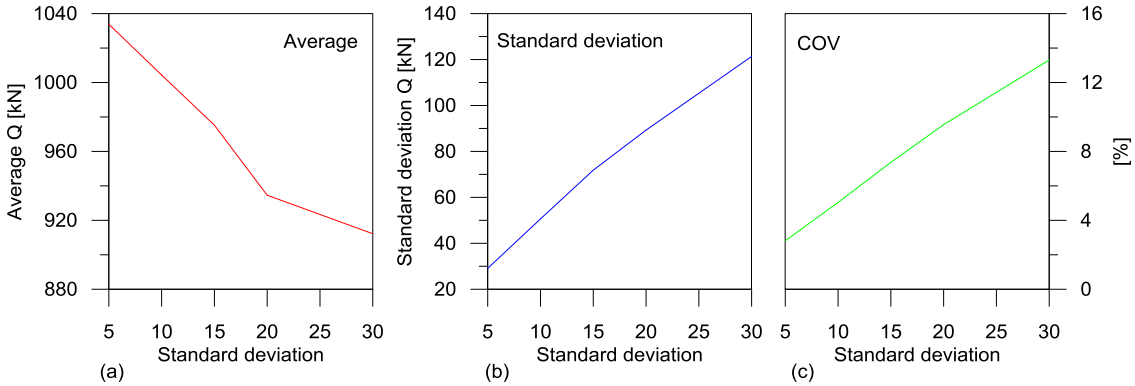


Figure 4.7 – Average, standard deviation and covariance variation with standard deviation of the input variable

Table 8 – Fitting parameters and probability of bearing capacity with standard deviation of the input variable

| **Standard Deviation** | **Fitting parameters of normal distribution** | | | **Probability of bearing capacity within interval** | | |
|---|---|---|---|---|---|---|
| | **μ (kN)** | **σ (kN)** | **K-S** | **1028±5%** | **1028±10%** | **1028±20%** |
| 5 | 1033.9 | 29.1 | -2.31 | 61.3% | 91.7% | 100.0% |
| 10 | 1004.3 | 50.7 | 0.02 | 35.2% | 63.6% | 100.0% |
| 15 | 975.2 | 71.9 | -0.34 | 21.6% | 41.9% | 98.3% |
| 20 | 934.6 | 89.3 | 0.00 | 13.2% | 26.7% | 89.4% |
| 30 | 912.2 | 121.3 | 4.97 | 10.7% | 21.4% | 69.6% |

## 4.3 Twin Strip Footings

### 4.3.1 General Considerations

A study on twin strip footings subject to simultaneous vertical loading was performed in order to evaluate the impact of the introduction of variability on risk analysis. The mesh considered, presented in Figure 4.8, is comprised of 798 quadrilateral elements with 8 nodal points and 4 Gauss points for tension control. Two equal sized strip footings having 1m width (B=1m) and distance between centres of 3m (3B) were placed at the upper middle point of the mesh. As in previous application, the single strip foundation, the soil beneath the footings was assumed to have an elasto-plastic behaviour with a Tresca yield surface where only undrained bearing was considered. The following properties were considered for the soil: average value of $S_u$=100kPa with truncation values set so that no truncation effects were expected (minimum equal to 0 and maximum equal to 200 kPa), $E_u$=100MPa, $\upsilon$=0.49 and $\gamma$=20kPa. Vertical distributed loads were applied simultaneously to both foundations along 23 stages until a value of 514kN (theoretical maximum bearing capacity for this problem according with Prandtl (1920)) was reached. For both footings vertical displacements were registered at the extremities and centre of the footing, which allowed for the calculation of the individual rotation of each footing and the relative rotation between the centres of the two.

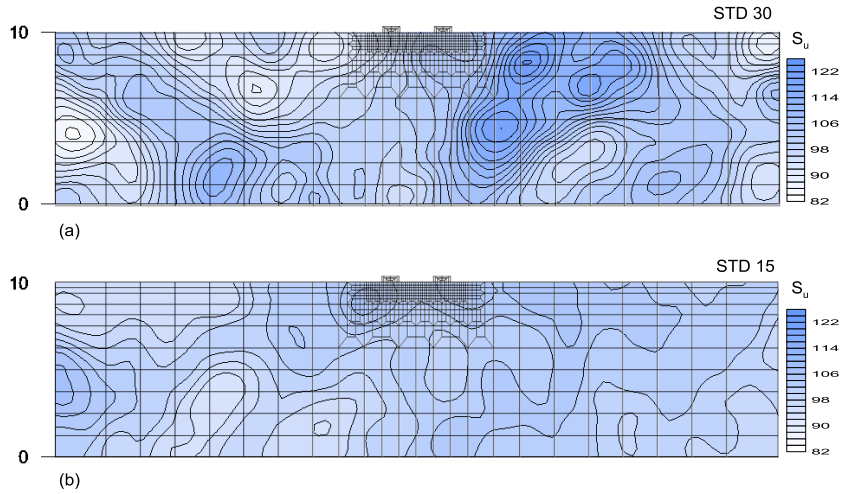


Figure 4.8 – Mesh used ($\theta_x$=$\theta_y$=4): (a) standard deviation of 30; (b) standard deviation of 15

In order to introduce variability a lognormal distribution was considered for the undrained strength of the soil. Several variations of the parameters that control the generation of the random fields were evaluated in this application. In Figure 4.8 are presented two cases of the undrained strength random field considered in the analyses. As it is possible to observe there are significant differences between the fields just when a different standard deviation is considered. The cases analysed are summarised in Table 9 and comprise three different studies.

The first study case aims to infer the effect of the standard deviation (***STD***) of the input variable has on the behaviour of the footings. The second study case is performed in order to assess the influence of the isotropic spatial correlation distance ($\boldsymbol{\theta_x}$). In the third and final study case the variability of the undrained deformation modulus, $E_u$, is added to the variability of the undrained strength of the soil by multiplying the value of $S_u$ at each Gauss point of the mesh by a constant (***K***). The value chosen for the constants represent the limits for clay and silt and silty or sandy clay as proposed by Bowles (1996) and already presented in Table 2. Finally, based on the overall obtained results a brief discussion about the possible failure mechanisms of the footings is presented.

Is important to refer that also in this application and for each case 999 calculations were performed. This number has proven to be sufficient to establish a pattern as can be seen in Figure 4.9 where the moving average of the relative vertical displacements ($d_R$) of the footings for the last stage of the analyses are presented. As can be seen from the figure stabilisation of the relative displacement occurs for around 500 analyses and for a value almost equal to the predicted in the deterministic case (solid black line).

Table 9 – Twin strip footings study cases

| Case | | ***STD*** | $\boldsymbol{\theta_x}$ | ***K*** |
|---|---|---|---|---|
| 1 | Standard deviation (*STD*) | 5,10; 15; 20,30 | 4m | - |
| 2 | Isotropic spatial correlation | 15 | 2m, 4m, 8m | - |
| 3 | Multivariable | 15 | 4m | 500, 1000, 1500 |

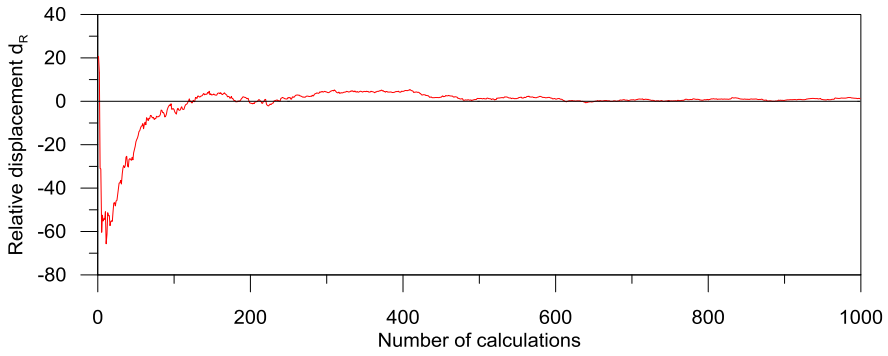


Figure 4.9 – Relative displacements moving average ($\theta_x$=4m; STD=15)

### 4.3.2 Case 1: Standard deviation

In this study 5 different standard deviation (5, 10, 15, 20 and 30) of the $S_u$ were analysed while maintaining whole the other parameters unchanged. As to be expected the variation of the standard deviation of the input variable has a major impact on the response of the soil underneath the footings. In Figure 4.10 the minimum, average and maximum load-vertical

displacement curves for a point located in the centre of the footings of all the analysis performed for standard deviation of 5, 15 and 30 are presented. (a), (b) and (c) figures correspond to the left footing and (d), (e) and (f) to the right footing. As can be shown, when considering minimum displacements, the soil is proven to have an almost elastic behaviour throughout the entire loading, except in the case of standard deviation of 5 where some plastification occurs for loads above 450kN. This is to be expected since the increment in the standard deviation value directly increases the probability of occurrence of values of $S_u$ significantly higher than the average value, consequently increasing the soil strength directly underneath the footings. The average values, (b) and (e), show an increase of displacements with the increment of the standard deviation due to the fact that the variable $S_u$ was introduced having lognormal statistical distribution which makes it so that for the same average value, the higher the value of standard deviation, the lower the mean value of $S_u$, originating an increase in the average of the displacements. The maximum values, presented in (c) and (f), increase significantly with the increment of standard deviation as expected. This is caused by fact that zones with lower strength beneath the footings are also more likely to occur with the increment of standard deviation. It is interesting to note that minimum, maximum and even average curves predicted in all cases differ significantly from the deterministic case where no variability was introduced, highlighting the role that variability can have to detect different scenarios.

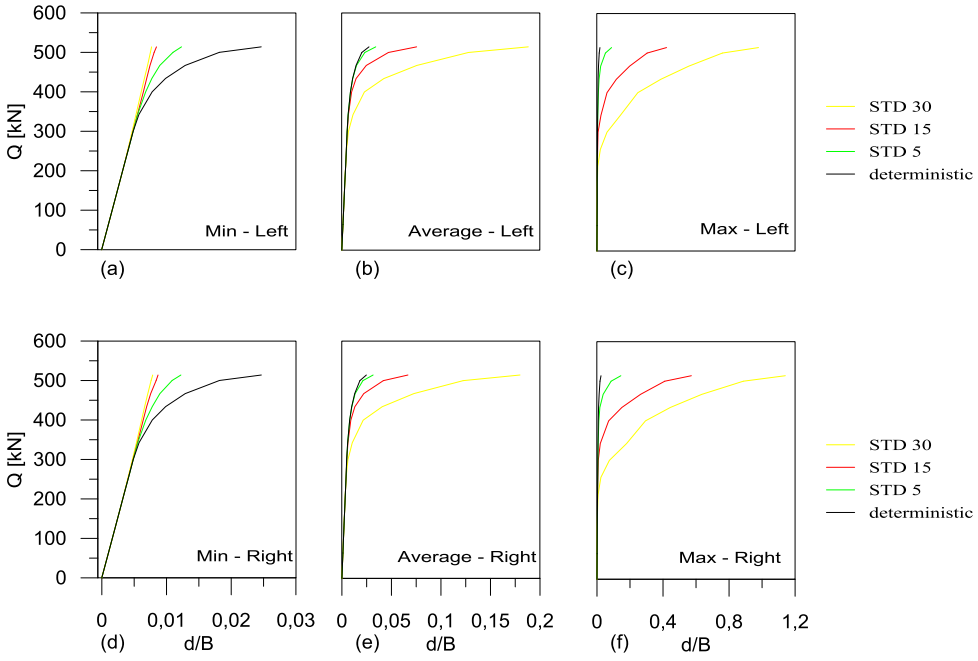


Figure 4.10 – Minimum, average and maximum load displacement curves (standard variation)

In Figure 4.11 the distribution of the total rotations, $w_{tot}$, between the footings determined for the 999 analysis performed with standard deviations of 5, 15 and 30 is shown for safety factors of 3, 2, 1.5 and 1 in (a), (b), (c) and (d), respectively. The total rotation was determined

considering the relative vertical displacement at the centres of each footing divided by its distance and the safety factor (*SF*) was calculated by dividing the maximum load applied (514kN) by the load at a given stage. When the *SF* is equal to 3 in all three cases considered the rotations are almost zero (deterministic value) in the majority of the calculations. This is due to the fact that only 33% of the average maximum load is applied and, therefore, the soil is either within the elastic range or at the beginning of the plastic phase. For a *SF*=2 an increase of the range off the rotations is noticeable even though a concentration of values around the deterministic value (zero) is still visible especially for small standard deviation values. When the load is increased and a *SF*=1.5 is reached the range of values for the rotations increases significantly, although centred in the value of zero, for all standard deviations. In the limit case (*SF*=1) an even higher variability is observed, and particularly for standard deviation of 30. With the introduction of variability, the footings no longer settle equally and relative displacements and rotation occur. This new behaviour of the footings could not have been foreseen during the design stage if just deterministic analysis were performed.

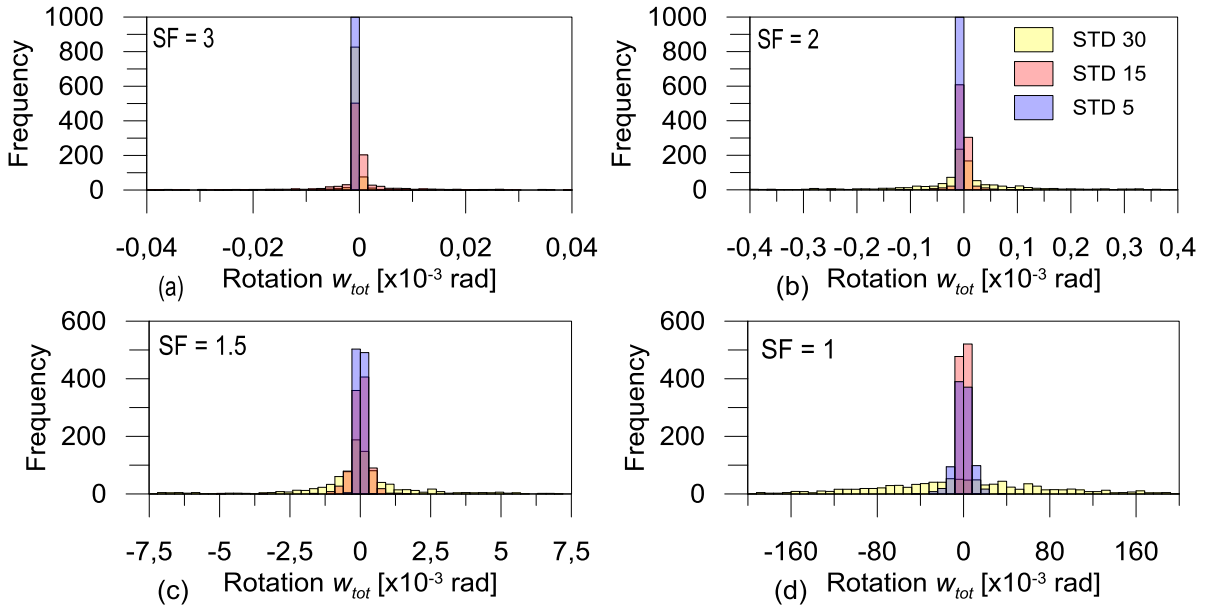


Figure 4.11 – Relative rotations – standard deviation: (a) *SF*=3, (b) *SF*=2, (c) *SF*=1.5, (d) *SF*=1

In order to further assess the impact of the results Gauss distribution curves were fitted to the distribution of the total rotation, between both footings, and to the individual rotation of each footing separately, $w_{right}$ and $w_{left}$, taken as the relative displacement measured at the extremities of the footing divided by its width (1m). In Figure 4.12 the evolution of the standard deviation values of the fitted Gauss distribution of the rotations with the standard deviation of the input variable is shown for (a) *SF*=3, (b) *SF*=2, (c) *SF*=1.5 and (d) *SF*=1. For *SF*=3 the standard deviation of the rotations only shows a minimal increase for standard deviation values of the input variable higher than 20. This a consequence of that for the loading applied at that stage

the soil underneath the footings is mostly in elastic behaviour, hence the settlements of both foundations will be equal in magnitude and no rotation is observed. For *SF*=2 and *SF*=1.5 the standard deviation values of the rotations will only increase noticeably for standard deviations of the input variable higher than 20, again due to the fact that for lower standard deviations of the input variable the values of $S_u$ will be closer to the average value and therefore, exhibit a behaviour close to the deterministic value. For *SF*=1 the standard deviation value of the rotations increases exponentially with the increment standard deviation value of the input variable due to the fact that the soil beneath the footings is mostly in plastic state, regardless of the standard deviation considered. Figure 4.12 also allows to observe that significant rotations within each footing are likely to occur although in lower values than those observed for the global rotation. This again is a behaviour that the deterministic case cannot foreseen and that might have significant implications in the design.

Finally, in Table 10 the fitted Gauss distribution parameters of the total rotation for each value of standard deviation of $S_u$ and for *SF*=2, *SF*=1.5 and *SF*=1 are presented. In the table are also displayed the probabilities of the total rotation exceeding the values of 1/500, 1/300 and 1/150 at each safety factor. The values of 1/500, 1/300 and 1/150 account for the values of differential rotations past which cracking in building coatings, cracking in structural walls and structural damage in common buildings are expected to occur respectively (Bjerrum, 1963; Rankin, 1988; Boscardin & Cording, 1989; Burland, 1995). From the table is possible to observe that despite the increase of variability given by the variation of the standard deviation only for the extreme cases and when a SF=1 a change in the average value of the distribution ($\boldsymbol{\mu}$) is observed. In the case of the standard deviation ($\boldsymbol{\sigma}$) that increase is more relevant particularly for *SF* higher than 2 as stated previously. The evaluation of the probability of damage in the footings shows that for *SF* higher than 2 no problems are likely to occur. When the *SF* decreases to 1.5 a reasonable risk of damage is observed for high standard deviation values of the $S_u$. In the limit case, as expected, the probability of damage is very high, regardless of the standard deviation considered. The results obtained show that if a *SF* higher than 2 is used in the design, as recommended by Bowles (1996), the probability of damage is very low although with the introduction of variability is possible to account for it.

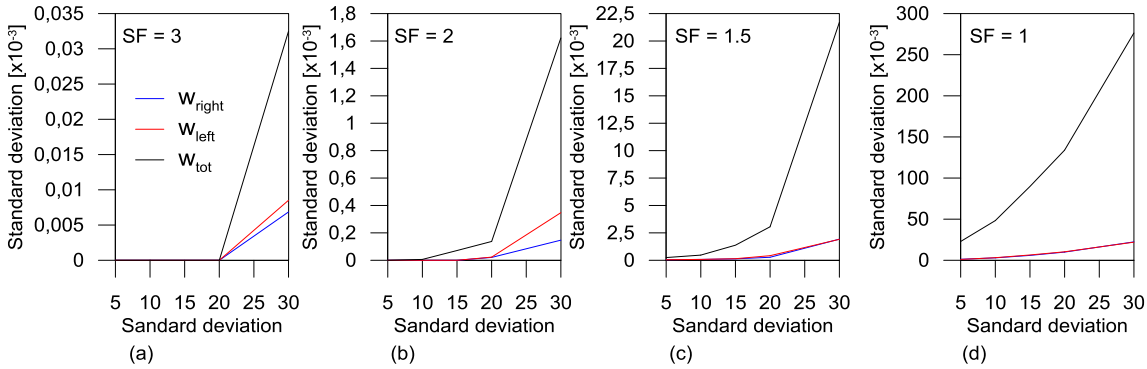


Figure 4.12 – Relative rotation standard deviation variation with input variable standard deviation: (a) *SF*=3, (b) *SF*=2, (c) *SF*=1.5, (d) *SF*=1

Table 10 – Structural damage probability effect of the standard deviation

| ***STD*** | **Fitting parameters** | | | | | | **Probability of rotation exceeding** | | | | | | | | |
|---|---|---|---|---|---|---|---|---|---|---|---|---|---|---|---|
| | ***μ*** | | | ***σ*** | | | ***1/500 [%]*** | | | ***1/300 [%]*** | | | ***1/150 [%]*** | | |
| | ***SF*** | | | ***SF*** | | | ***SF*** | | | ***SF*** | | | ***SF*** | | |
| | **2** | **1.5** | **1** | **2** | **1.5** | **1** | **2** | **1.5** | **1** | **2** | **1.5** | **1** | **2** | **1.5** | **1** |
| 5 | 0.0 | 0.0 | -0.6 | 0.0 | 0.2 | 23.0 | 0.0 | 0.0 | 45.6 | 0.0 | 0.0 | 43.3 | 0.0 | 0.0 | 37.8 |
| 10 | 0.0 | 0.0 | 0.3 | 0.0 | 0.5 | 48.3 | 0.0 | 0.0 | 48.7 | 0.0 | 0.0 | 47.6 | 0.0 | 0.0 | 44.8 |
| 15 | 0.0 | 0.0 | 1.2 | 0.1 | 1.4 | 89.8 | 0.0 | 7.5 | 49.6 | 0.0 | 0.8 | 49.2 | 0.0 | 0.0 | 47.6 |
| 20 | 0.0 | 0.1 | -0.8 | 0.1 | 3.1 | 134.0 | 0.0 | 26.9 | 49.2 | 0.0 | 14.7 | 48.8 | 0.0 | 1.6 | 48.0 |
| 30 | 0.0 | -0.1 | -10.4 | 1.6 | 21.7 | 276.4 | 11.3 | 46.4 | 49.4 | 2.1 | 43.6 | 48.0 | 0.0 | 37.8 | 47.6 |

### 4.3.3 Case 2: Isotropic spatial correlation distance

In the second study case the magnitude of the isotropic spatial correlation ($\theta_x$=$\theta_y$) was varied maintained all other parameters constant and assuming a standard deviation of 15. The impact of the magnitude of the isotropic spatial correlation on the behaviour of the footings was evaluated for 3 cases, $\theta_x$=2, 4 and 8m, which were considered relevant given the dimension of the model and the interaction zone of the two footings. In Figure 4.13 the minimum, average, and maximum load-vertical displacement curves for a point located in the centre of the footings of all the analysis performed are presented for the 3 cases analysed. As observed for the influence of the standard deviation, if the minimum values for the displacements are considered, (a) and (d), the soil beneath the footings behaves almost as an elastic material and the spatial correlation has a minimal effect resulting in displacements smaller than those determined for the deterministic case. The average values, presented in (b) and (e) show identical curves independently of the spatial correlation distance adopted and appear just to be influenced by the standard deviation of the input variable adopted. Finally, the maximum curves, (c) and (f), represent the most interesting results. As can be seen the smaller maximum curves are obtained for the smaller value of the spatial correlation distance (2m) and no visible difference is observable for the values of 4 and 8m. This is a direct consequence of the relationship between

the spatial correlation distance and the area affected by the footings. For values smaller than 4m (distance between the centres of the footings) and given the properties of the random fields at least a part of the soil underneath the footings has reasonable strength, while for higher values is possible to have analyses where all the soil underneath the footings presents poor strength characteristics, resulting in higher settlements. Naturally, for spatial correlation distances higher than the area affected by the two footings, the results will tend to became similar as obtained for the 4 and 8m studies.

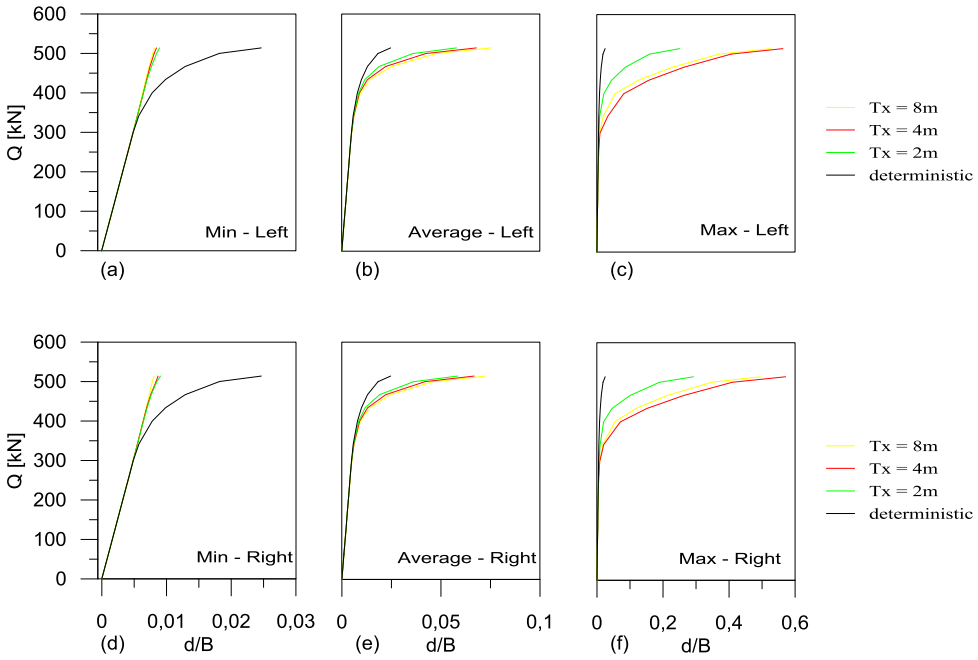


Figure 4.13 – Minimum, average and maximum load displacement curves (isotropic spatial correlation distance)

The distribution of the results of the 999 analysis performed for each case of the total relative rotations between the two footings is presented in Figure 4.14. As expected for a decrease of the *SF* a wider range of values is obtained for the total rotations, which are justified by the increase of plastification in the analysis. However, based the analysis of the histograms is not clear the influence of the variation of the spatial correlation distance, although it appears that higher values correspond to higher dispersion of values.

In order to clarify this point the evolution of the standard deviation of the total rotations, determined by fitting the Gauss distribution to the results presented in Figure 4.14, against the spatial correlation distance is plotted in Figure 4.15. Superimposed in the figures are also the results obtained for the adjustment of the rotations of the individual footings ($w_{right}$, $w_{left}$). It is possible to observe that *SF*=3 no rotations occur given the elastic behaviour of soil for this load. For the subsequent safety factors the standard deviation of the total rotation increases significantly. However, is possible to verify that for a spatial correlation higher than 4 the

standard deviation modifies its behaviour and appear to stabilise although is not possible to generalise a trend based solely in the cases analysed. As for the individual rotation of each footing it appears that there is no particular influence of the spatial correlation value adopted. This result was expected given the width of the footings (1m) being half of the smallest value studied (2m) and therefore there is a high probability that the entire footing is being located upon soil with poor strength characteristics.

In Table 11 the probability of exceeding a total rotation of 1/500, 1/300 and 1/150 when varying the isotropic spatial correlation is shown alongside the fitting parameters for the Gauss distribution. As can be observed the noticeable differences begin to occur for SF higher than *1.5,* where the probability of inducing cracking on building coatings (1/500) significantly increases when transitioning from a spatial correlation distance of 2 to 4m and stabilizing past that value. Once again this can be explained by the fact that 4m may be sufficient to influence both footings whilst a smaller spatial correlation is not. For *SF*=1 generalised plastification and consequence high probability of damage occurs regardless of the spatial correlation distance value adopted.

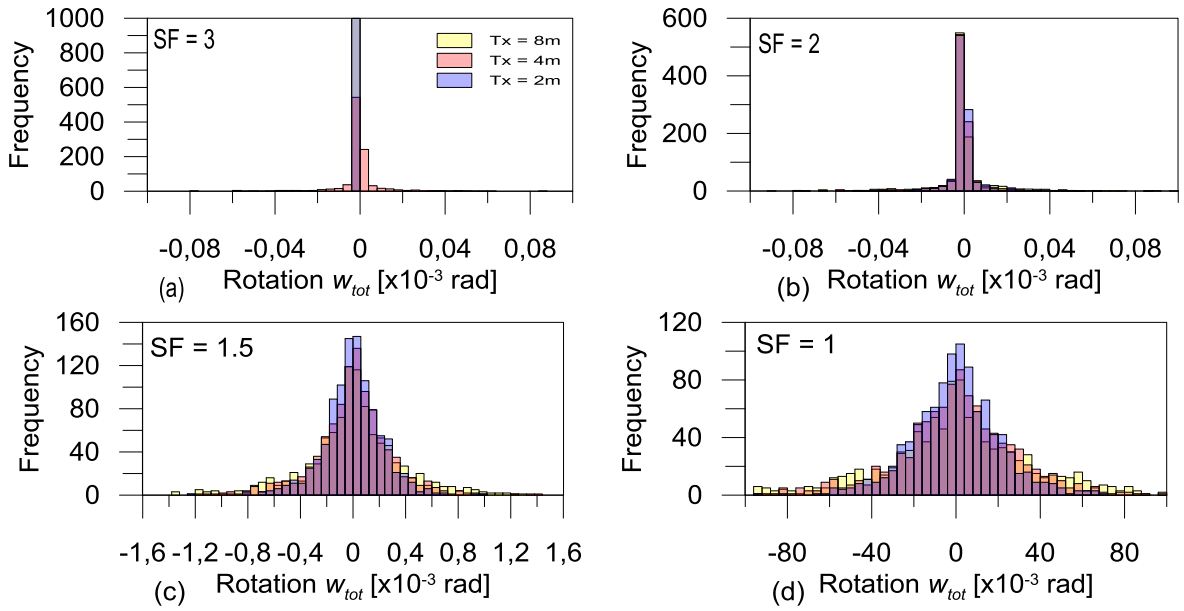


Figure 4.14 – Relative rotations – magnitude of isotropic spatial correlation distance (a) *SF*=3, (b) *SF*=2, (c) *SF*=1.5, (d) *SF*=1

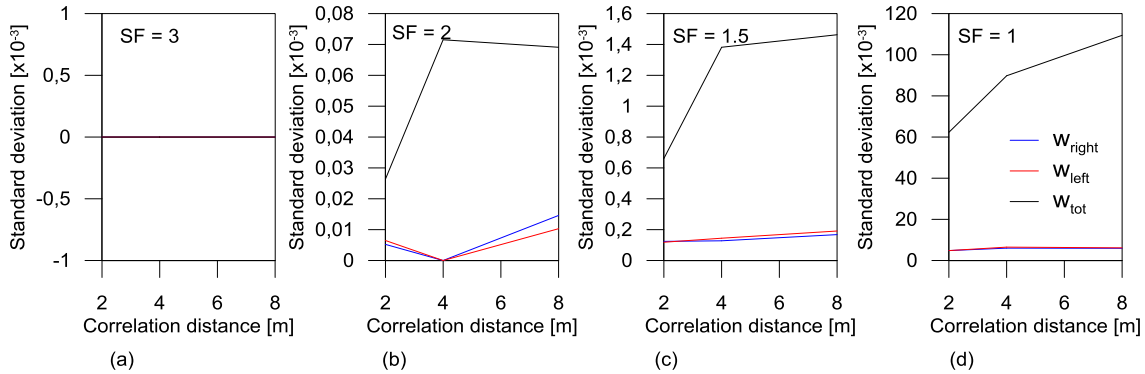


Figure 4.15 – Relative rotation standard deviation variation with magnitude of spatial correlation distance (a) *SF*=3, (b) *SF*=2, (c) *SF*=1.5, (d) *SF*=1

Table 11 - Structural damage probability effect of isotropic spatial correlation

| $\theta_x$ | **Fitting parameters** | | | | | | **Probability of rotation exceeding** | | | | | | | | |
|---|---|---|---|---|---|---|---|---|---|---|---|---|---|---|---|
| | ***μ*** | | | ***σ*** | | | ***1/500 [%]*** | | | ***1/300 [%]*** | | | ***1/150 [%]*** | | |
| | ***SF*** | | | ***SF*** | | | ***SF*** | | | ***SF*** | | | ***SF*** | | |
| | **2** | **1.5** | **1** | **2** | **1.5** | **1** | **2** | **1.5** | **1** | **2** | **1.5** | **1** | **2** | **1.5** | **1** |
| 2m | 0.0 | 0.0 | -0.6 | 0.0 | 0.7 | 62.3 | 0.0 | 0.1 | 48.4 | 0.0 | 0.0 | 47.6 | 0.0 | 0.0 | 45.6 |
| 4m | 0.0 | 0.0 | 1.2 | 0.1 | 1.4 | 89.8 | 0.0 | 7.5 | 49.6 | 0.0 | 0.8 | 49.2 | 0.0 | 0.0 | 47.6 |
| 8m | 0.0 | 0.0 | 2.7 | 0.1 | 1.5 | 109.4 | 0.0 | 8.9 | 50.4 | 0.0 | 1.2 | 49.6 | 0.0 | 0.0 | 48.8 |

### 4.3.4 Case 3: Multivariable

In the third and final case the influence of introducing variability into a second variable is evaluated by performed 3 additional analyses. In these, beside the variability of $S_u$, it was considered that the undrained deformation modulus, $E_u$, was also variable while all the other parameters remained unchanged. However, the variability of the latter was conditioned to the former through the application of Equation 15. Values of $K$ corresponding to 500, 1000 and 1500 were considered for the 3 analyses. It should be noted that the deterministic case and the analysis considering only the variability of $S_u$ the undrained deformation modulus, $E_u$, was kept constant and equal to 100MPa which correspond to adopt a K=1000.

The introduction of variability in more than one parameter is shown to influence decisively the behaviour of the footings. Figure 4.16 shows for the right and left footings the minimum, average and maximum load-vertical displacement curves for a point located in the centre of the footings for all the analysis performed of the 3 cases studied. In the figure are also plotted for reference the deterministic case and the equivalent analysis when only varying $S_u$ (*sing var*). The minimum curves, (a) and (d), reveal that a noticeable impact occurs in the stiffness of the soil beneath the footing showing that an increase of $K$ translate in higher $E_u$ and consequently in a stiffer response of the soil although within the elastic range. Identical results are observed for the average and maximum curves where the differences in stiffness are even more

perceptible due to the plastification of the soil. The comparison between the single variable calculation (blue solid line) with the results obtained from considering $E$=1000$S_u$ (red solid line) allow to directly evaluate the influence of considering a second parameter variable in the analysis. As expected the introduction of a second variable induces more variability in the results, although that is only very noticeable after plastification occurs.

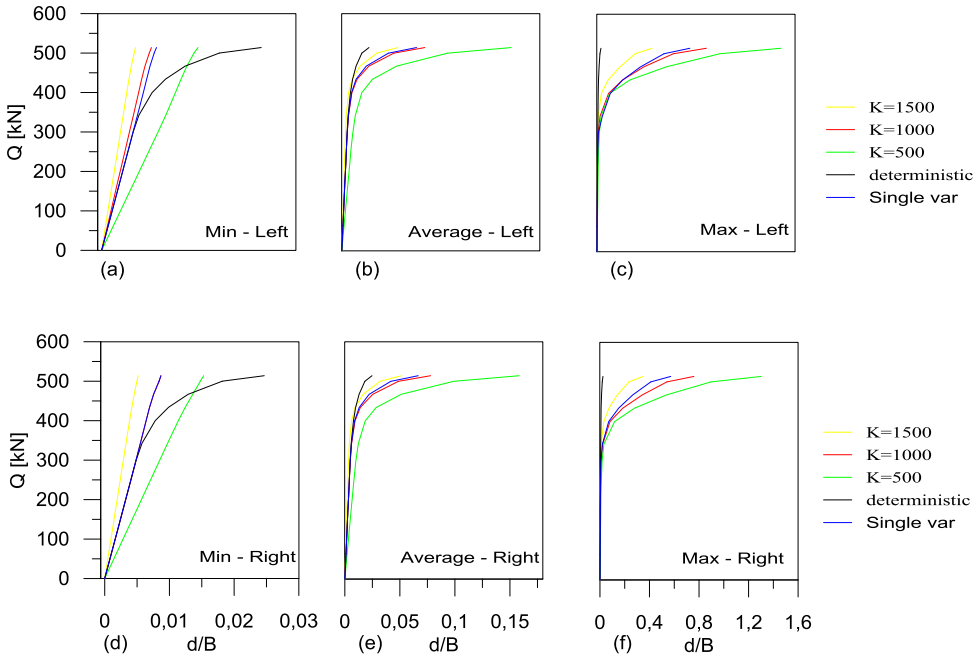


Figure 4.16 – Minimum, average and maximum load displacement curves (multivariable)

The distribution of the results of the 999 analysis performed for each case of the total rotation of the footings is shown to be directly influenced by the stiffness variation for every safety factor considered. Figure 4.17 shows those distributions for $SF$=3, $SF$=2, $SF$=1.5 and $SF$=1 in (a), (b), (c) and (d), respectively. When considering any safety factor it can be observed that the smaller the stiffness the larger is the range of the total rotations, even when only 33% of the maximum average load is applied, showing that the introduction of variability in multiple parameters translates into more variable results. This effect is even clearer on Figure 4.18 where the standard deviation of the fitted Gauss distribution to the results of the total rotation are plotted against parameter $K$. As expected an increase of $K$ (higher stiffness) translates in a lower standard deviation. However, the reference standard deviation value for a single variable is lower than the determined for the case where $K$=1000 highlighting the influence of variability. An identical result is observed, although at a smaller scale, for the individual rotations of each footing. Table 12 summarises the parameters of the fitted Gauss distribution and the probability of damage for different levels. The results confirm that the introduction of a second variable results in higher probabilities of damage, which naturally increase with the decrease of the stiffness ($K$).

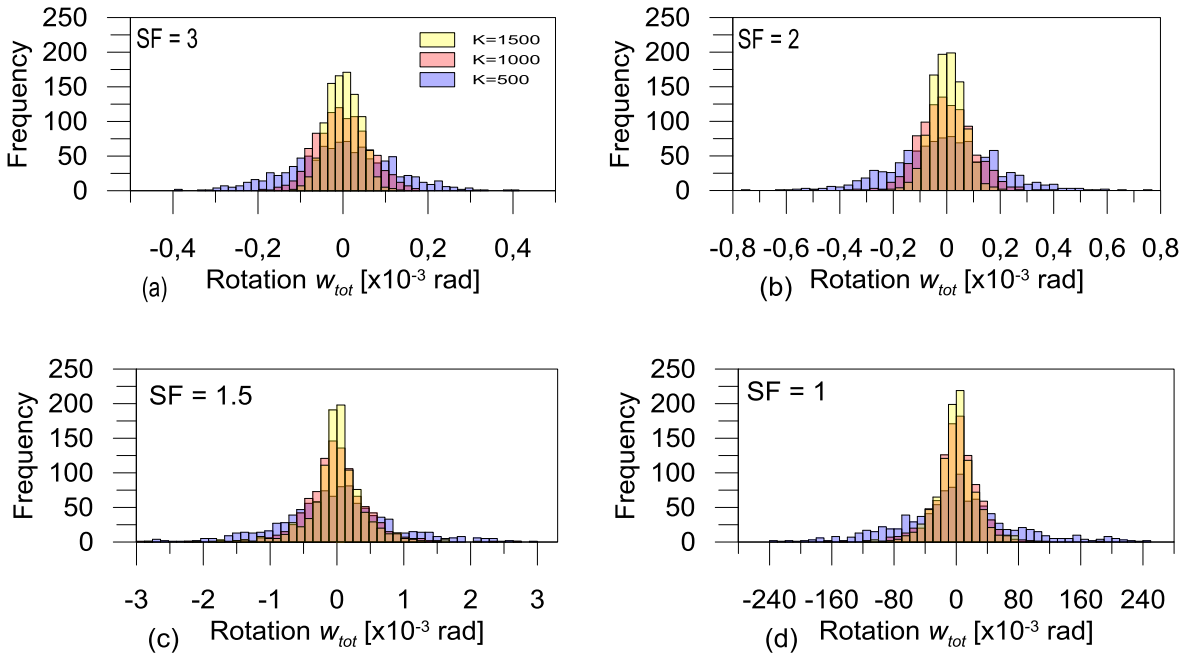


Figure 4.17 – Relative rotations - multivariable (a) *SF*=3, (b) *SF*=2, (c) *SF*=1.5, (d) *SF*=1

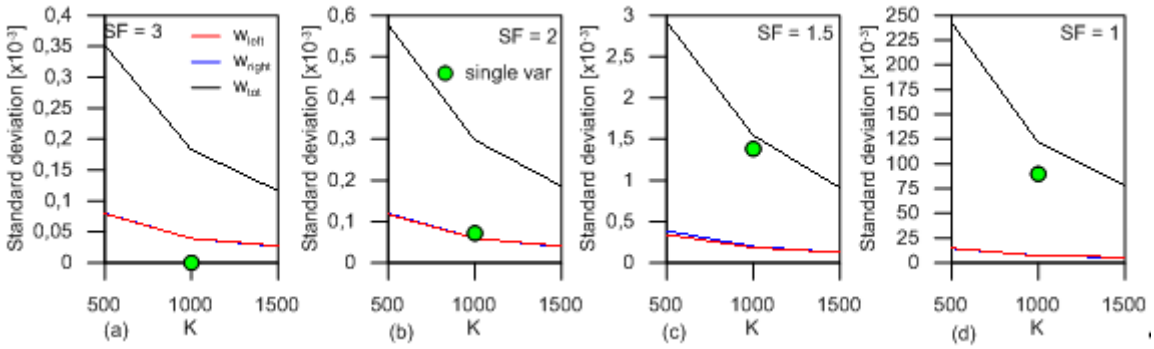


Figure 4.18 – Relative rotation standard deviation variation with introduction of multivariable variability (a) *SF*=3, (b) *SF*=2, (c) *SF*=1.5, (d) *SF*=1

Table 12 - Structural damage probability – multivariate variability

| K | Fitting parameters | | | | | | Probability of rotation exceeding | | | | | | | | |
|---|---|---|---|---|---|---|---|---|---|---|---|---|---|---|---|
| | μ | | | σ | | | *1/500 [%]* | | | *1/300 [%]* | | | *1/150 [%]* | | |
| | SF | | | SF | | | SF | | | SF | | | SF | | |
| | **2** | **1.5** | **1** | **2** | **1.5** | **1** | **2** | **1.5** | **1** | **2** | **1.5** | **1** | **2** | **1.5** | **1** |
| 500 | 0.0 | -0.1 | -4.5 | 0.6 | 2.9 | 242.5 | 0.0 | 23.9 | 49.2 | 0.0 | 12.1 | 48.8 | 0.0 | 0.0 | 48.0 |
| 1000 | *0.0* | *0.0* | *-2.4* | *0.3* | *1.5* | *121.1* | *0.0* | *9.5* | *48.7* | *0.0* | *1.5* | *48.0* | *0.0* | *0.0* | *47.2* |
| 1500 | 0.0 | 0.0 | -0.5 | 0.2 | 0.9 | 77.6 | 0.0 | 1.4 | 47.9 | 0.0 | 0.0 | 48.0 | 0.0 | 0.0 | 46.4 |

### 4.3.5 Failure mechanisms

The calculations performed show that there are 8 possible failure mechanisms for the footings. Each of the two footings can individually rotate clockwise or anticlockwise and the relative

rotation between them can also be clockwise or counter clockwise amounting to eight possible combinations. It should be mentioned that in the deterministic case there is no rotation between both footings (relative displacement at the centre equal to zero), the left footing rotates clockwise and the right footing anticlockwise, i.e., the footings rotates toward each other.

Figure 4.19 shows three different mechanisms identified for analyses which have the exact same input variables, average value of $S_u$ of 100, standard deviation of 15 and isotropic spatial correlation distances of 4m, and therefore only differ due to the randomly generated field. In (a) is possible to see that both foundations rotate anticlockwise and there is also a anticlockwise rotation between them, in (b) both foundations present a slight rotation anticlockwise with a significant clockwise rotation between them and, finally, in (c) both foundations rotate clockwise with also a relative clockwise rotation between them.

In each case performed throughout this study all 8 possible failure mechanism combinations were observed in the 999 analysis calculated. In total, in the nearly 10000 analysis performed, each mechanism occurred with an almost equal probability of roughly 12.5%. This nearly equal distribution leads to the conclusion that despite the footings being spaced only 3m apart they behave almost independently and show no significant mutual influence.

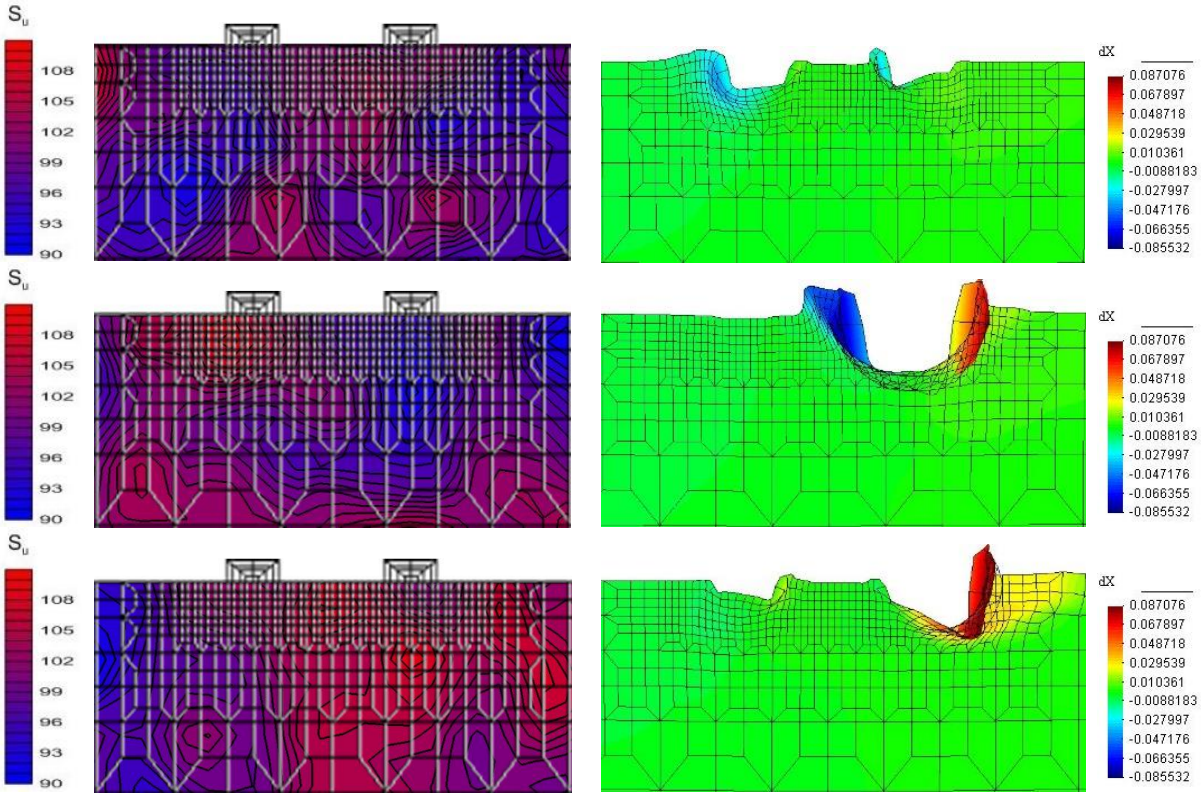


Figure 4.19 – Examples of failure mechanisms

## 4.4 Deep Tunnel

### 4.4.1 General considerations

So that the influence of rock mass variability on geotechnical structures can be assessed, a study on a deep tunnel having circular section subject to a uniform stress state was performed. The 2D mesh used is presented in Figure 4.20, and is a quadrilateral with dimension 120m having an 8m diameter tunnel centred. The mesh has 812 solid elements with 8 nodal points and 4 Gauss points for stress evaluation. The lining was simulated through solid elements with 0.20m thickness having linear elastic behaviour with a Young's modulus of 20 GPa and a Poisson's coefficient of 0.25. The boundary conditions were set so that no displacements were possible at the limits of the mesh. A uniform and isotropic stress state of 1MPa was assumed in order to simulate the typical conditions found in deep tunnels. The effect of gravity forces was neglected by considering that the elements of the mesh have null unit weight.

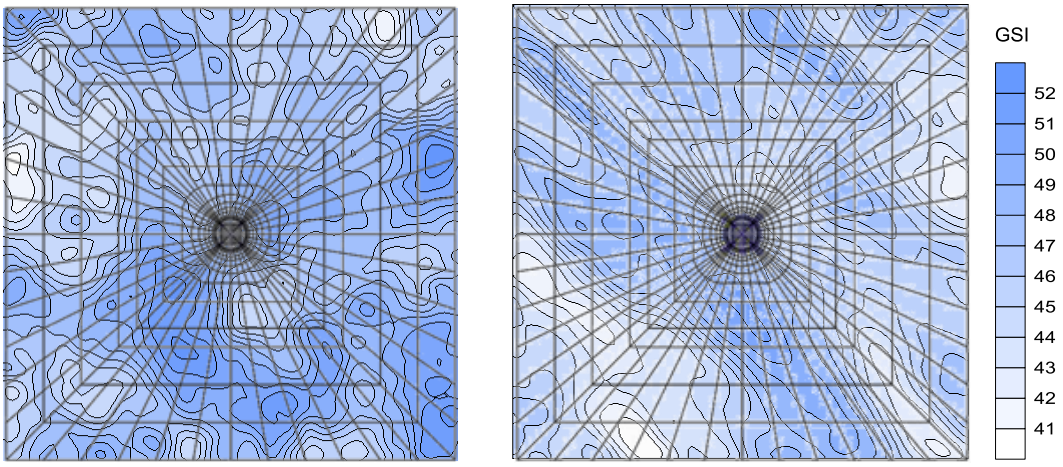


Figure 4.20 – Finite elements mesh used – deep tunnel: (a) STD=7, $\theta_x$=10m, $\theta_x/\theta_y$=1, α=0; (b) STD=7, $\theta_x$=75m, $\theta_x/\theta_y$=7.5, α=45

Simplifications were admitted so that the 3D effects normally associated to the excavations of tunnels could be reproduced in a 2D simulation (Moller, 2006). In order to account for the three-dimensional effects generated by the excavation, that usually translate in stress redistribution, through arch effect, onto the surrounding massif as well as into the lining, and the time delay with which the lining is installed in comparison to the front of the excavation, the stress relaxation method was employed (Potts et al., 2001). This method suggests that the simulation of the excavation can be performed in two separate stages. Firstly, the elements of the tunnel are removed and a percentage of resulting stresses ($\alpha$) are applied in the contour of the excavation, then, on a second stage, the lining is installed, and the remainder of the unbalanced stresses is applied (1-$\alpha$) so that a final equilibrium state is achieved. In deep tunnels the stress relief factor ($\alpha$) can be estimated through the convergence-confinement method (Panet &

Guenot, 1982). In the present analysis a stress relief factor of 80% was considered to be adequate given the dimensions of the tunnel, the stress state and the characteristics of the rock mass. Hence, the construction stages adopted were, the excavation of the tunnel through the removal of its elements (140) and application of 80% of the resulting stresses onto the contour of the excavation followed by a second stage where the lining was installed and applied the remaining stresses (20%).

For the rock mass the Hoek-Brown failure criterion was adopted (Hoek et al., 2002). As mentioned in section 3.3.2 the required parameters for the definition of the rock properties are the GSI, the constant of the intact rock $m_i$, the deformation modulus of the intact rock, $\sigma_{ci}$ , the Poisson's coefficient, $\upsilon$, and the disturbance factor, $D$. In order to have more realistic results the deterministic parameters adopted correspond to a real rock mass, in this case the complex C5 as presented in Pedro (2007). The GSI was the parameter elected to be variable within the field since it simultaneously affect the strength and deformability of the rock mass as demonstrated in 2.1.2. A normal distribution was considered for the *GSI* as suggested by Cai (2011). For the deterministic analysis the average value of 46 was adopted as proposed by Pedro (2007).

Table 13 – Rock mass parameters

| | |
|---|---|
| *GSI avg* | 46 |
| *GSI min* | 32 |
| *GSI max* | 60 |
| $E_i$ *(MPa)* | 8100 |
| $\sigma_{ci}$ *(MPa)* | 21 |
| $\upsilon$ | 0.25 |
| $m_i$ | 9 |
| $D$ | 0 |

Just like in the previous applications 999 analysis were run for each case considered. In Figure 4.21 the moving average of the relative displacements $D_r$ of points A and B, located at the centre of the upper and lower sides of the tunnel (vertical convergence), are presented for the 999 runs for a field having a standard deviation of 7 and isotropic spatial correlation of 10m. The moving average results of $D_r$ allows for the reasoning that 500 realizations would be sufficient. In this case it is possible to observe that the average value is almost identical to that obtained with the deterministic analysis. That occurs since for the geometry, conditions and parameters adopted there is almost no plastification in the rock mass, hence, being within the elastic range.

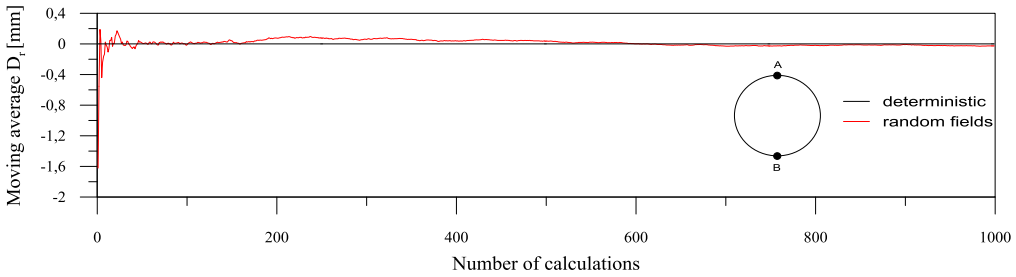


Figure 4.21 – Number of calculations – Deep tunnel

With this application it is intended to evaluate not just the influence of the standard parameters that control the generation of the field, standard deviation, isotropic spatial correlation, but also the advanced features implemented in UC2DRF, namely the degree and direction of the anisotropy in the field. The study cases analysed in this application are presented in Table 14. In the first case three values of the standard deviation and of the isotropic correlation distance were employed in a total of nine analysis performed. In the second case a degree of isotropic was introduced by varying $\theta_x$ and the ratio $\theta_x/\theta_y$. Finally, the rotation of the anisotropy of the field was evaluated by varying $\alpha$ while keeping all the other parameters constant.

Table 14 – Study cases – Deep tunnel

| Case | | *STD* | $\theta_x$ (m) | $\theta_x/\theta_y$ | $\alpha$ (°) |
|---|---|---|---|---|---|
| 1 | Standard deviation (*STD*) and isotropic spatial correlation | 5, 7, 9 | 5, 10, 20 | 1 | 0 |
| 2 | Anisotropic spatial correlation | 7 | 10, 20, 50, 100 | 0.1, 0.2, 0.5, 1, 2, 5, 10 | 0- |
| 3 | Rotation | 7 | 75 | 7.5 | -90, -62.5, -45, -22.5, 0, 22.5, 45, 62.5, 90 |

### 4.4.2 Deterministic analysis

So that the influence of variability can be asserted 3 deterministic calculations were performed for the average value of *GSI* as well as for the minimum and maximum values proposed by Pedro (2007). The Hoek-Brown parameters used in each analysis are presented in Table 15. As expected, given the initial stress conditions, each calculation originates uniform radial displacements, forces and pressures in the lining. The results are summarised in Table 16. It is worth mention that the minimum value considered for the GSI originates displacements, forces and pressures that are significantly larger in comparison with the ones resulting from the other analysis. These are consequence of the plastification of the rock mass that occurs for this small value of GSI. As a consequence of the radial symmetry of the mesh and the loading conditions the bending moment are equal to zero in all three analyses.

Table 15 – Hoek-Brown criterion parameters

| *GSI* | $\sigma_{ci}$ *(MPa)* | $m_b$ | *s* | *a* | $E_i$ *(MPa)* |
|---|---|---|---|---|---|
| 32 | 27 | 0.79346 | 0.00052 | 0.51953 | 751 |
| 46 | 27 | 1.30820 | 0.00248 | 0.50755 | 1934 |
| 60 | 27 | 2.15686 | 0.01174 | 0.50284 | 4212 |

Table 16 – Deterministic analysis results

| *GSI* | *Displacement (mm)* | *Convergence (mm)* | *Hoop Force (kN)* | *Lining Pressure (KPa)* |
|---|---|---|---|---|
| 32 | 6.03 | 12.06 | 533 | 128 |
| 46 | 2.47 | 4.93 | 338 | 82 |
| 60 | 1.17 | 2.35 | 199 | 48 |

### 4.4.3 Case 1: Standard deviation and isotropic spatial correlation distance

The impact of the variation of the standard deviation and of the isotropic spatial correlation is presented below. The values of standard deviation of 5, 7 and 9 were chosen so that the probability between the minimum and maximum values of the GSI are approximately 99.5%, 95% and 90% respectively.

In Figure 4.22 the results of the total displacements for 5 different analyses are presented. In (a) are illustrated for reference the total displacements of the deterministic analysis (*GSI*=46); in (b) the results obtained for a calculation having isotropic spatial correlation distance of 10m and standard deviation of 5; (c), (d) and (e) are, respectively the results obtained for random calculations with standard deviation of 7 and isotropic spatial correlation distances of 5, 10 and 20m, respectively, and (e) is the result of a random calculation having standard deviation of 9 and 10m spatial correlation distance. The differences between the results are both quantitatively and qualitatively noticeable. The spatial distribution of the total displacements is no longer radial and uniform as in the deterministic analysis and becomes preferably oriented according to the weak zones introduced in the massif. The effects are also noticeable in the magnitude of the displacements that are significantly different than those obtained in the deterministic case. The introduction of variability causes noticeable asymmetry in the deformation of the tunnel. This asymmetry implies the possibility of asymmetric hoop force and lining pressure diagrams that cannot be predicted by performing a simple deterministic analysis.

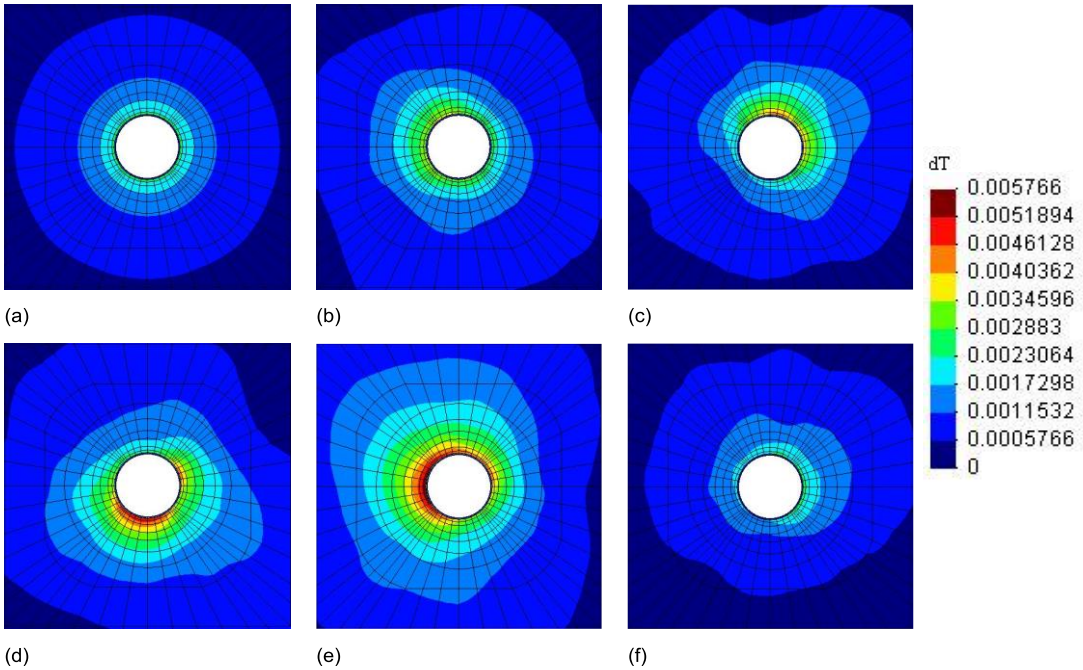


Figure 4.22 – Representative total displacements: (a) deterministic; (b) STD=5, $\theta_x$=10; (c) STD=7, $\theta_x$=5; (d) STD=7, $\theta_x$=10; (e) STD=7, $\theta_x$=20; (f) STD=9, $\theta_x$=10

When analysing the variation of the vertical displacement at the central point of the upper side of the tunnel (A) with *GSI* standard deviation and isotropic spatial correlation over the 999 calculations several conclusions can be drawn. Figure 4.23 presents the distribution of the displacement at point A for a standard deviation of (a) 5, (b) 7 and (c) 9 for the three spatial correlation distances analysed. Superimposed in the figure are the values obtained for the deterministic analysis for reference. The figure show that the increase of the spatial correlation distance implies a wider range of displacements. However, the effect of this parameter is smaller than the influence observed for the standard deviation were even wider distributions occur for the same isotropic correlation distance. The results appear to follow a lognormal distribution weak its peak around the deterministic average value of *GSI* and only for a higher standard deviations and spatial correlation distances surpass the values given by the limits of the *GSI*. This results are even more visible in Figure 4.24, where the average value of the vertical displacement (a) is shown to increase with the value of standard deviation between around 2 and 10% but to remain almost constant when varying the isotropic spatial correlation distance. The median value calculated for the 999 analysis of each case (b), is higher than the value obtained in the deterministic analysis, tends to decrease with the isotropic spatial correlation distance but increases with standard deviation of *GSI*. The standard deviation values obtained for the displacement density curves are shown to increase with the standard deviation of *GSI* and with the spatial correlation distance, having a significant influence for a standard deviation value of 9. The statistical analysis shows that the determination of the probability of

occurrence of displacements exceeding a given value is directly influenced by the standard deviation and by the spatial correlation distance, increasing with both parameters.

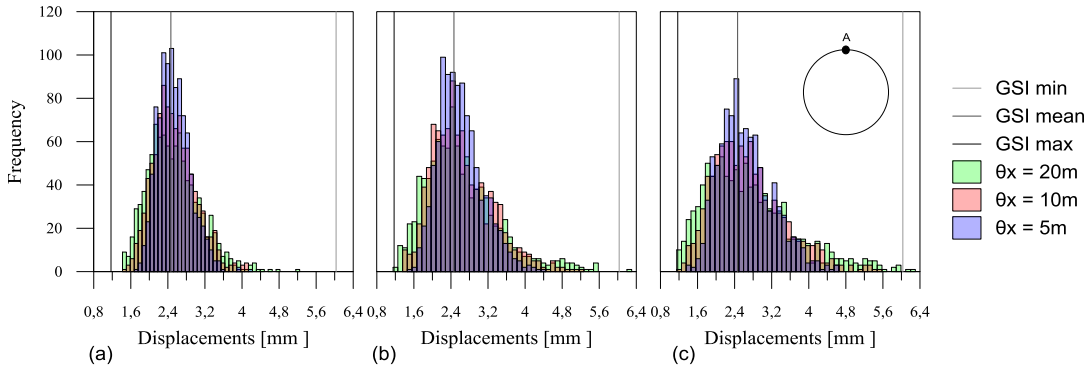


Figure 4.23 – Distribution of the vertical displacement with standard deviation and isotropic spatial correlation

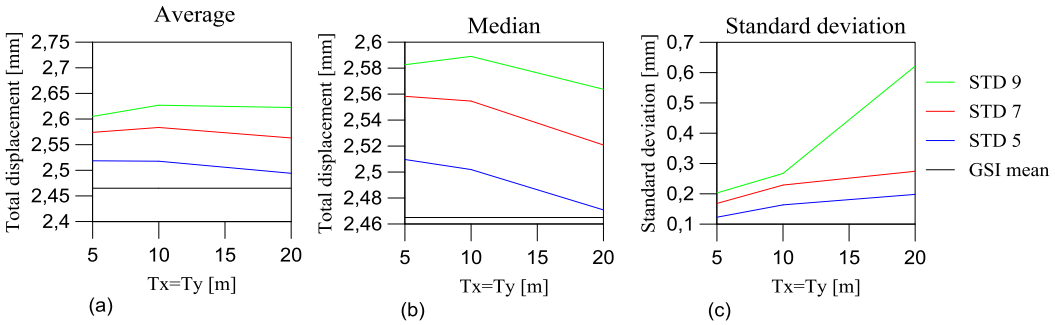


Figure 4.24 – Vertical displacements variation with standard deviation and isotropic spatial correlation

The effect of standard deviation and magnitude of the isotropic spatial correlation on the hoop force envelopes around the tunnel surface is presented in Figure 4.25. (a), (b) and (c) correspond to standard deviations of 5, 7 and 9 respectively. As can be observed, an increase of the value of the standard deviation and of the spatial correlation distance, corresponds to higher forces will be applied in the lining, which envelopes approaches the values expected for the minimum and maximum values of *GSI* although never surpassing the afore mentioned values. However, when the results are compared with the reference GSI value is possible to observe that the deterministic analysis is incapable of predicting the magnitude and asymmetry of forces that can be resultant of the introduction of variability in the rock mass. This can have a major impact in the design of the lining of the tunnel since an increase of nearly 28% on the hoop forces is predicted just when a small standard deviation is considered in the analysis. Furthermore, that increase is likely to be asymmetric causing additional problems in the lining design. A random result with isotropic spatial correlation and correspondent standard deviation was also plotted for each *STD* value further demonstrating the expected and random asymmetry resulting from the introduction of variability.

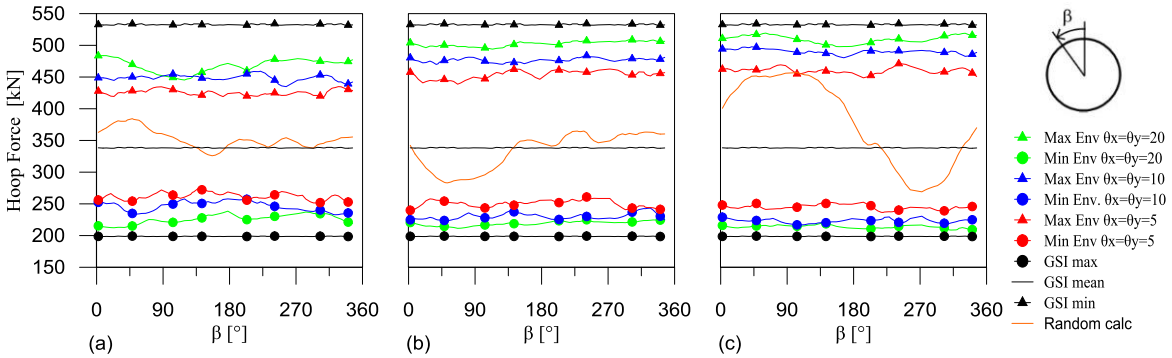


Figure 4.25 – Hoop force envelope variation with standard deviation and isotropic spatial correlation

### 4.4.4 Case 2: Anisotropic spatial correlation

In order to evaluate the anisotropy of the field 999 calculations were performed for values of $\theta_x/\theta_y$ of 0.1; 0.2; 0.5; 1; 2; 5 and 10 in fields generated having a standard deviation value of 7. In Figure 4.26 five examples of the fields considered in the analysis corresponding to $\theta_x/\theta_y$ (a) 0.2; (b) 2; (c) 5; (d) 0.5 are presented. The influence of anisotropy is clear in the figures where is possible to visualize that the ratio of 5 and 0.5 almost corresponds to having layers in the rock mass in the horizontal and vertical directions, respectively.

However, and despite the clear differences between the fields, the introduction of an anisotropic spatial correlation distance did not imply significant differences in the displacement distribution over all calculations, with the variation of the average and median values of the distribution being smaller than 2% in comparison with the corresponding isotropic case. A similar result was observed for the hoop force envelopes. Although these results appear strange they confirm that the execution of multiple analysis tend, in average, to resemble the deterministic case, which is an assurance that the analysis are well performed. Based solely on the average results the introduction of anisotropy, regardless of its degree, appear to bring no meaningful variations for this particular application. However, when the extreme results are analysed is possible to observe some influence of the anisotropy. In Figure 4.27 the vertical (A-B) and the horizontal (C-D) variations in percentage of the maximum convergence verified in the analyses relatively to the deterministic value are plotted against the anisotropy ratio. As shown both the vertical and horizontal convergence have a minimum difference when $\theta_x/\theta_y$=1, i.e. isotropic conditions. However, for values lower than 1 the difference of the vertical convergence (A-B) increases considerably with the decrease of the $\theta_x/\theta_y$ ratio. This result is justified since for ratios lower than 1 the rock mass becomes vertically layered (Figure 4.26(d)), hence, the probability of vertical weaker bands affecting simultaneously the crown and bottom of the tunnel is considerable resulting in higher variations of the convergence (up to 45%). For ratios higher than 1 the rock mass progressively becomes horizontally layered and a similar effect, increase of differences, is observed. Naturally this increase is smaller than the observed in the other

direction, since the bands are now horizontal, and is a direct function of the value of the spatial correlation distance, which in this case is 10m and consequently the entire tunnel can be located within a weaker band. It is also interesting to note that for high $\theta_x/\theta_y$ ratios there is a stabilisation of the variation, which is justified by the fact that the layering in the horizontal direction is already formed and, therefore, an increase of the anisotropy in this direction does not affect the result of the vertical convergence. Similar conclusions can be drawn for the convergence in the horizontal direction (C-D) that follows a mirrored behaviour.

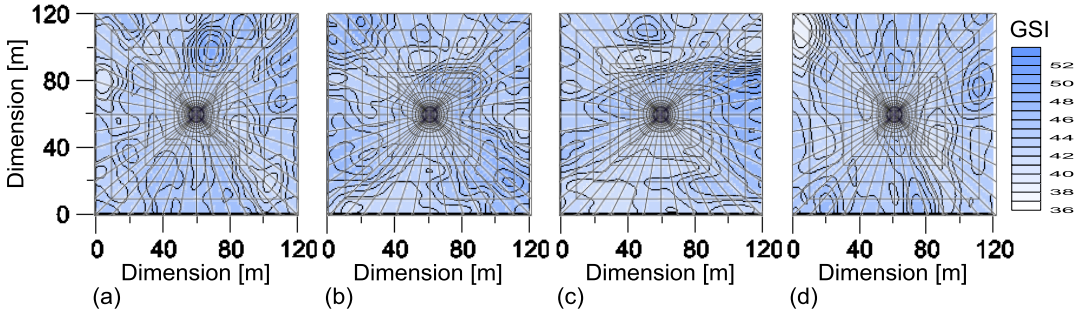


Figure 4.26 – Examples of random fields having anisotropic spatial correlations: (a) θx/θy=1; (b) θx/θy=0.5; (c) θx/θy=2; (d) θx/θy=0.2

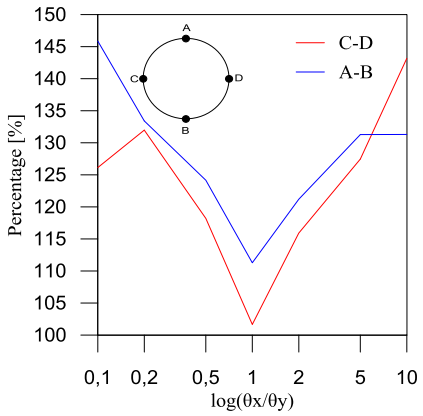


Figure 4.27 – Maximum convergence variation with anisotropic spatial correlation

### 4.4.5 Case 3: Field rotation

For evaluating the influence of the rotation of anisotropy random fields were generated for different angles α while keeping constant a standard deviation value of 7, a $\theta_x$=75m and an anisotropy ratio of $\theta_x/\theta_y$=7.5. In Figure 4.28 examples of random fields generated for (a) $\alpha$=-90°; (b) $\alpha$=-67.5°, (c) $\alpha$=--45°; (d) $\alpha$=-22.5°; (e) $\alpha$=0°; (f) $\alpha$=22.5°; (g) $\alpha$=45°; (h) $\alpha$=67.5° are presented. From the figures is possible to observe that bands of rock masses are created with approximately the direction imposed by α.

The rotation of the field is expected to have a similar impact to that observed when the degree of anisotropy was varied, with the only difference being the direction where the maximum convergence is observed. In fact, the results obtained for the hoop force, lining pressure and displacement envelopes lead to the conclusion that the minimum and maximum values are not a function of the rotation since no pattern could be established. A further analysis on the distribution of the convergence throughout the 999 runs show that the rotation of the anisotropy directly influences the standard deviation of the statistical distribution, as can be seen in Figure 4.29. From the figure is possible to verify that the standard deviation (a) is shown to have a minimum value for the vertical convergence (A-B) for α=0, which corresponds to the formation of horizontal bands, and a maximum in the opposite direction (α=-90 and 90). For the horizontal convergence (C-D) exactly the opposite occurs with the minimum observed for $\alpha$=-90 and 90 and the maximum for α=0. When the field presents different anisotropy directions a similar behaviour can be observed. For instance, the convergence E-F has a maximum for $\alpha$=-45° (anticlockwise rotation from the horizontal axis) and a minimum for $\alpha$=45°, and the opposite occurs for the convergence G- H. When analysing the covariation of the convergences (b) the afore mentioned conclusions become more evident. These results have a direct impact when computing the probability of the convergence exceeding a given value since the average value of the convergences throughout the calculations shows random and negligible variations between each rotation and therefore the probability becomes inversely proportional to the covariance.

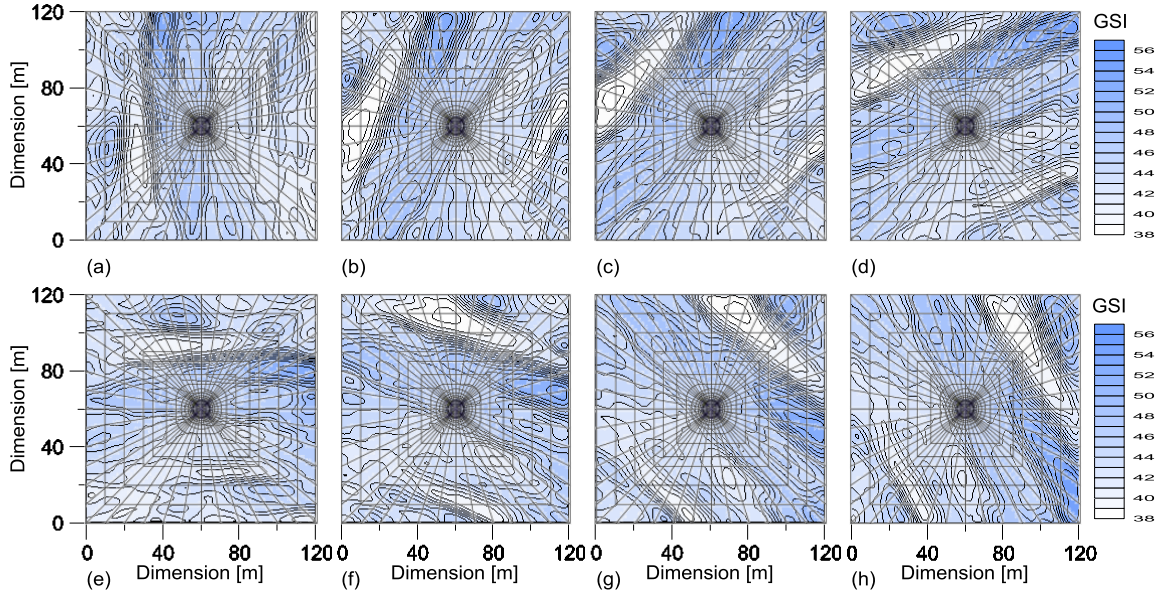


Figure 4.28 – Examples of rotated random fields: (a) α=-90º; (b) α=-62.5º; (c) α=-45º; (d) α=-22.5º; (e) α=0º; (f) α=22.5; (g) α=45º; (h) α=62.5º

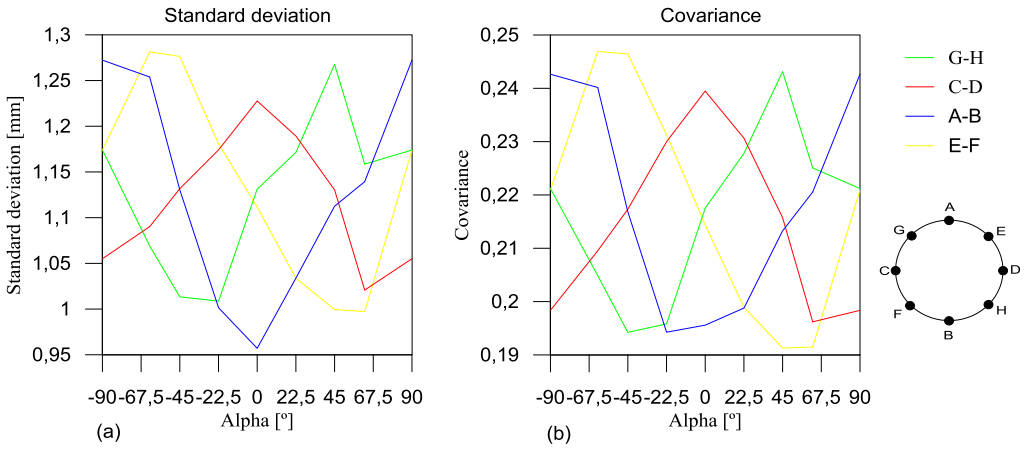


Figure 4.29 – Variation of (a) standard deviation and (b) covariance of the convergence distribution with the rotation of the field

# 5 CONCLUSIONS AND FURTHER WORKS

## 5.1 Conclusions

The existence of variability in soil and rock massifs is known to have implications in geotechnical and structural behaviour. So that this fact could be made evident several considerations regarding the existence and forms of variability as well as the parameters that condition its characterization were presented and discussed. From the most common algorithms available for numerically simulate variability in soils and rock massifs the LAS method was chosen due to its reliability as well as computation efficiency. The employment of random fields entails that multiple calculations have to be performed so that a pattern can be established and a tendency can be extrapolated. For the calculations presented in this work a substantial amount of computer capabilities were required due to the large number of parameters to vary as well as the number of calculations required.

In order to properly model variability within a given area a software capable of running the LAS algorithm for the generation of multiple random fields was further developed and several features were added to its routine, namely the possibility of varying the input statistical distribution, layering, non-stationary processes and field rotation, making it suitable to accurately simulate real case variability. A program capable of translate the random variable of the field into parameters of constitutive laws for soils and rocks through theoretical correlations as well as handling the interpolation between the random field and the finite element mesh was created. Furthermore, the already existing finite element algorithm was upgraded so that it could handle variable parameters and perform multiple calculations automatically. A couple of programs as well as an excel form were also developed so that result analysis could be efficiently performed in bulk.

So that the influence of variability could be assessed 3 applications were performed whose primordial objective was to infer the impact of the variation of the parameters required for the definition of the LAS algorithm namely the standard deviation, the isotropic spatial correlation distance and the degree and ratio of anisotropy.

The first application concerned the evaluation of the impact of introducing variability in the bearing capacity of a single strip footing. The random variable selected was the undrained strength of the soil, $S_u$. Based on the analyses performed several conclusions can be withdrawn:

- The statistical distribution of the input variable has a noticeable effect on the range of the bearing capacity with the normal distribution presenting wider values than the lognormal distribution essentially due to its tail. However, the average results show small variation regardless of the distribution chosen for input.

- It was also noticed that the distribution of the results of the bearing capacity followed a lognormal distribution for smaller stress levels in the soil than tended to change to a normal distribution when plastification occurs. These results were observed to be independent of the distribution selected for the input variable, $S_u$.

- The standard deviation is a very important parameter since it is shown to have influence not only in the minimum and maximum values obtained for the bearing capacity but also in the average values that decrease with the increment of standard deviation. In fact, the average bearing capacity is shown to decrease with the standard deviation of $S_u$ whilst the standard deviation of the bearing capacity is shown to increase.

- The obtained results highlight that the introduction of variability, even if small, can produce an impact of more than 30% in the value of the bearing capacity when compared with the theoretical or the deterministic value. This difference if not account in design can lead to a malfunction of the footing or ultimately to its failure.

The second application aimed to infer the implications of the variation of several parameters used to characterize variability on twin strip footings subject to simultaneous vertical loading. The parameters whose diversity was considered were standard deviation of $S_u$, the isotropic spatial correlation distance and multiple dependent variables. The main conclusions were:

- As before, standard deviation plays an important role in the displacement and rotation distribution of both footings. Increments in the standard deviation value will imply a wider range of results as well as condition the average value obtained in the load-displacement curves. As a result, the increase of the standard deviation value will imply the increase of the probability of structural damage due to the differential settlements and consequent rotations of the footings that occur.

- The higher the spatial correlation distance magnitude the higher the likelihood that zones of weaker resistance condition the response of each individual footing as well as their combined behaviour, having similar effects to the increment of standard deviation though less conspicuous.

- The introduction of variability in both strength and stiffness of the soil originates an even higher dispersion of displacements ad rotations in the footings. The results confirm that the introduction of a second variable translates in a higher probability of damage, which naturally increase with the decrease of the stiffness.

- The deterministic analysis is only capable of predicting one failure mechanism for the two footings. With the introduction of the variability eight different failure mechanism could be found enabling a more comprehensive behaviour of the footings that should be taken into consideration during design stages. The probability associated to each possible failure mechanism was roughly the same from which it can be concluded that despite its proximity the footings are not strongly affected by each other.

In the third application the influence of the variation of the rock mass standard deviation, of isotropic spatial correlation distance and of degree and direction of anisotropy on the excavation of a deep tunnel were analysed. The results obtained enabled the following conclusions:

- Standard deviation and isotropic spatial correlation have similar effects to those presented in previous applications having direct impact on the displacements of the tunnel and forces acting on the lining, which increases substantially (more than 25%) comparatively with the deterministic analysis.

- Variations of the ratio of anisotropy ($\theta_x/\theta_y$) affect the maximum horizontal and vertical convergences. The horizontal convergence was shown to increase with the increment of $\theta x/\theta y$ and the vertical convergence to decrease with it. These results are justified by the vertical/horizontal bands (layering of soil) of weak rock mass that are formed when the anisotropy increases and that accentuate the displacements in those areas.

- The direction of anisotropy of the random fields is shown to influence the distribution of the convergences along the tunnel contour, most prominently, the standard deviation of it, which is a function of the direction of anisotropy. This fact conditions the probability of the convergence exceeding a given value.

- With the introduction of variability it was observed asymmetry on the displacements and forces of the lining which were not possible to predict by the deterministic analysis where only a uniform pattern was found. This result demonstrates the importance of modelling the variability of soils and rock massifs since abnormal behaviours can be discovered leading to an improvement in the design of this type of structures.

Based on the application performed it is possible to conclude that the standard deviation of the input variable has a significant impact on the variability, which increases with its increment. Identical conclusion, though in a smaller scale, was observed for the spatial correlation distance, although it was found that this parameter is problem dependent and consequently should be evaluated in each case. As for the degree and direction of anisotropy of the random field it was observed that these factors have only an impact in the extreme cases, although its analysis should be further investigated since they might be very significant in other applications such as slope stability and excavations.

The adopted methodology, though certainly can be upgraded, has proven to be useful when modelling variability of soils and rocks. The applications performed with this methodology provided results, both in magnitude and behaviour, which simple deterministic analysis could not predict. Consequently, the use of this tool can improve and optimise the design of geotechnical structures making them both more reliable and profitable.

## 5.2 Further works

Following the present work some remarks must be made. Despite the fact that the developed methodology represents a step forward in the right direction there are features whose implementation would be deemed as useful:

- Ability to condition the random fields at set locations allowing for the direct integration of field test results in the generation of the random fields. This would represent a more reliable approach to simulate practical applications that could even have the advantage of reducing the number of realizations required for each parameter. Though this is theoretically possible in the current version of UC2DRF, the software is not capable of integrating the influence that a fixed value may have on its neighbourhood;

- 3D random field generation making the study of problems with three-dimensional nature possible such as tunnels, excavations, drainage, wave propagation among others;

- Possibility of having multiple independent variables without the need of them to be correlated. This can be performed by combining multiple single variable random fields.

- Integration of variability on dynamic calculations making it possible to analyse the behaviour of a given soil with heterogeneous properties in case of dynamic solicitations.

The analyses performed are merely theoretical, although representative of common geotechnical structures. For this methodology to be used in practice a combined approach using random fields and geo-statistics must be followed in order to properly establish the magnitude

of the parameters used. The influence that the introduction of variability has on the response of structures must be studied independently for each case. Furthermore, there are combinations of parameters that are not covered on the present work that are expected to influence the geotechnical and structural behaviour of such structures. It must be stated that due to the introduction of variability in the studied applications the results obtained for each application cannot be directly extrapolated to similar structures though similar methodologies are expected to be suitable.

# REFERENCES

Almeida e Sousa, J. (1998) *Tunnels in soils. Behaviour and numerical modelling*. PhD thesis. University of Coimbra, Coimbra. (in Portuguese).

Ameratunga, J., Sivakugan, N. & Das, B. M. (2015) *Correlations of Soil and Rock Properties in Geotechnical Engineering.* Springer.

Arsyad, A. (2008) *The effect of limited site investigations on the design and performance of pile foundations*. MSc thesis. University of Adelaide, Adelaide, Australia.

Bieniawski, Z. T. (1973) Engineering classification of jointed rock masses. *Civil Engineer in Sout Africa*, **15** (12), p. 353-343.

Bjerrum, L. (1963) Discussion. In *Proceedings of the European Conference on Soil Mechanics and Foundation Engineering, Wiesbaden*. Vol. 2, pp. 135-137.

Bond, A. & Harris, A. (2008) *Decoding Eurocode 7*. CRC Press.

Boscardin, M. D. & Cording, E. J. (1989) Building response to excavation induced settlement. *Journal of Geotechnical Engineering-Asce*, **115** (1), 1-21.

Bourdeau, P. L. & Amundaray, J. I. (2005) Non-parametric simulation of geotechnical variability. *Geotechnique*, **55** (2), 95-108.

Bowles, J. E. (1996) *Foundation analysis and design.* McGraw-Hill, New York.

Breysse, D., Niandou, H., Elachachi, S. & Houy, L. (2004) A generic approach to soil–structure interaction considering the effects of soil heterogeneity.

Burland, J. B. (1995) Assessment of risk of damage to buildings due to tunnelling and excavation. In *Proceedings of the 1st International conference on earthquake geotechnical engineering, IS Tokyo '95*. Vol. 3, pp. 1189-1201.

Cai, M., Kaiser, P., Uno, H., Tasaka, Y. & Minami, M. (2004) Estimation of rock mass deformation modulus and strength of jointed hard rock masses using the GSI system. *International Journal of Rock Mechanics and Mining Sciences*, **41** (1), 3-19.

Cai, M. (2011) Rock Mass Characterization and Rock Property Variability Considerations for Tunnel and Cavern Design. *Rock Mechanics and Rock Engineering*, **44** (4), 379-399.

Chen, Q., Seifried, A., Andrade, J. E. & Baker, J. W. (2012) Characterization of random fields and their impact on the mechanics of geosystems at multiple scales. *International Journal for Numerical and Analytical Methods in Geomechanics*, **36** (2), 140-165.

Ching, J., Wu, S.-S. & Phoon, K.-K. (2015) Statistical characterization of random field parameters using frequentist and Bayesian approaches. *Canadian Geotechnical Journal*, **53** (2), 285-298.

Cho, S. E. & Park, H. C. (2010) Effect of spatial variability of cross-correlated soil properties on bearing capacity of strip footing. *International Journal for Numerical and Analytical Methods in Geomechanics*, **34** (1), 1-26.

Christian, J. T. (2004) Geotechnical engineering reliability: How well do we know what we are doing? *Journal of Geotechnical and Geoenvironmental Engineering*, **130** (10), 985-1003.

Cochran, W. T., Cooley, J. W., Favin, D. L., Helms, H. D., Kaenel, R. A., Lang, W. W., Maling Jr, G. C., Nelson, D. E., Rader, C. M. & Welch, P. D. (1967) What is the fast Fourier transform? *Proceedings of the IEEE*, **55** (10), 1664-1674.

Cruz, F. (2008) *Implementação do fenómeno de consolidação num programa de elementos finitos 3D*. MSc thesis. Universidade de Coimbra, Coimbra. (in Portuguese).

Dasaka, S. M. & Zhang, L. M. (2012) Spatial variability of in situ weathered soil. *Geotechnique*, **62** (5), 375-384.

Décourt, L. (1989) The standard penetration test: state-of-the-art-report. *Norwegian Geotechnical Institute Publication*, **179**.

Degroot, D. J. & Baecher, G. B. (1993) Estimating autocovariance of insitu soil properties. *Journal of Geotechnical Engineering-Asce*, **119** (1), 147-166.

Dershowitz, W. & Einstein, H. (1988) Characterizing rock joint geometry with joint system models. *Rock Mechanics and Rock Engineering*, **21** (1), 21-51.

Duhamel, P. & Vetterli, M. (1990) Fast Fourier transforms: a tutorial review and a state of the art. *Signal processing*, **19** (4), 259-299.

Duncan, J. M. & Buchignani, A. L. (1976) *An engineering manual for settlement studies.* University of California, Department of Civil Engineering.

EC7: Part 1 (2004), EN 1997-1, *Eurocode 7: Geotechnical design - Part 1: General rules*.

EC7: Part 2 (2007), EN 1997-2, *Eurocode 7 - Geotechnical design - Part 2: Ground investigation and testing*.

Fenton, G. (1994) Error Evaluation of Three Random-Field Generators. *Journal of Engineering Mechanics*, **120** (12), 2478-2497.

Fenton, G. & Griffiths, D. V. (2008) *Risk assessment in geotechnical engineering.* John Wiley & Sons. pp. 467.

Fenton, G. A. & Vanmarcke, E. H. (1990) Simulation of random fields via local average subdivision. *Journal of Engineering Mechanics-Asce*, **116** (8), 1733-1749.

GID (2012) *GID v7.0: user manual.*

Griffiths, D. V. & Fenton, G. A. (2001) Bearing capacity of spatially random soil: the undrained clay Prandtl problem revisited. *Geotechnique*, **51** (4), 351-359.

Griffiths, D. V. & Fenton, G. (2008) *Probabilistic methods in geotechnical engineering.* CISM COURSES AND LECTURES. Springer. pp. 346.

Hanataka, M. & Uchida, A. (1996) Empirical Correlation between Penetration Resistance and Internal Friction Angle of Sandy Soils. *Soils and Foundations*, **36** (4), 1-9.

Hara, A., Ohta, t., Masanori, N., Shumpei, T. & Tadashi, B. (1974) Shear modulus and shear strength of cohesive soils. *Soils and Foundations*, **14** (3), 1-12.

Hoek, E. (1994) Strength of rock and rock masses. *ISRM News Journal*, **2** (2), 4-16.

Hoek, E., Carranza-Torres, C. & Corkum, B. (2002) Hoek-Brown failure criterion-2002 edition. *Proceedings of NARMS-Tac*, **1**, 267-273.

Hoek, E. & Diederichs, M. S. (2006) Empirical estimation of rock mass modulus. *International journal of rock mechanics and mining sciences*, **43** (2), 203-215.

Hoek, E. (2007) *Practical Rock Engineering.*

Jones, A. L., Kramer, S. L. & Arduino, P. (2002) *Estimation of uncertainty in geotechnical properties for performance-based earthquake engineering.* Pacific Earthquake Engineering Research Center, College of Engineering, University of California.

Kulhawy, F. H. & Mayne, P. W. (1990) *Manual on estimating soil properties for foundation design*. Electric Power Research Inst., Palo Alto, CA (USA); Cornell Univ., Ithaca, NY (USA). Geotechnical Engineering Group.

Lacasse, S. & Nadim, F. (1996) Uncertainty in characterising soil properties (plenary). In *Proceedings of the Uncertainty in the geologic environment, from theory to practice*.

Le Ravalec, M., Noetinger, B. & Hu, L. Y. (2000) The FFT moving average (FFT-MA) generator: An efficient numerical method for generating and conditioning Gaussian simulations. *Mathematical Geology*, **32** (6), 701-723.

Li, X. Y., Zhang, L. M., F., A. & Li, J. H. (2015) Using conditioned random field to characterize the variability of geological profiles. *Geotechnical and Geoenvironmental Engineering*.

Lumb, P. (1966) The variability of natural soils. *Canadian Geotechnical Journal*, **3** (2), 74-97.

Marinos, P. & Hoek, E. (2001) Estimating the geotechnical properties of heterogeneous rock masses such as flysch. *Bulletin of engineering geology and the environment*, **60** (2), 85-92.

Mayne, P. W. (2007) Cone penetration testing state-of-practice. *Transportation Research Board. Synthesis Study. NCHRP Project*, 20-05.

Moller, S. (2006) *Tunnel induced settlements and structural forces in linings*. PhD thesis. University of Stuttgard, Stuttgard.

Nishimura, S. (2005) *Laboratory study on anistropy of natural London clay*. PhD thesis. Imperial College of London, London.

Orchant, C., Kulhawy, F. & Trautmann, C. (1988) Reliability-based foundation design for transmission line structures: Critical evaluation of in-situ test methods. *Report EL-5507 (2)*.

Orr, T. L. L. (2012) How Eurocode 7 has affected geotechnical design: a review. *Proceedings of the Institution of Civil Engineers-Geotechnical Engineering*, **165** (6), 337-350. (in English).

Panet, M. & Guenot, A. (1982) Analysis of convergence behind the face of a tunnel. In *Proceedings of the Conference Tunnelling '82, London, UK*. Institute of Mining and Metallurgy, London, 197-204.

Pedro, A. (2007) *Mato Forte Tunnel - Back Analysis of its behaviour*. MSc thesis. Universidade de Coimbra, Coimbra. (in Portuguese).

Pedro, A., Taborda, D., Coelho, P. A. L. F. & Almeida e Sousa, J. (2012) The variability of massifs: numerical modelling and its influence on the behaviour of geotechnical structures. In *Proceedings of the XIII National Conference in Geotechnics, Lisboa, Portugal*. 14 (in Portuguese).

Phoon, K. K. & Kulhawy, F. H. (1999) Characterization of geotechnical variability. *Canadian Geotechnical Journal*, **36** (4), 612-624.

Potts, D. M., Zdravkovic, L. & Zdravković, L. (2001) *Finite element analysis in geotechnical engineering: application.* Thomas Telford.

Prandtl, L. (1920) Uber die harte plasticher korper. *Nachr Ges Wiss. Gottingen Math Phys Kl*, **12**, 74-85.

Rackwitz, R. (2000) Reviewing probabilistic soils modelling. *Computers and Geotechnics*, **26** (3-4), 199-223.

Rankin, W. J. (1988) Ground movements resulting from urban tunnelling: predictions and effects. *Eng. Geol. of Underground Movements*, 79-92.

Robertson, P. (2012) The James K. Mitchell Lecture: Interpretation of in-situ tests–some insights. In *Proceedings of the Proc. 4th Int. Conf. on Geotechnical and Geophysical Site Characterization–ISC'4*, 3-24.

Robertson, P. K. & Campanella, R. (1983) Interpretation of cone penetration tests. Part I: Sand. *Canadian geotechnical journal*, **20** (4), 718-733.

Shioi, Y. & Fukui, J. (1982) Application of N-value to design of foundations in Japan. In *Proceedings of the Proceeding of the Second European Symposium on Penetration Testing*, Vol. 1, pp. 159-16.

Suchomel, R. & Masin, D. (2009) Calibration of an advanced soil constitutive model for use in probabilistic numerical analysis. In *Proceedings of the Int. Symposium on Computational Geomechanics (ComGeo I), Juan-les-Pins, France*. 265-274.

Suchomel, R. & Masin, D. (2010) Spatial variability of soil parameters in an analysis of a strip footing using hypoplastic model. In *Proceedings of the 7th European Conference on Numerical Methods in Geotechnical Engineering (NUMGE 2010), Trondheim, Norway*. 383-388.

Tanabe, K. & Sagae, M. (1992) An exact Cholesky decomposition and the generalized inverse of the variance-covariance matrix of the multinomial distribution, with applications. *Journal of the Royal Statistical Society. Series B (Methodological)*, 211-219.

Uzielli, M., Lacasse, S., Nadim, F. & Phoon, K. (2006) Soil variability analysis for geotechnical practice. In *Proceedings of the second international workshop on characterisation and engineering properties of natural soils, Singapore. Balkema, The Netherlands*, 1653-1752.

Vanmarcke, E. H. (2010) *Random fields: analysis and synthesis.* The MIT press. pp. 394.

Wang, C. Z. Y. (2014) Bayesian model comparison and selection of spatial correlation functions for soil parameters. *Structural Safety*, **49**, 10-17.

Webb, D. (1970) Settlement of structures on deep alluvial sandy sediments in Durban, South Africa.

Wolff, T., Hassan, A., Khan, R., Ur-Rasul, I. & Miller, M. (1995) Geotechnical reliability of dam and levee embankments. *Report for the US Army Corps of Engineers, Experiment Station, Michigan State University*.

Zhang, L. M. (2013) Characterizing geotechnical anisotropic spatial variations using random field theory. *Canadian Geotechnical Journal*, **50** (7), 723-734.